ONDEMAND Drug Delivery: The Role of Conducting Polymers and Wirefree Electrochemistry



Áine Brady, B.Sc
A thesis submitted at Dublin City University for the degree of PhD

School of Chemical Sciences

Supervisors:

Dr. Tim McCormac and Prof. Robert J. Forster

July 2024

I. Declaration

We, the undersigned declare that this thesis entitled 'ONDEMAND Drug Delivery: The Role of Conducting Polymers and Wirefree Electrochemistry' is entirely the author's own work and has not been taken from the work of others, except as cited and acknowledged within the text.

The thesis has been prepared according to the regulations of Dundalk Institute of Technology and has not been submitted in whole or in part for an award in this or any other institution.

Author Name: Áine Brady

Author Signature: Live Frady

Date: July 29, 2024

Supervisor Name: Dr. Timothy McCormac

Supervisor Signature:

Date:

Supervisor Name: Prof. Robert Forster

Robert Forter

Supervisor Signature:

Date: July 29, 2024

II. Dedication

I dedicate this to my Grandad, keep watching over us.

III. Acknowledgements

Firstly, I'd like to acknowledge my Mam. You are such a strong, independent, resilient woman, and I owe all of my character to you. Without you I certainly wouldn't have achieved all I have done to date, and for this I am forever grateful. To Aishling, I followed in your footsteps down the pathway of science, what great advice! You have always been such a caring, supportive, role model in my life, fulfilling all the 'big sister' criteria. Thank you for always being only a phone call away. And finally, Jarlaith, you are a remarkable young man. Your passion for all things engineering will always be inspiring, and your kind, curious, nature will assist you in doing wonderful things in life.

Christopher, my best friend, and life partner. I simply cannot thank you for all you have done for me since we met. You were the first person that encouraged me to pursuit this path and you've been with me this whole journey, through the many ups and downs. You've supported me in many ways, and I will forever be grateful for that. Thank you for always being by my side, giving the right advice when needed. As you always say, "anything you do is everything you do".

To my second family, Philip, Martina, and Caitríona. Since the first day I met you, you welcomed me into your family with open arms. I will never be able to repay your generosity and kindness over the past three years. From the bottom of my heart, thank you.

Noel and Lynne, my home from home. I am forever grateful that we met all those years ago. You have always taught me that there is no limit. Thank you for being such wonderful, supportive, positive people. We will be over when this is submitted!!

I would like to give a special thanks to Prof. Robert Forster and Dr. Loanda Cumba for encouraging me to pursuit a PhD in this field during my undergraduate degree. To Robert, you have continuously guided, supported and challenged me throughout my studies to become the best version of myself. You are an incredible scientist, and I am honoured to have worked alongside you. I look forward to continuing doing great things in the future!

I would like to thank Dr. Tim McCormac for giving me this opportunity. Your knowledge and guidance throughout this project are greatly appreciated. You have allowed me to grow and develop into an independent researcher, which will assist me in future years. Thank you.

To the FRGs! What a group of people. Indher, Oisín, and Michał, thank you for all the laughs in the lab and the office. I look forward to working alongside you all in 2024! To the DkIT crew, Athira, Suganya, and Indher (again), thank you for being so welcoming when I joined the group. You are such caring, generous people, and I am so lucky to have had you as part of my PhD journey.

To the 'Nomadians', and in particular, Stephanie and Dave. I am incredibly lucky to have worked alongside such a wonderful bunch of people, making weekend working such a laugh! Thank you so much for giving me the opportunity of working with you, and I wish you all the success in your future!

Finally, I would like to acknowledge the Ballyhaise Ladies Gaelic Football Team, or shall I say the 2023 Intermediate Champions? What a year! Thank you to the management, the girls, and the community for all the laughs and the wonderful memories.

IV. Table of Contents

I. Declaration	i
II. Dedication	ii
III. Acknowledgements	iii
IV. Table of Contents	v
V. List of Abbreviations	vii
VI. List of Symbols	viii
VII. List of Figures	ix
VIII. List of Tables	xvi
IX. Abstract	xvii
1. Introduction	2
1.1. Breast Cancer	2
1.2. Classification of Anti-Cancer Drugs	3
1.3. Conducting Polymers	
1.3.1. Doping	7
1.3.2. Electrical Characteristics	
1.4. Drug Delivery	
1.4.2. Pharmacokinetics of Drug Delivery Systems	
1.4.3. Polymers in Drug Delivery Systems	14
1.4.4. Conducting Polymers in Drug Delivery Systems	15
1.5. Wireless Electrochemistry	17
1.5.1. Conducting Polymers in Bipolar systems	19
1.6. Techniques	20
1.6.1. Introduction to Electrochemistry	
1.6.2. Electrochemical Setup	
1.6.3. Cyclic Voltammetry	
1.6.4. Electrochemical Quartz Crystal Microbalance	
1.6.6. Scanning Electron Microscopy	
1.6.7. Chronoamperometry	
1.6.8. Chronocoulometry	
1.6.9. Chronopotentiometry	
1.6.10. Electrochemical Impedance Spectroscopy	
1.7. Conclusion	29
1 & References	30

2. Electrochemical and Surface Characterisation of Poly(5,4-	
ethylenedioxythiophene) Dodecylbenzenesulfonate Layers	43
2.1. Introduction	43
2.2. Experimental	44
2.3. Results and Discussion	46
2.4. Conclusion	55
2.5. References	56
3. Electrochemical Doping and De-doping of Therapeutics	62
3.1. Introduction	62
3.2. Materials and Methods	63
3.3. Results and Discussion	
3.3.2. The Effects of Film Thickness on Drug Loading and Release	
3.4. Conclusion	
3.5. References	81
4. Wirefree and Conventional Electrodeposition of PEDOT Films	85
4.1. Introduction	85
4.2. Materials and Methods	86
4.3. Results and Discussion	90
4.4. Conclusion	109
4.5 References	110
5. The Effects of Bipolar Size on Electric Field Distribution	115
5.1. Introduction	115
5.2. Materials and Methods	116
5.3. Results and Discussion	120
5.3.1. The Effects of Electrode Size on Electric Field Distribution	120
5.3.2. Shaping the Electric Field	129
5.3.3. Electric Field Mapping using Simulation Software	
5.4. Conclusion	139
5.5. References	140
6. Thesis Conclusion	145
7. Future Work: Wireless Release of Naproxen from Poly(3,4-	
ethylenedioxythiophene) Films	148
7.1. Aim	
7.2. Conclusion	
7.2. Conclusion	150

V. List of Abbreviations

Acronyms Explanation

ABS Acrylonitrile Butadiene Styrene

AFM Atomic Force Microscopy

API Active Pharmaceutical Ingredient

BP Bipolar

BPE Bipolar Electrode

BPE Bipolar Electrochemistry
BPES Bipolar Electrostimulation

CAD Computer Aided Design

CV Cyclic Voltammetry

DBS Dodecylbenzenesulfonate

DDS Drug Delivery System

EIS Electrochemical Impedance Spectroscopy

EPR Enhanced Permeability and Retention

EQCM Electrochemical Quartz Crystal Microbalance

FE-SEM Field Emission Scanning Electron Microscopy

FTO Fluorine-Doped Tin Oxide

GCE Glassy Carbon Electrode

HOMO Highest Occupied Molecular Orbital

Hz Hertz

LUMO Lowest Occupied Molecular Orbital

MDC Mitoxantrone Dihydrochloride

NPX Naproxen Sodium Salt

PEDOT Poly(3,4-ethylenedioxythiophene)

SEM Scanning Electron Microscopy

VI. List of Symbols

Symbol	Explanation	Unit
D	Diffusion Coefficient	cm ² /s
v	Scan Rate	V/s
Q	Charge	C
i_p	Peak Current	A
f_0	Resonant Frequency	Hz
$ ho_q$	Density of Quartz	g/cm ³
μ_q	μ_q Shear Modulus of Quartz	
E_{pc}	Cathodic Peak Potential	V
E_{pa}	Anodic Peak Potential	V
R_s	R _s Solution Resistance	
R_{ct}	R _{ct} Charge Transfer Resistance	
A_{W}	Warburg Diffusion	
M_t	Mass of Drug Released at Any Time t	
M_{∞}	Total Drug Mass	
k	Rate Constant	
ΔE_{elec}	Interfacial Potential of the BPE	V
E_{tot}	Total Voltage Applied to the BP System	V
l_{elec}	Length of the BPE	cm
$oldsymbol{l_{channel}}$	channel Distance Between Driving Electrodes	
Γ	Surface Coverage	
F	Faraday's Constant	
Q_p	Polymerisation Charge	
M_w	Molecular Weight	g/mol
η_e	Number of Electrons	-
$ ho_f$	Film Density	g/cm^3

VII. List of Figures

Chapter 1. Literature Review

Figure 1. 1. Schematic representation of the wirelessly stimulated drug release from
conducting polymers
Figure 1. 2. A diagram of the structure of the female breast including the two most
common breast diseases, ductal carcinoma in situ and invasive ductal carcinoma. This
illustration is extracted from Song et al. ⁸
Figure 1. 3. Illustration of the various applications of conducting polymers extracted from
Namsheer et al. ²¹ 6
Figure 1. 4. Chemical structures of (a) Poly(3,4-ethylenedioxythiophene) (PEDOT) (b)
Polyethylene
Figure 1. 5. Graphical representation of electronic band gap and oxidation process of
polypyrrole extracted from Le et al. ²⁵
Figure 1. 6. Schematic of the conductivity levels of doped and undoped conjugated
polymers. Extracted from Le et al. ²⁵
Figure 1. 7. (a) Possible mechanism for the electropolymerisation of EDOT. Extracted
from Ramalingam et al. 30 (b) Oxidation and doping processes of PEDOT. Extracted from
Cameron et al. ³¹
Figure 1. 8. Classification of conventional drug delivery systems. Extracted from Adpeu
et al. ³⁵
Figure 1. 9. Adapted from the National Institute of Diabetes, Digestive and Kidney
Diseases, National Institutes of Health. ³⁷
Figure 1. 10. Schematic of bipolar electrolysis extracted from Crooks. ⁷⁴
Figure 1. 11. Schematic of a bipolar electrochemical system, side view. (a) Typical
bipolar setup including the BPE in the centre of the cell located between two feeder
electrodes. (b) Linear potential decay model that occurs across the BPE. Extracted from
Crooks. ⁷⁴
Figure 1. 12. Schematic of an (a) open and (b) closed bipolar electrochemical system
extracted from Wang et al. ⁷⁸
Figure 1. 13. Schematic of a three-electrode electrochemical cell. Extracted from Elgrishi
et al. ⁸⁴
Figure 1. 14. Schematic of an EQCM set up. Extracted from Ji et al. 92

Figure 1. 15. (a) one step chronoamperometric waveform where analyte O is not			
electroactive at E_1 and is reduced at E_2 (b) two step chronoamperometric waveform where			
analyte O is not electroactive at $E_{1} \text{and}$ is reduced at $E_{2}.$ From time 0 to $\tau,$ the reduced			
product builds up near the electrode surface. After τ , the oxidised species is available at			
the electrode due to the change in potential to E_1 . Extracted from Bard and Faulkner. 83			
26			
Figure 1. 16. Schematic of a Nyquist plot extracted from Mei et al. 103			
Chapter 2. Electrochemical and Surface Characterisation of Poly(3,4-			
ethylenedioxythiophene) Dodecylbenzenesulfonate Layers			
Figure 2. 1. (a) 10 mC PEDOT/Cl film cycled in 0.1 M KCl. Scan rate: 50 mV/s. (b) 10			
mC PEDOT/DBS film (250 cycles) in 1 M KCl. Scan rate: 100 mV/s			
Figure 2.2. Overlay of 10 mC PEDOT/DBS film on GCE cycled in (a) 1M LiCl and 1M			
BaCl ₂ (b) 1M LiCl and 1M CsCl. Scan rate 50 mV/s			
Figure 2.3. (a) Electropolymerisation of PEDOT/DBS by cyclic voltammetry in 10 mM			
EDOT 5 mM SDBS in aqueous solution on Pt quartz crystal electrode. Scan rate 100			
mV/s. (b) Mass changes obtained simultaneously during electropolymerisation of			
PEDOT/DBS film using QCM			
Figure 2.4. (a) PEDOT/DBS film cycled in 0.1M KCl on Pt quartz crystal electrode (b)			
EQCM frequency response of PEDOT/DBS cycled in 0.1 M KCl (c) EQCM mass			
response of PEDOT/DBS cycled in 0.1 M KCl (d) PEDOT/DBS film cycled in 0.1 M			
LiCl, 0.1 M NaCl and 0.1 M KCl (third cycle). Scan rate 50 mV/s50			
Figure 2.5. Nyquist plot of 10 mC PEDOT/DBS film in 1 M KCl on GCE. AC impedance			
was performed at different applied potentials (0.1 V, -0.3 V, -0.8 V, -1,0V) (vs. Ag/AgCl)			
from 0.01 to 1×10^5 Hz			
Figure 2.6. Representative FE-SEM images of specimens (a) PEDOT/DBS and (b)			
PEDOT/Cl. AFM micrographs of samples (c) PEDOT/DBS and (d) PEDOT/Cl 54			

Chapter 3. Electrochemical Doping and De-doping of Therapeutics
Figure 3.1. Chemical structure of (a) naproxen sodium salt (b) mitoxantrone
dihydrochloride62
Figure 3.2. (a) Electrochemical polymerisation of PEDOT/ClO ₄ by cyclic voltammetry
for 25 cycles in 10 mM EDOT 0.1 M LiClO $_4$ solution on an Au quartz crystal at 100 mV/s
(b) Electropolymerisation of PEDOT/NO ₃ by cyclic voltammetry for 25 cycles in 10 mM
EDOT 0.1 M KNO ₃ solution on an Au quartz crystal (c) EQCM frequency response for
PEDOT/ClO ₄ film formation (d) EQCM frequency response for PEDOT/NO ₃ film
formation
Figure 3.3. (a) Cyclic voltammogram of PEDOT/ClO ₄ film cycled in 0.1 M LiClO ₄ a
$0.1~\mbox{V/s}$ (b) Cyclic voltammogram of PEDOT/NO3 film cycled in $0.1~\mbox{KNO}_3$ at $0.1~\mbox{V/s}$
Both cyclic voltammograms were started at open circuit potential
Figure 3.4. Mass change versus time graph of (a) ClO_4 de-doping at -0.5 V for 600
seconds in 0.1 M LiClO $_4$ by chronoamperometry (b) $\mathrm{NO_{3}^{-}}$ de-doping at -0.2 V for 600
seconds in 0.1 M KNO ₃ by chronoamperometry
Figure 3.5. (a) PEDOT/ClO $_4$ film naproxen loading for 600 seconds at $\pm 0.5~\mathrm{V}$ using
chronoamperometry in 10 mM naproxen sodium salt (b) PEDOT/NO3 film naproxen
loading for 600 seconds at ± 0.5 V using chronoamperometry in 10 mM naproxen sodium
salt71
Figure 3.6. Mass versus time graph of (a) PEDOT/ClO ₄ spontaneous release using open
circuit potential for 600 seconds and controlled release at -0.5 V for 600 seconds (b)
PEDOT/NO ₃ spontaneous release using open circuit potential for 600 seconds and
controlled release at -0.2 V for 600 seconds
Figure 3.7. Mass versus time response of PEDOT/ ClO ₄ film de-doping ClO ₄ in 0.1 M
LiClO ₄ for 300 seconds at –0.5 V using chronoamperometry. Film thicknesses include (a)
10 mC and (b) 20 mC. Film formation was performed in 10 mM EDOT 0.1 M LiClO
solution using chronocoulometry
Figure 3.8. Mass versus time response of PEDOT/ClO ₄ film loading with 5 mM anti-
cancer drug mitoxantrone in DI water for 300 seconds at + 0.5 V using
chronoamperometry. (a) 10 mC and (b) 20 mC
Figure 3.9. Mass versus time response of (a) 10 mC PEDOT/ClO ₄ film spontaneous and
controlled release of mitoxantrone (b) 20 mC PEDOT/ClO ₄ film spontaneous and
controlled release of mitoxantrone.

Chapter 4. Wirefree and Conventional Electrodeposition of PEDOT Films
Figure 4. 1. Diagram depicting the diverse applications for wireless electrostimulation.
Extracted from Forster. ² 85
Figure 4. 2. (a) FreeCAD design of the in house bipolar electrochemical cell with two
feeder electrodes, FTO slot, and tweezer slot (b) 3D printed bipolar electrochemical cell
printed in acrylonitrile butadiene styrene (ABS)91
Figure 4. 3. (a) Bipolar electrode (BPE) after bipolar polymerisation in a two-feeder set
up as shown in Figure 4.2. BP polymerisation was performed in a 10 mM EDOT DI water
solution at 30 V for 20 minutes on FTO glass (BPE) (b) linear potential decay model
currently used to describe the bipolar system91
Figure 4. 4. (a) Galvanostatic polymerisation of EDOT for 300 s at 200 μA in 10 mM
EDOT 0.1 M LiClO ₄ on FTO glass (b) Images from top to bottom of PEDOT polymerised
at 200 μA for 100, 200, 300 and 600 seconds in 10 mM EDOT 0.1 M LiClO ₄ solution on
FTO glass93
Figure 4. 5. (a) Scan rate study of the PEDOT/ClO ₄ film in 0.1 M LiClO ₄ from 5 mV/s
to 100 mV/s (b) Conventional film capacitance versus polymerisation time (c) Film
thickness versus polymerisation time calculated using Eqt. 4.1 (d) Capacitance versus
film thickness for the conventional PEDOT film
Figure 4. 6. Normalised absorbance of 400 nm – 1000 nm wavelength light through (a)
conventionally deposited PEDOT/ClO ₄ on FTO by applying 200 µA for 300 seconds in
10 mM EDOT 0.1 M LiClO ₄ (purple) and (b) bipolar deposited PEDOT on FTO
polymerised at 30 V for 20 minutes in 10 mM EDOT Milli-Q water (green)96
Figure 4. 7. The influence of time on BP polymerisation (a) The quantity of PEDOT
deposited at constant 30 V for 5 to 30 minutes in a 10 mM EDOT DI water solution (b)
Film surface coverage across the length of the BPE. Polymerisation was performed at a
constant 30 V for varying times of 5 to 30 minutes
Figure 4. 8. The influence of the voltage applied to the feeder electrodes on BF
polymerisation. (a) Dependence of the quantity of PEDOT deposited on the BPE as the
voltage dropped across the two feeder electrodes is varied. The deposition time is 15
minutes. Diagram of the bipolar polymerised PEDOT on the FTO surface at varying
voltages for constant time 15 minutes. BP polymerisation was performed in 10 mM
EDOT Milli-Q water solution from 5 V to 30 V

Figure 4. 9. (a) Diagram of a BP PEDOT film deposited on FTO using a feeder voltage
drop of 30 V for 20 minutes in 10 mM EDOT Milli-Q water solution. Half of the deposited
film was removed to create a clean step for the stylus, as described in Section 4.2.4. The
arrows show the stylus paths. The stylus distance represents the location across the length
of the BP. (b) Dependence of the film thickness with increasing distance from edge of the
BPE anode towards the centre of the BPE
Figure 4. 10. Schematic representation of a 30 V 30 minute bipolar polymerisation in 10
mM EDOT Milli-Q water solution. The maximum possible voltages, calculated using
Eqt. 1.1, are indicated along the length of the BPE
Figure 4. 11. SEM images of (a) bipolar electrode negative pole after polymerisation at
30 V for 20 minutes in 10 mM EDOT Milli-Q water (b) bipolar electrode positive pole
after polymerisation at 30 V for 20 minutes in 10 mM EDOT in Milli-Q water (c) edge
of the bipolar electrode positive pole after 30 V 20 minute polymerisation of 10 mM
EDOT in Milli-Q water film (d) Horizontal edge (2 cm side) of the bipolar positive pole
after 30 V 20 minute polymerisation of 10 mM EDOT in Milli-Q water 106
Figure 4. 12. Contact angle measurement of (a) bare FTO, (b) and (c) BP PEDOT film
polymerised at 30 V for 20 min in a 10 mM EDOT Milli-Q solution on an FTO slide (d)
conventionally deposited PEDOT on an FTO electrode (2 cm x 1 cm) at 200 μA for 300
seconds in 10 mM EDOT 0.1 M LiClO ₄ .
Chapter 5. The Effects of Bipolar Size on Electric Field Distribution
Figure 5. 1. Schematic of the electric field distribution generated by four feeder
electrodes using COMSOL software. Extracted from Forster. ⁴
Figure 5. 2. Diagram of BP PEDOT polymerisation on BPEs of varying lengths.
Polymerisation was performed on an FTO BPE in 10 mM EDOT Milli-Q water solution
at 30 V for 20 minutes. Percentage coverage was determined experimentally as described
in Section 5.2.5. Maximum voltages at the tip of the BPE anode were calculated using
Eqt. 1.1. Theoretical voltages where polymerisation stops was calculated by measuring
the polymerisation distance as described in Section 5.2.5. The voltage where the
polymerisation stopped was then calculated using Eqt. 1.1
Figure 5. 3. BP PEDOT polymerisation on FTO BPEs of increasing length, ranging from
1.4 cm to 2.7 cm. Polymerisation was performed in an electrolyte free solution.
Theoretical voltages were calculated using Eqt. 1.1
Figure 5. 4. Capacitance of BP polymerised EDOT in 10 mM EDOT Milli-Q water on
FTO BPEs of varying lengths (1.4 cm, 2.0 cm, and 2.6 cm) at voltages of 10, 20, 30, and

40 V for 10 minutes. Capacitance was calculated from scan rates studies. Samples were
performed in triplicate. 124
Figure 5. 5. EIS and CV data of the BPEs of varying length in 0.1 M LiClO ₄ . (a) 1.4 cm
BPE capacitance results for initial EIS (EIS 1), scan rate study (CV), and second EIS
measurement (EIS 2). (b) 2.0 cm BPE capacitance results for initial EIS (EIS 1), scan rate
study (CV), and second EIS measurement (EIS 2). (c) 2.6 cm BPE capacitance results for
initial EIS (EIS 1), scan rate study (CV), and second EIS measurement (EIS 2). BP
PEDOT films were formed by BP polymerisation at 30 V for 20 minutes in 10 mM EDOT
in Milli-Q water. A frequency range of $1x10^5\ Hz$ to $0.1\ Hz$ at $0.2\ V$ was used for all
impedance results. (d) The circuit used for EIS data fitting using Nova software 126
Figure 5. 6. SEM images of BP polymerised PEDOT at 30 V for 20 minutes in 10 mM
EDOT Milli-Q water solution. (a) 1.4 cm BPE (b) 2.1 cm BPE (c) 2.7 cm BPE (d) 2.7 cm
BPE. BP films were polymerised using a two-feeder electrode system (Figure 5.2) 128
Figure 5. 7. (a) FreeCAD design of the four-feeder set up including four 2 cm x 1 cm x
2 mm feeder electrode slots and one 1.5 cm x 1.5 cm FTO BPE slot (b) four feeder BP
cell printed in acrylonitrile butadiene styrene
Figure 5. 8. FTO BPE polymerised in 10 mM EDOT Milli-Q water solution at 30 V for
20 minutes (a) Configuration 1: Positive and negative feeders are opposing each other (b)
Configuration 2: Positive feeders and negative feeders are located beside each other. 130
Figure 5. 9. Four feeder BP polymerisation of 10 mM EDOT in Milli-Q water at 30 V
for 20 minutes. Each BPE was cycled in 0.1 M LiClO ₄ . Scan rates of 5, 10, 20, 50 and
100 mV/s were used for the scan rate study. (a) Configuration 1 (b) Current versus scan
rate of configuration 1 (c) Configuration 2 (d) Current versus scan rate of configuration
2
Figure 5. 10. SEM images for PEDOT deposited by bipolar polymerisation using four
feeder electrodes at $30~\mathrm{V}$ for $20~\mathrm{minutes}$ in $10~\mathrm{mM}$ EDOT Mill-Q water solution. (a) and
(b) represent Configuration 1, (c) and (d) represent Configuration 2
Figure 5. 11. Electric field modelling of the two-feeder electrode set up, investigating (a)
potential gradient (b) electric field and (c) electric flux
Figure 5. 12. Electric field mapping of the four-feeder setup without the BPE
(Configuration 1), investigating (a) potential gradient (b) electric field (c) electric flux
and (d) image of PEDOT deposited by Configuration 1 on FTO (1.5 x 1.5 cm). Applied
potential of -10 V on the negative feeders and +10 V on the positive feeders

Figure 5. 13. Electric field mapping of the four-feeder electrode set up (Configuration 2),
investigating (a) potential gradient (b) electric field (c) electric flux and (d) image of
PEDOT deposited by Configuration 2 on FTO (1.5 x 1.5 cm). Applied potential of -10 V
on feeder cathodes and +10 V on feeder anodes
Chapter 7. Future Work
Figure 7.1. Schematic representation of the wirelessly stimulated drug release from
conducting polymers

VIII. List of Tables

Chapter 1. Literature Review	
Table 1.1. List of Taxane and Anthracycline Drugs used for Cancer Treatment.	5
Table 1.2. Polymeric nanoparticle formulations that are currently on the market. Adap	ted
from Ferrari et al. ⁴⁹	15
Chapter 2. Electrochemical and Surface Characterisation of Poly(3	,4-
ethylenedioxythiophene) Dodecylbenzenesulfonate Layers	
Table 2.1. Table of hydrated radii of ions extracted from literature	48
Table 2.2. Numerical values of solution resistance (R _s), capacitance (C), charge trans	fer
resistance (Rct), and Warburg diffusion (Aw). Data obtained by fitting to the circuit	in
Figure 2.5.	53
Chapter 3. Electrochemical Doping and De-doping of Therapeutics	
Table 3.1. Drug loading and release of naproxen from ClO ₄ and NO ₃ films. M	ass
calculated in ng cm ⁻² using stated otherwise. Mass calculated using Eqt 3.2	73
Table 3.2. Calculated quantity of polymer film, drug loading and drug release from	om
PEDOT/ClO ₄ and PEDOT/NO3 films	74
Table 3.3. Release kinetics of both PEDOT/ClO ₄ and PEDOT/NO ₃ films for be	oth
spontaneous and controlled release. The Avrami equation was used to calculate the r	ate
constants and kinetic exponents (Eqt. 3.5).	74
Table 3.4. Mass changes of PEDOT/ClO ₄ films of varying thicknesses at 300 secon	ds.
Mass calculated using Eqt 3.2	79
Table 3.5. Calculated quantity of mitoxantrone for PEDOT/ClO4 films of vary	
thicknesses after 300 seconds.	_

IX. Abstract

At the moment, breast cancer is one of the most dominant forms of cancer globally, diagnosing 2.3 million people in 2020 alone, according to the World Health Organization. While current treatments exhibit some encouraging outcomes, the associated side effects are profound and severe. The aim of this project is the creation of an 'on demand' drug delivery system, tackling one of the most formidable issues in modern society. The drug delivery system is based on the use of biocompatible, multifunctional, electronically conducting polymers so as to enable more effective therapy for cancer patients, whilst reducing common side effects. Based on the redox switching of conducting polymers, a drug delivery system was created using poly(3,4-ethylenedioxythiophene) as the drug release vehicle, having the ability to load and release materials upon oxidation and reduction. The second part of the project focuses on the fundamentals of 'wirefree' or bipolar electrochemistry. The main focus of this work is to challenge current theories in the field, to provide a thorough, in-depth understanding of the technique. In combining the work presented in this thesis, a thorough understanding of conducting polymer drug delivery and wireless electrochemistry has been established. Further building on this work could see the development of a wirelessly triggered conducting polymer-based drug delivery system that could be used as a minimally or non-invasive method for delivering therapeutics to patients.

Keywords: Poly(3,4-ethylenedioxythiophene), electrochemical quartz crystal microbalance, breast cancer, drug delivery, bipolar electrochemistry.

Chapter 1Literature Review

1. Introduction

The overarching aim of this thesis is to develop a wirelessly stimulated drug delivery system through the use of the well-known redox characteristics of conducting polymers and 'wirefree' electrochemistry. The purpose of this work includes the wireless delivery of therapeutics in a safe, controlled, and targeted manner, minimising the cytotoxic effects of many drugs. By using conducting polymers, particularly poly(3,4-ethylenedioxythiophene), therapeutics are doped and de-doped upon the application of a potential, resulting in an 'on-demand' 'on/off' switch like behaviour. The innovation behind this work is the implementation of 'wirefree' electrochemistry which allows the application of a potential without any physical wiring to the working electrode. This 'wirefree' electrochemical stimulation would then result in the wireless release of therapeutics from conducting polymer films as shown in Figure 1.1 and discussed in Chapter 7.

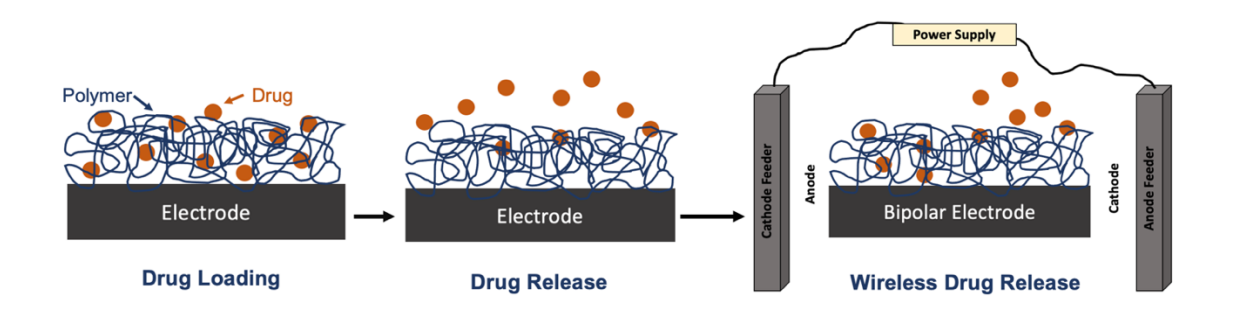


Figure 1. 1. Schematic representation of the wirelessly stimulated drug release from conducting polymers.

1.1. Breast Cancer

At this moment, after skin cancer, breast cancer is the most dominant form of cancer globally, diagnosing 2.3 million people in 2020 alone, according to the World Health Organization.² Since the 1980s, breast cancer mortality rates have decreased with the implementation of routine breast check screening, which has only improved with advances in healthcare and technology.^{3,4} Mammography has become an established screening method for breast cancer, with a sensitivity level of 75 to 95% and an accuracy of 80 to 95%.⁵ The introduction of screening has greatly improved breast cancer survival

rates, especially in reoccurring breast cancer patients. After five years post cancer treatment, patients are considered cancer free.⁶ However, according to the publication by Norgaard Pedersen et al. the risk of breast cancer reoccurrence can range from 13 to 41% between 5 and 20 years, subject to the status of the initial tumour.⁷

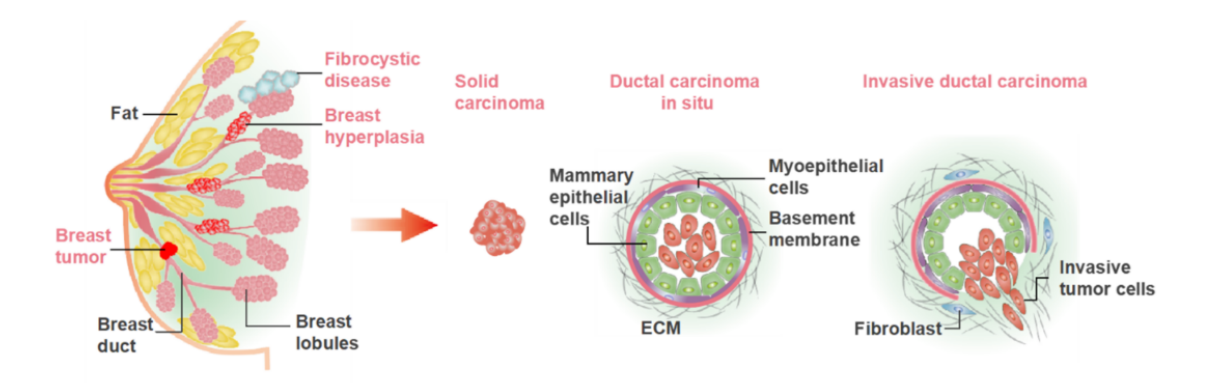


Figure 1. 2. A diagram of the structure of the female breast including the two most common breast diseases, ductal carcinoma in situ and invasive ductal carcinoma. This illustration is extracted from Song et al.⁸

1.2. Classification of Anti-Cancer Drugs

(i) Alkylating Agents

Alkylating agents operate by obtaining an alkyl group (R-CH₂⁺) which interacts with nucleic acids and proteins by inhibiting DNA transcription and replication.⁹ Examples include Cytoxan, Platinol, Neosar, and Platinol-AQ.¹⁰

(ii) Antimicrotubular Agents

Antimicrotubular agents work by inhibiting topoisomerase II, which in turn prevents DNA replication and RNA synthesis, resulting in cell death.⁹ Anthracyclines are a subdivision of anticancer drugs which are extracted from *Streptomyces bacterium* and used to treat a variety of cancers.¹¹ They are used in the treatment of breast, stomach, ovarian, uterine, bladder, lung, leukemia and lymphoma cancers. Anthracyclines are one of the most effective forms of cancer drugs, operating by intercalating with cell DNA which gives rise to DNA metabolism and RNA production impairments.¹² The drugs efficiently target the topoisomerase II cleavage complex (Top2cc), consequently breaking the DNA in proliferating cells.^{12,13} The structure of anthracyclines include an

anthraquinone backbone to a tetracyclic molecule, connected to a sugar group. The structure of anthracycline derivatives has a direct affect to their level of cytotoxicity.¹⁴ Taxanes are another class of anticancer drugs known as diterpenes.¹⁵ They originate from the Taxus brevifolia yew.¹⁵ Taxanes demonstrate their anticancer effects by hindering the mitotic spindle during cell division. They do so by binding to the microtubules, inhibiting the depolymerisation of the microtubules which results in the apoptosis of proliferating cells.¹⁶ Taxanes are used in solid tumours such as lung, breast and ovarian cancers.

(iii) Anti-Metabolites

Antimetabolites function by destroying nucleotides which results in DNA being incapable of replication.¹⁷ Its interactions with nucleic acids can also cause structural deformations which can also lead to cell death.¹⁷ Antimetabolites are subdivided into four categories: Cytidine analogs, folate antagonists, purine analogs and pyrimidine analogs.⁹

(iv) Antibiotics

Antibiotics are used in chemotherapy for inhibiting DNA and DNA synthesis. Examples of these drugs include daunomycin, bleomycin and actinomycin.⁹

 Table 1.1. List of Taxane and Anthracycline Drugs used for Cancer Treatment.

Group	Name	Drug	Water Soluble	Soluble in	Dosage	Usage
Taxane	Taxol	Paclitaxel	0.1 μg/ml	Castor oil, ethanol	175mg/m ² IV	Used following anthracycline and cyclophosphamide therapy, metastatic treatment
	Taxotere	Docetaxel	No	Methanol, acetone, acetonitrile	75mg/m ²	Used following anthracycline treatment, used for advanced or metastatic cancer
	Abraxane	nab- paclitaxel	No	-	-	For metastatic breast cancer patients who have failed first-line treatment for metastatic cancer
Anthra- cycline	Adriamycin	Doxorubicin	Readily	-	60- 75mg/m ²	Metastatic cancer in patients with an increased cardiac risk
	Ellence	Epirubicin	Yes	•	100-120 mg/m ²	Monotherapy
	Mitoxantrone	Novantrone	Readily 2.59 mg/ml	Ethanol, DMSO	14mg/m ²	Metastatic breast cancer

1.3. Conducting Polymers

The first recording of conducting polymers dates back to 1862, where Henry Letheby oxidised aniline, forming a 'thick layer of bluish-green pigment' on the surface of a platinum electrode. Initially, polymers were recognised as insulating materials before the work of Shirakawa, MacDiarmid, and Heeger in 1977. Their work transformed the use of polymers to electrically conducting materials, which resulted in the award of the Nobel Prize in Chemistry in 2000. In recent years, conducting polymers are being used in the fabrication of sensors, photovoltaic cells, energy storage devices, and drug delivery systems (Figure 1.3). 20-24

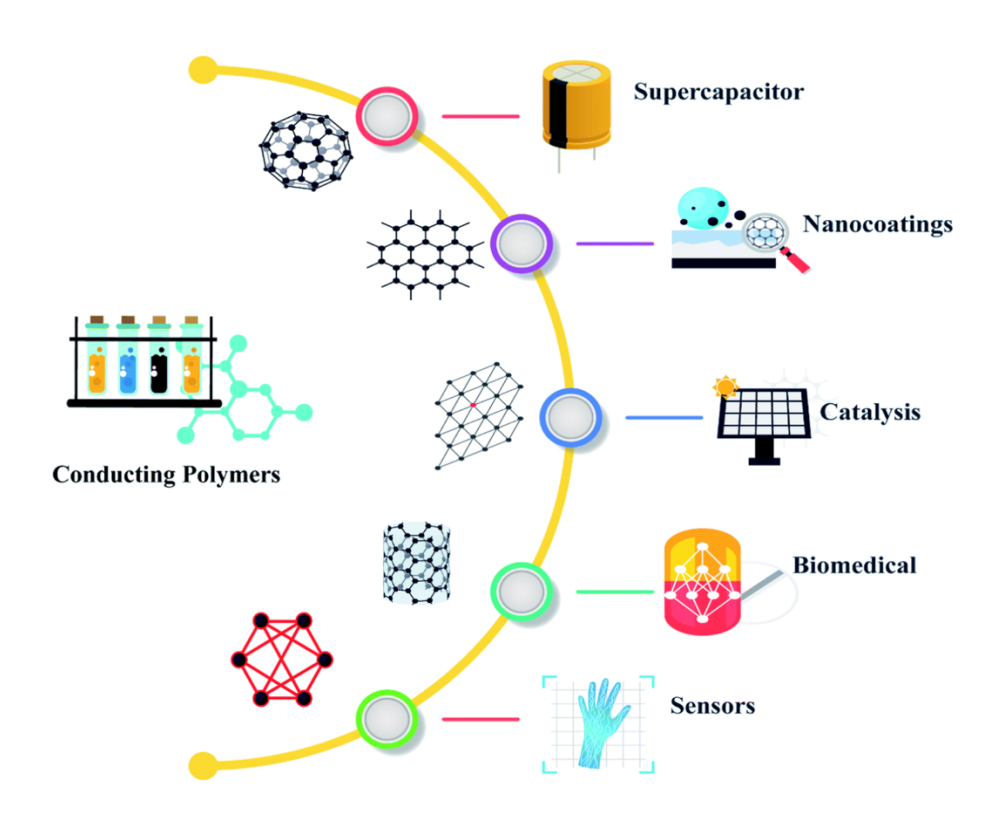
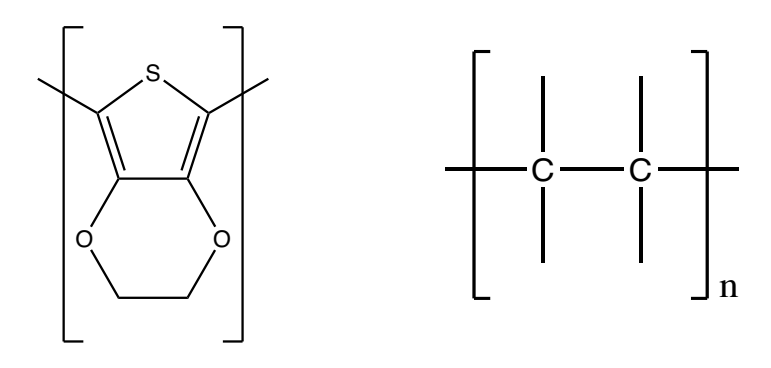


Figure 1. 3. Illustration of the various applications of conducting polymers extracted from Namsheer et al.²¹

Polymers can be categorised as conjugated or saturated. These polymers are composed of different electronic configurations. Saturated polymers were investigated by Ziegler, Natta, Staudinger and Flory and are insulators due to the four carbon valence electrons being used in covalent bonding, such as polyethylene in Figure 1.4 (b).²² For conjugated

polymers there is an unpaired electron, π -electron, for each carbon atom. Carbon orbitals of sp^2p_z configuration, overlap along the backbone of the polymer, resulting in electron delocalisation along the polymer backbone, promoting charge mobility.²² This shows that the electrical conductivity of conducting polymers is dictated by the type and number of atoms in a repeating unit.²² The presence of π -electrons enable the polymer to store or carry charge, resulting in their semi-conductive, metallic like behaviour.²³



Poly(3,4-ethylenedioxythiophene) Conjugated Polymer

Polyethylene Saturated Polymer

Figure 1. 4. Chemical structures of (a) Poly(3,4-ethylenedioxythiophene) (PEDOT) (b) Polyethylene.

1.3.1. Doping

Polymers can increase their levels of conductivity through a process called doping. Doping occurs through the movement of charged species into the polymer backbone.²⁴ Doping can occur in a variety of ways, the most common being electrochemical doping, followed by chemical doping, photodoping and acid-based doping. In chemical doping, charge-transfer redox chemistry is used to (a) oxidise (*p*-type doping) or (b) reduce (*n*-type doping) the polymer.¹⁹ This process is simple to conduct, however, it is difficult to control the reaction. Electrochemical doping operates by providing the conducting polymer with the redox charge via the electrode. The level of doping can be controlled by the potential generated at the electrode. This process causes ions to transfer in or out of the polymer film from the electrolyte in order to compensate charge.²² Additionally, the type of dopant can alter film properties such as homogeneity, porosity and volume. In

addition, these processes are reversible allowing the polymer to return back to its neutral form via reduction or oxidation depending on its doping type.

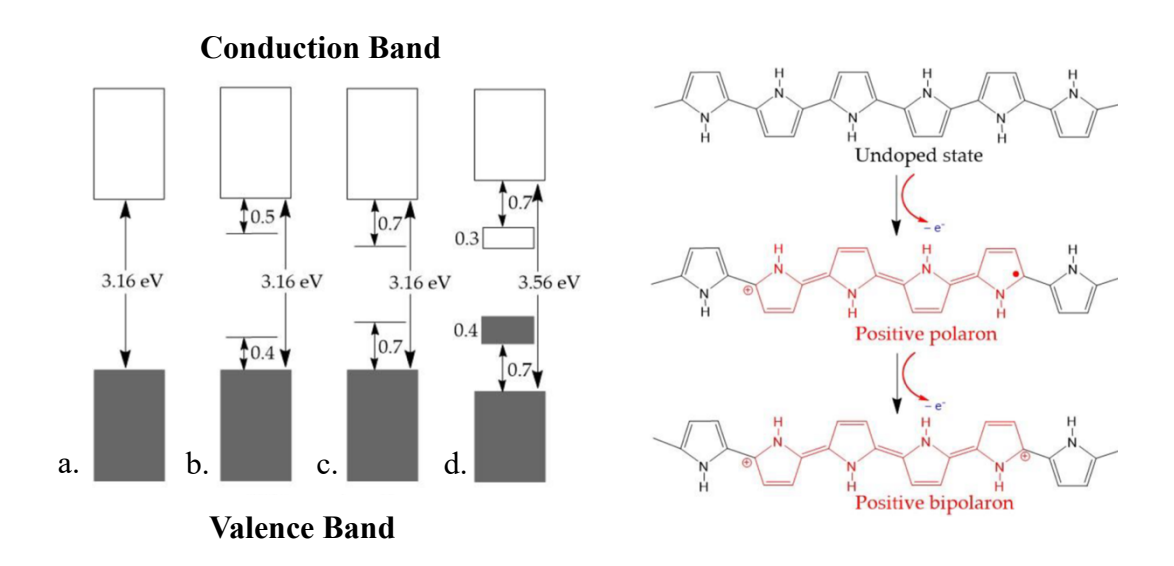


Figure 1. 5. Graphical representation of electronic band gap and oxidation process of polypyrrole extracted from Le et al.²⁵

Figure 1.5 provides a graphical representation of p-type doping in pyrrole from Le et al. The oxidation and reduction processes results in the creation of charge carriers known as polarons which are radical ions and bipolarons which are dications or dianions. These charge carriers result in the movement of electrons along the polymer chain, resulting in conductivity. In Figure 1.5 (a), polypyrrole is in its undoped form, which is shown by the large band gap of 3.16 eV. Oxidation of polypyrrole causes a π -electron to be removed from the polymer backbone, causing the benzenoid structure to change to a quinoid structure, with the formation of a polaron. The outcome is two localised electronic levels in the band gap (Figure 1.5 (b)). Further oxidation results in the removal of a second electron forming a double charged bipolaron. As oxidation continues, bipolarons overlap resulting in a decrease in band gap energy as a result of the bipolaronic bands (Figure 1.5 (d)). 25,26

1.3.2. Electrical Characteristics

Indeed, the conductivity of the conducting polymer is essential in determining the application. In conjugated polymers, π -electrons have a considerable role to partake, determining the conductivity of the system as a result of polarisation and delocalisation.²⁵ As described in Section 1.3.1, polymer doping assists in the generation of a semiconducting, metallic like state. The doping process reduces the morphological and structural disorder of the polymer, enhancing conductivity. PEDOT has shown conductivity levels of 0.1 S/cm in the undoped state, to 5400 S/cm in the doped state.^{28,29}

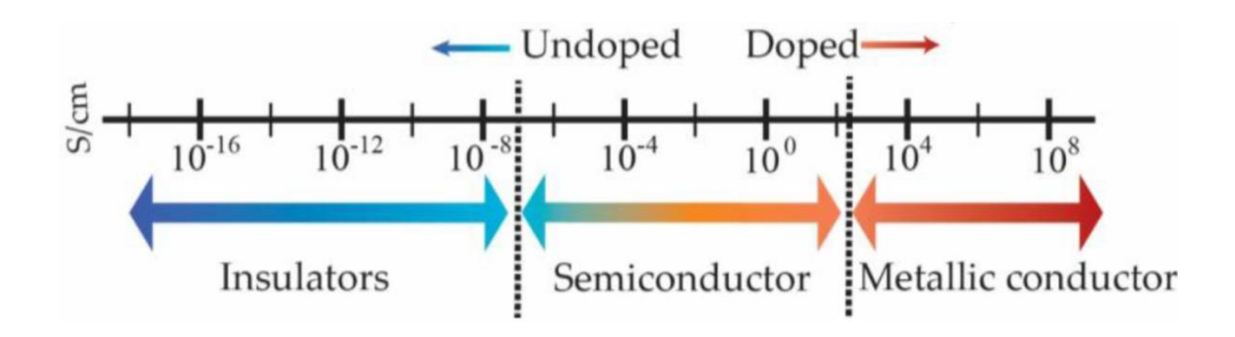


Figure 1. 6. Schematic of the conductivity levels of doped and undoped conjugated polymers. Extracted from Le et al.²⁵

1.3.3. Poly(3,4-ethylenedioxythiophene)

PEDOT is the conducting polymer used throughout this project. It is renowned for its conductivity, flexibility and stability, making it ideal for use in sensors, photovoltaic cells, and drug delivery systems. PEDOT is derived from the conducting polymer polythiophene, having an additional dioxane group.

(a)
$$\stackrel{\bullet}{\longrightarrow} \left[\stackrel{\bullet}{\longrightarrow} \right] \left[\stackrel{\bullet}{\longrightarrow} \right] \xrightarrow{-2H^{+}} \left[\stackrel{\bullet}{\longrightarrow} \right] \xrightarrow{-$$

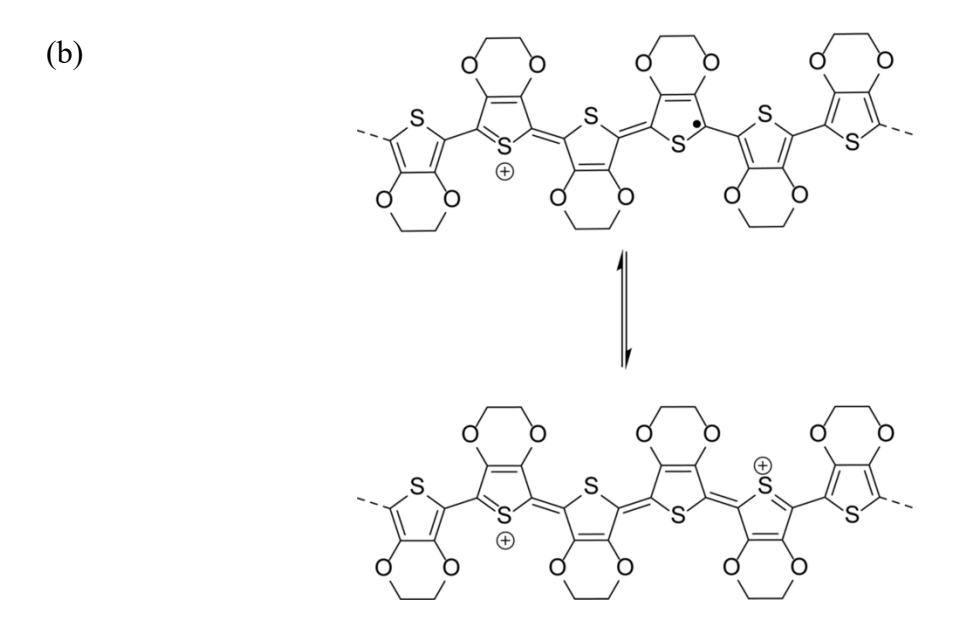


Figure 1. 7. (a) Possible mechanism for the electropolymerisation of EDOT. Extracted from Ramalingam et al. ³⁰ (b) Oxidation and doping processes of PEDOT. Extracted from Cameron et al.³¹

PEDOT is commonly electrochemically polymerised by applying a constant potential to the electrode surface. Upon oxidation, an electron is removed, leading to the formation of a cation radical (Figure 1.7 (a)). ³² Cation radicals can undergo radical-radical coupling or they can interact with neutral monomers, dimers and oligomers, resulting in the formation of the polymer chain. ¹⁸ During the oxidation process, anions from the solution enter the polymer chain to achieve charge neutrality (doping)(Figure 1.7 (b)). ³² Similarly to the mechanism described for polypyrrole in Section 1.3.1, polarons and bipolarons are responsible for the electrical conductivity. Examples of PEDOT being used in drug delivery systems can be seen in work performed by Krukiewicz et al. ^{33,34} In this work the inflammatory drug Naproxen is used as the dopant in the PEDOT film. Krukiewicz et al., uses chronoamperometry to apply a set potential, allowing the drug to be doped and dedoped depending on the positive or negative potential used. This work is promising in the use of polymers for targeted and controlled drug delivery.

1.4. Drug Delivery

1.4.1. Conventional Drug Delivery System Classification

Drug delivery systems (DDS) aim to control the release of Active Pharmaceutical Ingredients (APIs) in a targeted manner. Currently drug delivery includes the use of tablets, syrups, capsules and many more, as shown in Figure 1.8.35 These systems lack target specificity, drug bioavailability and are incapable of maintaining a constant release rate.35 Controlled drug delivery systems are being implemented to eliminate the issues with conventional drug delivery. It does so by delivering the drug at a specific rate to a target site, optimising the drug's ability and preventing toxicity.35 This section will investigate the use of nanomaterials as drug delivery systems and their ability to target specific sites.



Figure 1. 8. Classification of conventional drug delivery systems. Extracted from Adpeu et al.³⁵

1.4.2. Pharmacokinetics of Drug Delivery Systems

Pharmacokinetics is the study and understanding of the movement of a drug through the body, how it is absorbed, distributed, metabolised, and excreted. The success of drug delivery systems are reliant on the behaviour of the carrier within the body.³⁶ This section emphasises the importance of specific DDS functions to achieve optimal therapeutic effect.

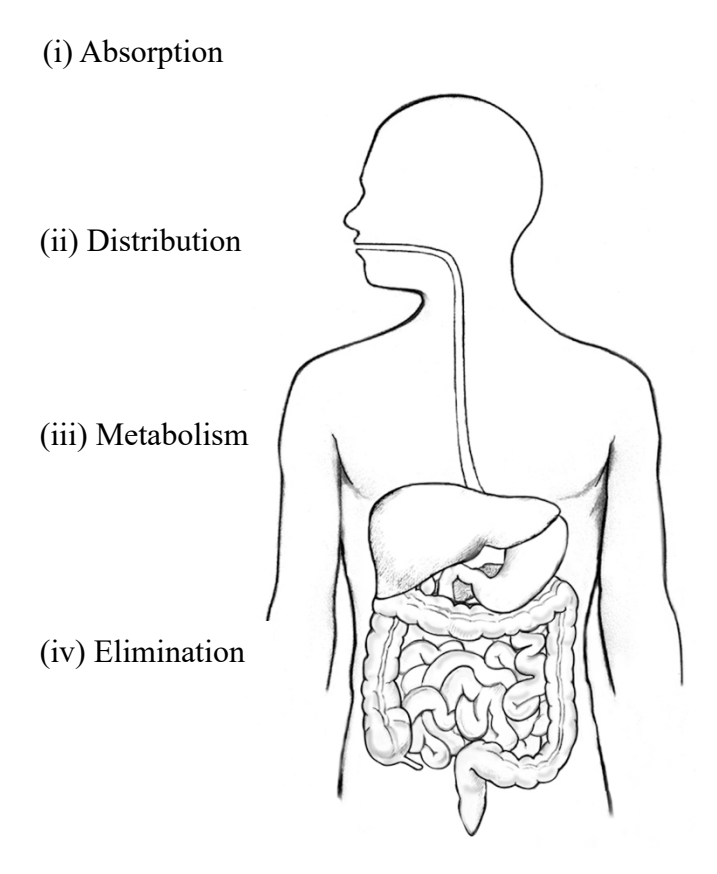


Figure 1. 9. Adapted from the National Institute of Diabetes, Digestive and Kidney Diseases, National Institutes of Health.³⁷

(i) Absorption

Drug absorption is the migration of the drug into the bloodstream after administration. The rate and quantity of the absorption of a drug is reliant on the administration method, drug formulation and the physicochemical characteristics of the drug.^{35,38} Bioavailability refers to the quantity of drug that reaches the target site. Oral doses tend to have substandard bioavailability as a result of poor absorption and drug metabolism in the

liver.³⁵ Intravenous drug administration presents full bioavailability as it is administered directly into the bloodstream.³⁵

- (a) Passive transport is the migration of a drug through the cell membrane. The movement occurs from high drug concentration to low drug concentration. Example: From the gastrointestinal tract to the bloodstream.³⁵ This process does not require energy.
- (b) Active transport involves the transportation of molecules, using energy, withstanding a concentration gradient which takes place in the small intestine.³⁸

(ii) Distribution

Distribution refers to the reversible transfer of drug molecules into the blood and tissues. This is a crucial role as it determines the efficacy of the treatment while also dictating toxicity.³⁶ The circulation of the drugs are dependent on the blood flow, the size of the drug molecules, the drug's binding affinity with plasma proteins, as well as lipophilicity.³⁵ There are also anatomical barriers such as the blood-brain barrier which inhibits the movement of certain drugs into the brain tissue. Only low molecular weight, small size and high lipophilicity drugs can move through the blood-brain barrier.³⁹

(iii) Metabolism

Drugs are metabolised in the liver and the wall of the gut. This process reduces the concentration of the drug, especially oral administered drugs, before moving into the blood.⁴⁰ The liver enzyme cytochrome P450 is responsible for the metabolism of approximately 70 to 80% of drug molecules.³⁶

(iv) Elimination

Elimination involves the excretion of any drug that is unchanged from the body.⁴¹ The predominant methods of elimination include the liver, lungs, bone marrow and spleen. The phagocytic cells present in these tissues remove foreign bodies from circulating.³⁶ Other forms of excretion include bile, sweat, urine, saliva, and stool.³⁸

1.4.3. Polymers in Drug Delivery Systems

Nanomedicine has been used to revolutionise how patients can and will be treated in the future. The use of nanocarriers as drug delivery devices is becoming increasingly sophisticated, using their size, solubility, and high specificity to create an innovative drug release profile.⁴² Polymeric nanoparticles are of particular interest due to their adaptable characteristics, allowing some polymeric nanoparticles to possess biocompatible and biodegradable properties as well as having the ability to be modified for personalised therapy. Polymeric nanocarriers are ideal carriers of multiple cytotoxic compounds, providing long circulation half-lives, reducing drug toxicity, and improving drug efficacy. These nanoparticles have the potential to be adapted with ligands such as proteins and antibodies which enhances target selectivity. Nanocarriers also exhibit superior permeability and retention (EPR effect) as a result of their accumulation within cancer cells.⁴² Another advantage of using nanocarriers as drug delivery systems, is the drug encapsulation mechanism. Drug encapsulation in nanocarriers improves transport within the body, substantially enhancing biodistribution as well as decreasing biodegradation.⁴³ Additionally, these nanocarriers present an improved circulation half-life of the therapeutics, therefore promoting drug efficacy resulting in lower dosages.^{44,43} The polymeric nanoparticle drug release is more efficient, producing minimal side effects in comparison to traditional chemotherapy.⁴⁵

The objective of drug delivery systems is to transfer a therapeutic agent to a specific target site and to release the drug. In recent times, these schemes have become more advanced, focusing on preserving the efficacy of the drug, specifically targeting the malignant cells and controlling the release of the drug.⁴⁶ The variety of combinations allows for a vast range of possibilities for personalising the delivery methods. These treatments are specifically targeted and designed to obstruct biological pathways and cancer proteins contributing to tumour progression.⁴⁷ Biocompatibility, biodegradability, and stability are vital components necessary for the assembly of an effective drug delivery system. Recently, polymers such as polyglycolic acid (PGA), polyethylene glycol (PEG), polylactic acid (PLA), and polylactic-*co*-glycolic acid (PLGA) demonstrate good biocompatible and biodegradable characteristics.⁴⁸ In 2018, as stated by Ferrari et al, there were four polymer based drug formulations on the market which are stated in Table 1.2.⁴⁹

Table 1.2. Polymeric nanoparticle formulations that are currently on the market. Adapted from Ferrari et al.⁴⁹

Name	Company	Polymer	Drug	Indication	Approval	Ref
Genexol-	Samyang	PEG-poly(d,l-lactide)	Paclitaxel	Breast Cancer	2007 South	50, 51
PM	Pharmaceuticals			NSCLC	Korea	
Transdrug	BioAlliance Pharma	Poly(isohexylcyanoacry late)	Doxorubicin	Hepatocarcinoma	2005 USA	52, 53
Zinostatin	Astellas	Poly(styrene-co-maleic	Neocarzinosta	Hepatocellular	1994 Japan	54, 55
stimalamer	Pharma, Inc.	acid)	tin	Carcinoma		
Paclical	Osmia	Poly(glutamic acid)	Paclitaxel	Ovarian Cancer	2015	56, 57
	Pharmaceutical				Russian	
					Federation	

Natural polymers such as alginate, hyaluronic acid, chitosan and cellulose have acquired more attraction for their biocompatible and biodegradable properties. He also renowned for their antibacterial aspects as well as their low immunogenicity. Nonetheless, synthetic polymers are proven to be more diverse, having the ability to adjust the polymer's morphology to cater to the patients' needs. Using nanoparticle drug delivery has the potential to overwrite current treatments being used. In traditional treatments, the drug only has the ability to act outside the cell as the cell membrane prevents admission to the cell. Therefore, the drug's activity is not long lasting, leading to regular higher concentrations of the drug. In terms of bacterial infections, another advantage to the nanosized drug delivery systems is the inability of resistant bacteria to form due to the drugs nanostructure, which in turn increases the longevity of the drug. Castro et al. discusses the possibilities for these polymeric nanoparticles, having the ability to be modified for specific stimulus-responsive activity for drug delivery in normal and extreme environments, e.g. temperature and pH.

1.4.4. Conducting Polymers in Drug Delivery Systems

Conducting polymers have been investigated for their electrical properties for their application in a multiple of disciplines, including drug delivery.⁵⁸ Poly(3,4-ethylenedioxythiophene) (PEDOT), polypyrrole (PPy), polyaniline (PANI) and polythiophene (PT), are some of the most researched conducting polymers in the field of 'smart biomaterials'.⁵⁸ The first developed controlled drug delivery system was reported in the 1980s by Miller et al., using cyclic voltammetry to release dopamine, glutamate

and ferrocyanide with PPy.^{59,60} The doping and de-doping characteristics of conducting polymers allows for materials, referred to as 'dopants' to enter and leave the polymer upon the application of a specific potential. The dopant moves in and out of the film by ion exchange processes as explained in Section 1.3.1. For example, a polymer exhibiting p-type doping will encourage the incorporation of a negatively charged drug upon oxidation (Figure 1.7 (b)). An interesting observation is that therapeutics are commonly being incorporated after the polymer formation, with the removal of the primary doping agent first, followed by the incorporation of the drug. 61,62 Previously, polymers such as polypyrrole were investigated as potential drug delivery systems, possibly due to the extensive level of research; however, compared to newer synthetic polymers, polypyrrole can lack in biocompatibility, exhibiting cytotoxicity at high concentrations.^{63,64} Some examples of PPy based DDSs include electrochemically triggered release of dexamethasone, naproxen, and nerve growth factor. 65-66 Another commonly used polymer with potential in drug delivery systems is PEDOT. PEDOT has shown biocompatibility, being used in applications for medical devices; however, the degradability of this material within the body is not extensively researched. ^{67,68,69}

1.5. Wireless Electrochemistry

Bipolar electrochemistry is being investigated as a contactless method by converting the conventional electrostimulation system to a wireless process called bipolar electrostimulation (BPES).⁷⁰ This system has been known for years with Fleischmann et al. recording the 'electrical conduction of spherical particles fluidised by electrolyte flow' in the late 1960s.⁷¹ BPES operates by depositing an electrical conducting bipolar electrode in an electric field. The electric field is a result of driving electrodes, also referred to as feeder electrodes, which have no direct contact to the bipolar electrode.^{70,72,73} These wireless bipolar electrodes undergo anodic and cathodic reactions.

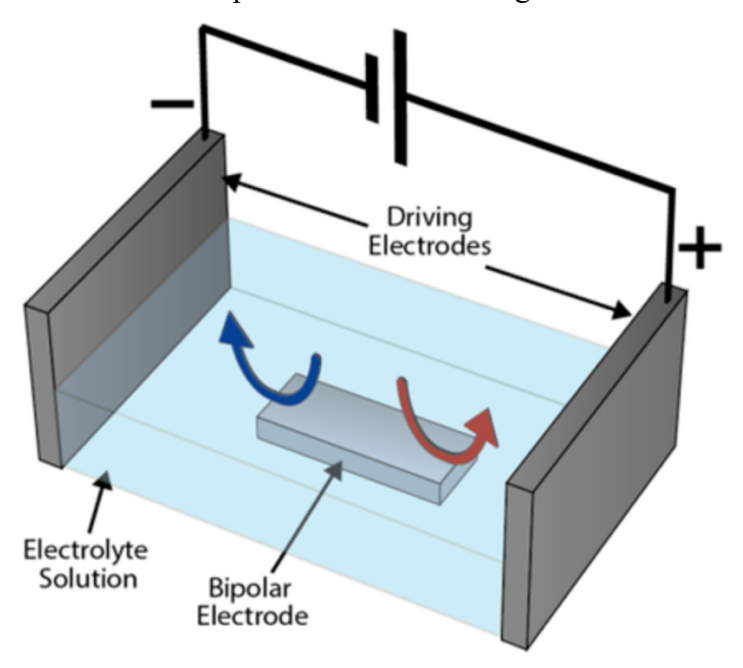


Figure 1. 10. Schematic of bipolar electrolysis extracted from Crooks.⁷⁴

Figure 1.10 shows a standard set up for a bipolar electrostimulation system. The setup includes two driving electrodes which are connected to power. The bipolar electrode is located between the driving electrodes without any electrical connection. The bipolar electrode (BPE) is operated by the electric field generated from the driving electrodes. Therefore, the BPE acts as its own electrochemical cell, undergoing oxidation and reduction reactions at either poles.⁷⁵ In electrostatic field theory, the surrounding electrolyte causes a potential gradient between the electrode and the electrolyte. An important aspect to consider is the concentration of the electrolyte solution. In BP

systems, if the solution conductivity is high, the double layer of the BPE will be thick, resulting in a dissipation of the electric field near the feeder electrodes.⁷⁵

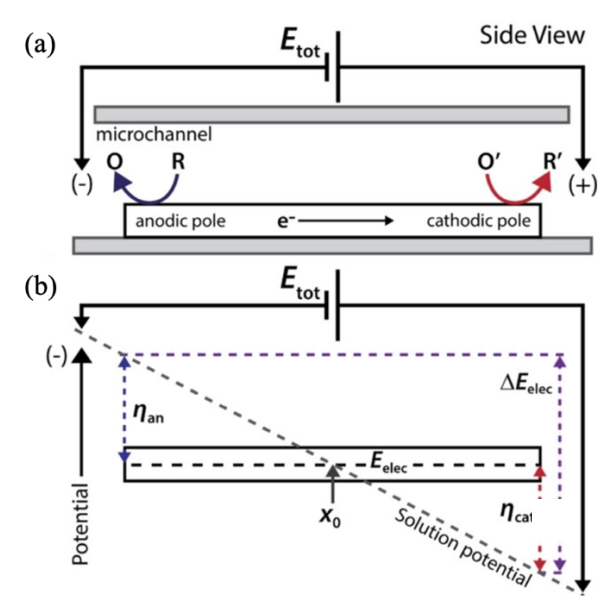


Figure 1. 11. Schematic of a bipolar electrochemical system, side view. (a) Typical bipolar setup including the BPE in the centre of the cell located between two feeder electrodes. (b) Linear potential decay model that occurs across the BPE. Extracted from Crooks.⁷⁴

 E_{tot} refers to the voltage being applied to the driving electrodes causing the electric field. As a result of the electric field, the bipolar electrode settles at an equilibrium potential, also known as ΔE_{elec} (Eqt. 1.1). This potential is dependent on the electrolyte solution and the BPE location in the electric field.⁷⁴ There are variations in the interfacial potential between the solution and the BPE because of the electric field. In Figure 1.11 (b), Crooks explains that the applied potential and length of the bipolar electrode are the two variables that alter the magnitude of the overpotentials. X_0 is defined as the point of the BPE at which the overpotential is zero.⁷⁴ The quantity of voltage experienced by the BPE is noted as ΔE_{elec} , and can be calculated by the following equation (Eqt. 1.1).^{76,77}

$$\Delta E_{elec} = E_{tot} \left(\frac{l_{elec}}{l_{channel}} \right)$$
 Eqt. 1.1

Where $l_{channel}$ is the distance between the driving electrodes, l_{elec} is the BPE length, E_{tot} is the total applied voltage by the power supply, and ΔE_{elec} is the change in voltage experienced across the BPE.

Bipolar electrochemical setups can occur in two difference forms, open and closed systems. Open Bipolar Electrochemical System: An open BPE system in when current flows through the electrolyte and the bipolar electrode. Closed Bipolar Electrochemical System: A closed BPE system consists of two isolated solutions, one containing the anode and the other containing the cathode. The movement of current between the two solutions is caused by the bipolar electrode.

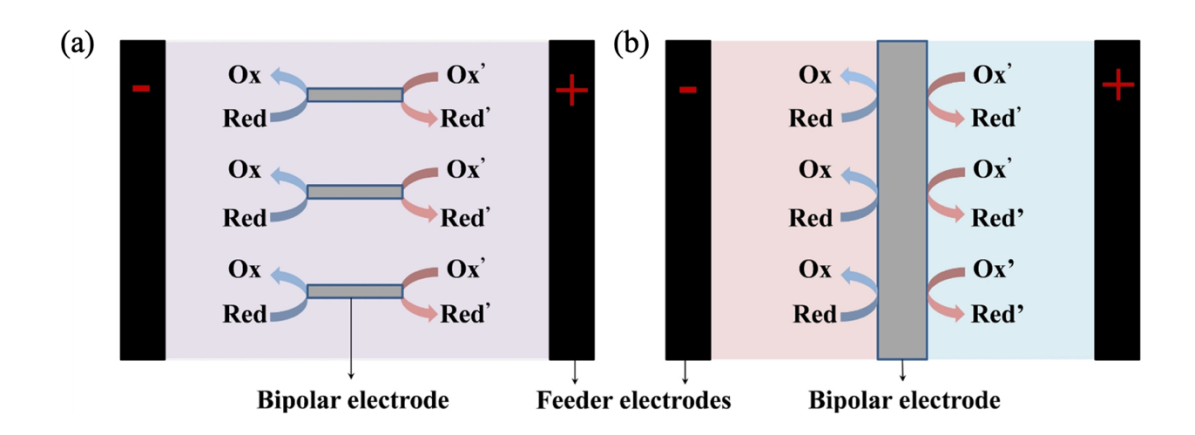


Figure 1. 12. Schematic of an (a) open and (b) closed bipolar electrochemical system extracted from Wang et al.⁷⁸

1.5.1. Conducting Polymers in Bipolar systems

Conducting polymers are appealing materials as a result of their high conductivity, flexibility, and stability. These materials have the ability to be altered in terms of redox potential, conductivity and surface charge.⁷⁵ When used in conjunction with bipolar electrochemistry, conducting polymers can be used in applications such as electroceuticals for the treatment of disease and drug delivery.^{70,79} Advantages of conducting polymers include their low toxicity levels depending on dopant and chain

length. Their surface roughness can also play a significant role in cell adhesion, as rough surfaces promote cell adhesion while smoother surfaces may result in a reduction in cell adhesion.⁷⁵

Traditional drug administration is impactful for illnesses requiring an immediate dosage of drugs (eg. asthma attack, sudden injury). However, for more chronic long-term diseases such as diabetes and cancers, controlled, targeted and long lasting release systems are highly desireable. Since conducting polymers undergo voltage dependant oxidation and reduction reactions, these materials have the ability to be doped with active pharmaceutical ingredients (APIs) and in turn release these materials in the presence of an applied electric field. Conducting polymers have also been used in the electrostimulation of cells. Electrostimulation can affect the differentiation and proliferation of living cells which has potential for clinical applications such as nerve cell stimulation for injury repair. The use of wireless systems provides the benefits of conventional electrochemistry without the need for physically wired connections.

1.6. Techniques

1.6.1. Introduction to Electrochemistry

Electrochemistry is a domain of chemistry that focuses on the correlation of electrical and chemical effects.⁸³ It concentrates on chemical effects caused by the passing of an electrical current and the formation of electrical energy as a result of chemical processes.⁸³ The Nernst equation is the fundamental equation of electrochemistry. This equation is used to combine information between the concentrations of analytes and electrode potential. The equation was formulated by German chemist, Walther Nernst and is as follows (Eqt. 1.2):^{83,84}

$$E = E^0 - \frac{RT}{nF} lnQ$$
 Eqt. 1.2

Where E is the cell potential (V), E^0 is the standard cell potential (V), R is the gas constant (J/mol.K), T is temperature (K), n is number of electrons transferred, F is Faraday's constant (C/mol), and Q is the reaction quotient.

1.6.2. Electrochemical Setup

A three-electrode set up is common for electrochemical experiments such as cyclic voltammetry, chronocoulometry and chronoamperometry. It consists of a working electrode, reference electrode and counter electrode. A three-electrode setup is necessary to measure and control reactions at the electrode interface.

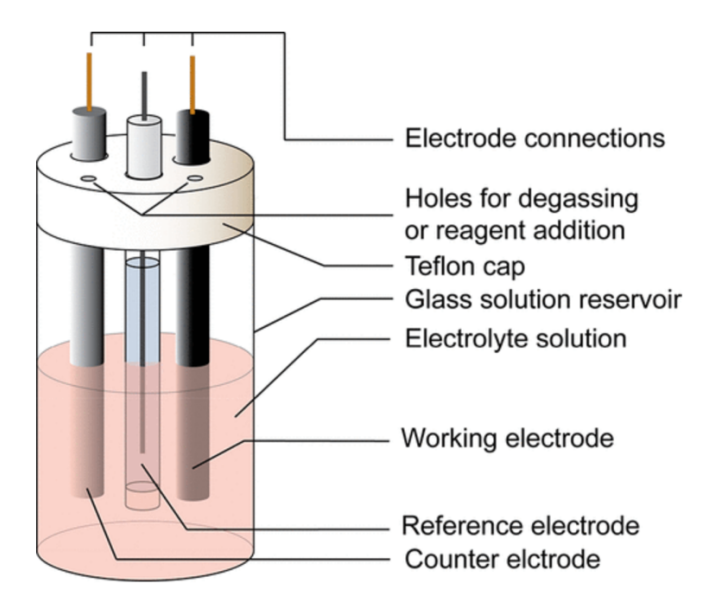


Figure 1. 13. Schematic of a three-electrode electrochemical cell. Extracted from Elgrishi et al.⁸⁴

(i) Working Electrode

The working electrode is the location at which the electrochemical reaction occurs. It is essential that the electrode material is electrochemically inert. The potential of the working electrode is controlled by the potentiostat throughout the experiements.⁸⁴ The working electrode can be comprised of materials such as gold, glassy carbon, and platinum.

(ii) Reference Electrode

The reference electrode possess a stable potential from which the working electrode potential is measured.⁸⁴ If the electrochemical cell did not have a reference electrode the potential at the working electrode would fluctuate causing inaccurate and unreproducible measurements. A commonly used reference electrode is a saturated silver silver chloride electrode (Ag/AgCl).⁸³

(iii) Counter Electrode

Current flows between the working and counter electrodes.⁸⁴ It is also made of an inert material and is typically two and a half times the surface area of the working electrode to ensure that the reaction at the counter electrode does not inhibit the reaction at the working electrode. While oxidation occurs at the working electrode, reduction occurs at the counter electrode. The counter electrode assures that the potential of the working electrode does not shift due to polarisation effects. Polarisation can occur when reaction kinetics effects the potential of the working electrode.⁸⁵

1.6.3. Cyclic Voltammetry

Cyclic voltammetry (CV) is a common electrochemical technique that is used to monitor the oxidation reduction reaction of a species in solution. It involves the application of a voltage sweep across the electrochemical cell, resulting in a current response. ⁸⁶ This technique offers data on the redox potential of species and electron transfer kinetics. In this thesis, CV is used to electropolymerise EDOT and to understand doping and dedoping processes.

$$Fe(CN)_6^{3-} + e^- \rightleftharpoons Fe(CN)_6^{4-}$$

Consider the standard redox probe ferricyanide. When ferricyanide is scanned cathodically the species becomes reduced, resulting in formation of the ferrocyanide ion due to the gain of an electron. When reduction occurs and the film is scanned negatively, the quantity of the ferricyanide ion at the electrode surface depletes. He reduction product, ferrocyanide, continues to increase at the electrode surface, known as the diffusion layer. This results in a growing cathodic peak current (i_{pc}). As reduction continues, the cathodic peak current begins to decrease due to the effects of mass transport from the bulk electrolyte solution. Furthermore, when the scan is reversed and oxidation occurs, the ferrocyanide ion is oxidised to form ferricyanide. Similarly, as the potential is swept more positively, more ferricyanide ions are available in the diffusion layer, thus a current increase is observed (i_{pa}). Electron transfers can be reversible, quasi-reversible or irreversible. For ideally reversible systems, the peak-to-peak potential (ΔE_p), is 57 mV. The scanned reduced in the diffusion of the ferrocyanide ion is oxidised to form ferricyanide.

(i) Scan Rate

Scan rate plays a vital role in the speed at which the potential is scanned. When the potential is scanned at lower scan rates, a reduced peak current will be observed due to an increased size in the diffusion layer at the electrode solution interface. Conversely, as potential is swept at higher scan rates, higher peak currents will be observed due to the decreased diffusion layer.⁸³ The Randles-Sevcik equation can be used to describe the proportional relationship between square root scan rate and peak current (Eqt. 1.3).^{83,88} It is important to note that the Randles-Sevcik equation is only applicable in reversible systems.

$$i_p = 0.446 nFAC^0 \left(\frac{nFvD_o}{RT}\right)^{1/2}$$
 Eqt. 1.3

Where ip is the peak current (A), n is the number of electrons transferred, F is Faraday's constant, A is the electrode surface area (cm²), C^0 is the bulk analyte concentration (mol/cm³), v is the scan rate (V/s), D_o is the diffusion coefficient (cm²/s), R is the gas constant and T is temperature (K).⁸⁴

(ii) Electrolyte Solution

The electrolyte solution should be of sufficient concentration to ensure solution conductivity. It should be electrochemically inert within the parameters of the experimentation.⁸⁴ Within the bulk solution, three mass transportations can take place; diffusion, migration and convection. Diffusion involves the movement of the analyte due to a concentration gradient. Migration is the movement of charged particles through an electric field and is prevented by using high concentration electrolytes. Convection is due to mechanical forces such as stirring.⁸³ Ideally, migration and convection should be prevented to reduce mass transport.

1.6.4. Electrochemical Quartz Crystal Microbalance

Electrochemical Quartz Crystal Microbalance (EQCM) is a technique which is used to record mass changes that occur as a result of reactions at the working electrode. 89 Such reactions taking place may include ion exchange processes or polymer film deposition.

EQCM operates by using a quartz crystal oscillator which acts as a working electrode.⁸⁹ The setup is a conventional three electrode set up.⁹⁰ Measurements are obtained through changes to the crystal's resonant frequency which can then be related to mass by the Sauerbrey equation (Eqt. 1.4):⁹¹

$$\Delta f = \frac{-2f_0^2}{A(\mu\rho)^{1/2}} \Delta m$$
 Eqt. 1.4

Where Δf is the change in frequency, f_0 is the resonant frequency of the fundamental mode of the crystal, A is the area of the Au disk on the crystal (0.196 cm²), μ is the shear modulus of quartz (2.947 x 10^{11} g/cm s²), ρ is the density of quartz (2.684 g/cm³) and Δm is the change in mass.

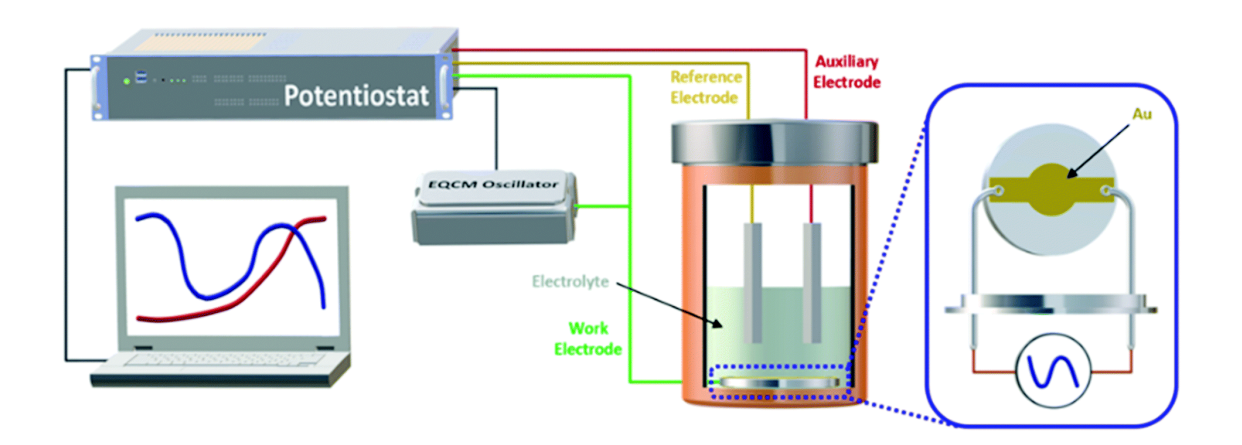


Figure 1. 14. Schematic of an EQCM set up. Extracted from Ji et al. 92

The Sauerbrey equation is used in Chapter 2 and Chapter 3 to investigate electropolymerisation and doping/de-doping procedures. It is important to note that there are some limitations to the Sauerbrey equation such as the (1) thin, rigid film assumption (2) film homogeneity and (3) viscoelastic effects.⁹²

1.6.5. Ultraviolet-Visible Spectroscopy

UV-Vis spectroscopy is a technique capable of performing both quantitative and qualitative analysis through the absorption, reflection, or transmission of UV and visible light by molecules. ⁹³ The ultra-violet wavelength ranges between 200 – 400 nm while the

visible region is between 400-700 nm. When molecules absorb the light, they ensure electronic transitions which involves the movement of electrons from ground states to excited states.⁹⁴ UV-Vis spectroscopy is used in Chapter 4 to understand the electronic states of the bipolar polymerised PEDOT film. The Beer-Lambert law can also be used to correlate peak absorption with concentration (Eqt. 1.5):⁹⁵

$$A = \varepsilon bc$$
 Eqt. 1.5

Where A is the absorbance, ε is the molar absorption (L.mol⁻¹.cm⁻¹), b is the path length and c is the concentration of the material absorbing.

1.6.6. Scanning Electron Microscopy

Scanning Electron Microscopy (SEM) involves the emission of electrons from a lanthanum hexaboride or tungsten cathode which are then accelerated by the anode toward the specimen surface.⁹⁸ This technique provides information about the morphology of a specimen. Tungsten is mainly used as the electron gun because of its low vapour pressure and high melting point. 96 The electron beam is deflected by spinning coils of the objective lens, covering the sample surface area. 96 The electron beam can have energy of 100 to 50000 eV which is condensed to a focal spot of 1 to 5 nm. 96 The presence of a high vacuum setting prevents electrons being absorbed by air or being scattered.⁹⁷ SEM is a superior optical technique because of its high resolution. SEM resolution is greater than that of light microscopes due to electron wavelengths being approximately one hundred thousand time smaller than that of light. In this thesis, SEM is used to investigate the surface morphologies of different conducting polymer films and how doping ions can affect the structure of the polymer film. Secondary electrons arise from the specimen surface, making them important for investigating the surface morphology. They are low energy electrons, possessing energies of <50 eV and resolutions of approximately 100 Å.99 Back scattered electrons are derived from reemitted electrons from the samples as a result of elastic scattering by atoms. 99 These are high energy electrons with resolutions of approximately 500 Å being achieved.⁹⁹

1.6.7. Chronoamperometry

Chronoamperometry is a potentiostatic technique by which the potential of the working electrode is maintained at a constant voltage while current is recorded as a function of time.⁸³ In this technique the working electrode experiences a square-wave potential.¹⁰⁰ Chronoamperometry involves a potential step from a potential where no reaction is occurring to a potential where an electrode reaction is taking place.¹⁰¹ The current obtained corresponds to the diffusion of an analyte toward the surface of the electrode.¹⁰⁰ Double-step chronoamperometry involves a second step where the electrode reaction is reversed. This method is used for complex electrode reactions where the initial step results in a product, then the reversal allows for the first product to be examined.⁸³ Chronoamperometry was used in the one step waveform in Chapter 3 to apply a specific potential during doping and de-doping procedures.

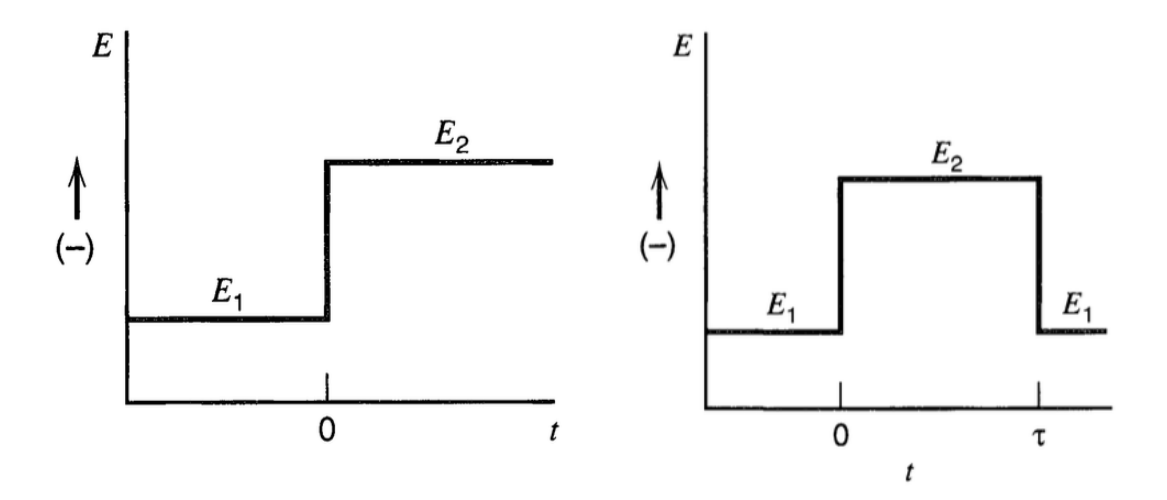


Figure 1. 15. (a) one step chronoamperometric waveform where analyte O is not electroactive at E_1 and is reduced at E_2 (b) two step chronoamperometric waveform where analyte O is not electroactive at E_1 and is reduced at E_2 . From time 0 to τ , the reduced product builds up near the electrode surface. After τ , the oxidised species is available at the electrode due to the change in potential to E_1 . Extracted from Bard and Faulkner.⁸³

The Cottrell equation describes the relationship between current and time in a potential controlled experiment. It considers the effects of diffusion and depletion and is described as (Eqt. 1.6):⁸³

$$i = \frac{nFAC_0\sqrt{D}}{\sqrt{\pi t}}$$
 Eqt. 1.6

Where *i* is current (A), *n* is the number of electrons transferred, *F* is Faradays constant (C/mol), *A* is the electrode area (cm²), C_{θ} is the analyte concentration (mol/cm³), *D* is the diffusion coefficient (cm²/s) and *t* is time (s).

1.6.8. Chronocoulometry

Chronocoulometry is a similar technique to chronoamperometry however in this case the current is converted to charge which is recorded as a function of time. ¹⁰¹ Charge versus time is obtained by the integral of current versus time. ⁸³ Chronocoulometry can also be performed in a one-step or two-step process as shown in Figure 1.17. In this work, chronocoulometry was used in Chapter 2 and Chapter 3 to electropolymerise EDOT. Comparable polymer films could be formed as the polymerisation is based on charge.

1.6.9. Chronopotentiometry

Chronopotentiometry is a technique which involves the application of constant current resulting in a potential change. The potential change is caused by the electroactive species, ensuring that the supply is sufficient for the applied current.¹⁰² As time passes, the influx of electroactive material at the electrode surface is incapable of maintaining the current, causing potential changes due to other species such as electrolyte or solvent.¹⁰² Chronopotentiometry was as another form of electropolymerisation (Chapter 4) where a specific current was applied to the system and a voltage response was obtained.

1.6.10. Electrochemical Impedance Spectroscopy

Electrochemical Impedance Spectroscopy (EIS) is a technique used to provide information on the electrochemical properties of systems. This technique is used in the study of batteries, capacitors, fuel cells and energy storage devices. ^{103,104} Impedance is performed by applying a sinusoidal signal (AC voltage or current) over specific frequencies. ¹⁰⁵ These frequencies can range between millihertz to megahertz. It is a complex quantity and is typically represented in a Nyquist plot with real (Z) and imaginary (Z") axis.

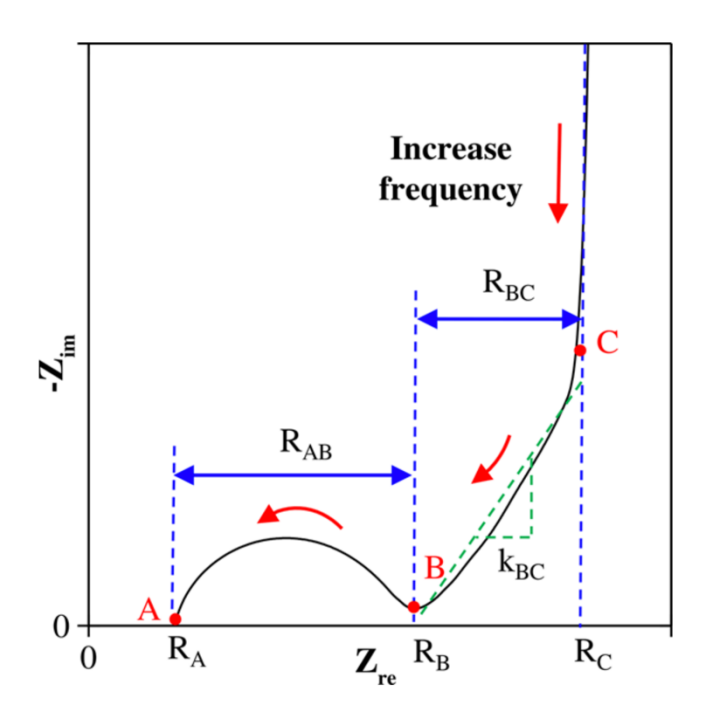


Figure 1. 16. Schematic of a Nyquist plot extracted from Mei et al. 103

Point 0 to R_A displayed in Figure 1.18 is related to the resistance of the bulk electrolyte solution, known as solution resistance, and the equivalent series resistance (ESR) which is an accumulation of electrolyte, electrode and contact resistance (between electrode and current collector). The semi-circle from point R_A to R_B is referred to as charge transfer resistance. Charge transfer resistance is the resistance caused by the movement of ions across the electrode-electrolyte interface and settling in the electrodes. 107,108 R_{BC} consists of a non-vertical line and is a result of ion transport limitations in the bulk electrolyte, or from the electrolyte to the electrode surface. 104 The vertical lines observed at point R_C is due to the capacitive nature of the double layer at the electrode-electrolyte

interface.¹⁰³ In this thesis, AC impedance was used to gain insight into the doping and dedoping procedures of polymer films at various potentials (Chapter 2).

1.7. Conclusion

As the mortality rates for cancer increase globally, it is ever more evident that research into safe, effective, and reliable treatments is at the upmost importance for society. The development of a new method of drug administration is vital to revolutionise treatments, providing patients with a specific personal treatment plan based on their level of illness. The following work takes into account the various disadvantages to current treatments and aims to rectify these problems. The main objective of this work is the development of a controlled, minimally invasive drug release procedure, focusing specifically on breast cancer. As seen in current research, drug delivery has been performed using conducting polymers because of their biocompatible properties and high conductivities, making them ideal materials for the electrochemical 'doping' and 'de-doping' of materials. This procedure would act as a controllable method to load or release a specific drug within seconds while applying a sufficient voltage, performing similar to that of a switch. Bipolar electrochemistry is a resurfacing area of electrochemistry, allowing 'wirefree' stimulation through a gradient electric field. This method is extremely attractive due to its low cost of instrumentation and ease of use. BP work has been researched for many decades, providing a sufficient understanding of the fundamentals. Using the 'wirefree' technique in conjunction with the controlled release of therapeutics from conducting polymers, would allow for a minimally invasive controlled drug release system, with aims of minimising drug dosage, cytotoxicity, and improving patient outcomes through targeted release.

1.8. References

- (1) Rébé, C.; Ghiringhelli, F. Cytotoxic Effects of Chemotherapy on Cancer and Immune Cells: How Can It Be Modulated to Generate Novel Therapeutic Strategies? *Future Oncol* **2015**, *11* (19), 2645–2654. https://doi.org/10.2217/fon.15.198.
- (2) *Breast cancer*. https://www.who.int/news-room/fact-sheets/detail/breast-cancer (accessed 2022-04-27).
- (3) PDQ Screening and Prevention Editorial Board. Breast Cancer Screening (PDQ®): Health Professional Version. In *PDQ Cancer Information Summaries*; National Cancer Institute (US): Bethesda (MD), 2002.
- (4) Maroni, R.; Massat, N. J.; Parmar, D.; Dibden, A.; Cuzick, J.; Sasieni, P. D.; Duffy, S. W. A Case-Control Study to Evaluate the Impact of the Breast Screening Programme on Mortality in England. *Br J Cancer* 2021, 124 (4), 736–743. https://doi.org/10.1038/s41416-020-01163-2.
- (5) Elmore, J. G.; Armstrong, K.; Lehman, C. D.; Fletcher, S. W. Screening for Breast Cancer. *JAMA* 2005, 293 (10), 1245–1256. https://doi.org/10.1001/jama.293.10.1245.
- (6) Hortobagyi, G. N. The Curability of Breast Cancer: Present and Future. *European Journal of Cancer Supplements* **2003**, *I* (1), 24–34. https://doi.org/10.1016/S1359-6349(03)00003-X.
- (7) Pedersen, R. N.; Esen, B. Ö.; Mellemkjær, L.; Christiansen, P.; Ejlertsen, B.; Lash, T. L.; Nørgaard, M.; Cronin-Fenton, D. The Incidence of Breast Cancer Recurrence 10-32 Years After Primary Diagnosis. *JNCI: Journal of the National Cancer Institute* 2022, 114 (3), 391–399. https://doi.org/10.1093/jnci/djab202.
- (8) Song, K.; Zu, X.; Du, Z.; Hu, Z.; Wang, J.; Li, J. Diversity Models and Applications of 3D Breast Tumor-on-a-Chip. *Micromachines* **2021**, *12* (7), 814. https://doi.org/10.3390/mi12070814.
- (9) Amjad, M. T.; Chidharla, A.; Kasi, A. Cancer Chemotherapy. In *StatPearls*; StatPearls Publishing: Treasure Island (FL), 2022.
- (10) Huang, C.-Y.; Ju, D.-T.; Chang, C.-F.; Muralidhar Reddy, P.; Velmurugan, B. K. A Review on the Effects of Current Chemotherapy Drugs and Natural Agents in Treating Non–Small Cell Lung Cancer. *Biomedicine (Taipei)* 2017, 7 (4), 23. https://doi.org/10.1051/bmdcn/2017070423.

- (11) Venkatesh, P.; Kasi, A. Anthracyclines. In *StatPearls*; StatPearls Publishing: Treasure Island (FL), 2022.
- (12) Marinello, J.; Delcuratolo, M.; Capranico, G. Anthracyclines as Topoisomerase II Poisons: From Early Studies to New Perspectives. *Int J Mol Sci* **2018**, *19* (11), 3480. https://doi.org/10.3390/ijms19113480.
- (13) Nitiss, J. L. Targeting DNA Topoisomerase II in Cancer Chemotherapy. *Nat Rev Cancer* **2009**, *9* (5), 338–350. https://doi.org/10.1038/nrc2607.
- (14) Shaul, P.; Frenkel, M.; Goldstein, E. B.; Mittelman, L.; Grunwald, A.; Ebenstein, Y.; Tsarfaty, I.; Fridman, M. The Structure of Anthracycline Derivatives Determines Their Subcellular Localization and Cytotoxic Activity. *ACS Med Chem Lett* **2013**, *4* (3), 323–328. https://doi.org/10.1021/ml3002852.
- (15) Holton, R. A. Chapter 5 Total Synthesis of Taxusin: An Initial Step Toward Taxol Synthesis. In *Strategies and Tactics in Organic Synthesis*; Lindberg, T., Ed.; Academic Press, 1991; Vol. 3, pp 165–197. https://doi.org/10.1016/B978-0-08-092430-4.50011-1.
- Alexa-Stratulat, T.; Luca, A.; Bădescu, M.; Bohotin, C.-R.; Alexa, I. D. Chapter 2
 Nutritional Modulators in Chemotherapy-Induced Neuropathic Pain. In *Nutritional Modulators of Pain in the Aging Population*; Watson, R. R., Zibadi, S., Eds.; Academic Press, 2017; pp 9–33. https://doi.org/10.1016/B978-0-12-805186-3.00002-3.
- (17) Lansiaux, A. [Antimetabolites]. *Bull Cancer* **2011**, *98* (11), 1263–1274. https://doi.org/10.1684/bdc.2011.1476.
- (18) Fomo, G.; Waryo, T.; Feleni, U.; Baker, P.; Iwuoha, E. Electrochemical Polymerization. In *Functional Polymers*; Jafar Mazumder, M. A., Sheardown, H., Al-Ahmed, A., Eds.; Polymers and Polymeric Composites: A Reference Series; Springer International Publishing: Cham, 2019; pp 105–131. https://doi.org/10.1007/978-3-319-95987-0_3.
- (19) Shirakawa, H.; Louis, E. J.; MacDiarmid, A. G.; Chiang, C. K.; Heeger, A. J. Synthesis of Electrically Conducting Organic Polymers: Halogen Derivatives of Polyacetylene, (CH)x. *J. Chem. Soc., Chem. Commun.* **1977**, No. 16, 578–580. https://doi.org/10.1039/C39770000578.
- (20) Cichosz, S.; Masek, A.; Zaborski, M. Polymer-Based Sensors: A Review. *Polymer Testing* **2018**, *67*, 342–348. https://doi.org/10.1016/j.polymertesting.2018.03.024.

- (21) K, N.; Sekhar Rout, C. Conducting Polymers: A Comprehensive Review on Recent Advances in Synthesis, Properties and Applications. *RSC Advances* **2021**, *11* (10), 5659–5697. https://doi.org/10.1039/D0RA07800J.
- (22) Heeger, A. J. Nobel Lecture: Semiconducting and Metallic Polymers: The Fourth Generation of Polymeric Materials. *Rev. Mod. Phys.* **2001**, *73* (3), 681–700. https://doi.org/10.1103/RevModPhys.73.681.
- (23) Müllen, K.; Scherf, U. Conjugated Polymers: Where We Come From, Where We Stand, and Where We Might Go. *Macromolecular Chemistry and Physics* **2023**, 224 (3), 2200337. https://doi.org/10.1002/macp.202200337.
- (24) Alshammary, B.; Walsh, F. C.; Herrasti, P.; Ponce De Leon, C. Electrodeposited Conductive Polymers for Controlled Drug Release: Polypyrrole. *J Solid State Electrochem* **2016**, *20* (4), 839–859. https://doi.org/10.1007/s10008-015-2982-9.
- (25) Le, T.-H.; Kim, Y.; Yoon, H. Electrical and Electrochemical Properties of Conducting Polymers. *Polymers* **2017**, *9* (4), 150. https://doi.org/10.3390/polym9040150.
- (26) Bredas, J. L.; Street, G. B. Polarons, Bipolarons, and Solitons in Conducting Polymers. *Acc. Chem. Res.* 1985, 18 (10), 309–315. https://doi.org/10.1021/ar00118a005.
- (27) Optical properties of conducting polymers | Chemical Reviews. https://pubs.acs.org/doi/pdf/10.1021/cr00083a009 (accessed 2023-01-03).
- (28) Gueye, M.; Carella, A.; Massonnet, N.; Yvenou, E.; Brenet, S.; Faure-Vincent, J.; Pouget, S.; Rieutord, F.; Okuno, H.; Benayad, A.; Demadrille, R.; Simonato, J.-P. Structure and Dopant Engineering in PEDOT Thin Films: Practical Tools for a Dramatic Conductivity Enhancement. *Chemistry of Materials* **2016**, *28*. https://doi.org/10.1021/acs.chemmater.6b01035.
- (29) Nie, S.; Li, Z.; Yao, Y.; Jin, Y. Progress in Synthesis of Conductive Polymer Poly(3,4-Ethylenedioxythiophene). *Front Chem* **2021**, *9*, 803509. https://doi.org/10.3389/fchem.2021.803509.
- (30) Ramalingam, K.; Panchu, S.; Salunke, A. S.; Muthukumar, K.; Ramanujam, A.; Muthiah, S. Free-Standing Graphene/Conducting Polymer Hybrid Cathodes as FTO and Pt-Free Electrode for Quasi-State Dye Sensitized Solar Cells. *ChemistrySelect* **2016**, *1* (15), 4814–4822. https://doi.org/10.1002/slct.201600874.
- (31) Cameron, J.; J. Skabara, P. The Damaging Effects of the Acidity in PEDOT:PSS on Semiconductor Device Performance and Solutions Based on Non-Acidic

- Alternatives. *Materials Horizons* **2020**, 7 (7), 1759–1772. https://doi.org/10.1039/C9MH01978B.
- (32) Ren, M.; Zhou, H.; Zhai, H.-J. Obvious Enhancement in Electrochemical Capacitive Properties for Poly(3,4-Ethylenedioxythiophene) Electrodes Prepared under Optimized Conditions. *J Mater Sci: Mater Electron* **2021**, *32* (8), 10078–10088. https://doi.org/10.1007/s10854-021-05666-3.
- (33) Krukiewicz, K.; Kruk, A.; Turczyn, R. Evaluation of Drug Loading Capacity and Release Characteristics of PEDOT/Naproxen System: Effect of Doping Ions. *Electrochimica Acta* **2018**, 289, 218–227. https://doi.org/10.1016/j.electacta.2018.09.011.
- (34) Krukiewicz, K.; Kowalik, A.; Turczyn, R.; Biggs, M. J. P. In Vitro Attenuation of Astrocyte Activation and Neuroinflammation through Ibuprofen-Doping of Poly(3,4-Ethylenedioxypyrrole) Formulations. *Bioelectrochemistry* **2020**, *134*, 107528. https://doi.org/10.1016/j.bioelechem.2020.107528.
- (35) Adepu, S.; Ramakrishna, S. Controlled Drug Delivery Systems: Current Status and Future Directions. *Molecules* **2021**, *26* (19), 5905. https://doi.org/10.3390/molecules26195905.
- (36) Glassman, P. M.; Muzykantov, V. R. Pharmacokinetic and Pharmacodynamic Properties of Drug Delivery Systems. *J Pharmacol Exp Ther* **2019**, *370* (3), 570–580. https://doi.org/10.1124/jpet.119.257113.
- (37) *Digestive tract*. National Institute of Diabetes and Digestive and Kidney Diseases. https://www.niddk.nih.gov/news/media-library/18116 (accessed 2022-11-09).
- (38) Kendrick, J. Basic Pharmacokinetics. Can J Hosp Pharm 2010, 63 (1), 55.
- (39) Applied Biopharmaceutics & Pharmacokinetics, 6e | AccessPharmacy | McGraw Hill Medical.

 https://accesspharmacy.mhmedical.com/content.aspx?bookid=513§ionid=41
 488016 (accessed 2022-11-09).
- (40) Gillette, J. R. Factors Affecting Drug Metabolism. *Annals of the New York Academy of Sciences* **1971**, *179* (1), 43–66. https://doi.org/10.1111/j.1749-6632.1971.tb46890.x.
- (41) Taft, D. R. Chapter 9 Drug Excretion. In *Pharmacology*; Hacker, M., Messer, W., Bachmann, K., Eds.; Academic Press: San Diego, 2009; pp 175–199. https://doi.org/10.1016/B978-0-12-369521-5.00009-9.

- (42) Avramović, N.; Mandić, B.; Savić-Radojević, A.; Simić, T. Polymeric Nanocarriers of Drug Delivery Systems in Cancer Therapy. *Pharmaceutics* **2020**, *12* (4). https://doi.org/10.3390/pharmaceutics12040298.
- (43) Parveen, S.; Arjmand, F.; Tabassum, S. Clinical Developments of Antitumor Polymer Therapeutics. *RSC Adv.* **2019**, *9* (43), 24699–24721. https://doi.org/10.1039/C9RA04358F.
- (44) Bahrami, B.; Hojjat-Farsangi, M.; Mohammadi, H.; Anvari, E.; Ghalamfarsa, G.; Yousefi, M.; Jadidi-Niaragh, F. Nanoparticles and Targeted Drug Delivery in Cancer Therapy. *Immunol Lett* **2017**, *190*, 64–83. https://doi.org/10.1016/j.imlet.2017.07.015.
- (45) Feng, S.-S. Nanoparticles of Biodegradable Polymers for New-Concept Chemotherapy. *Expert Review of Medical Devices* **2004**, *1* (1), 115–125. https://doi.org/10.1586/17434440.1.1.115.
- (46) Begines, B.; Ortiz, T.; Pérez-Aranda, M.; Martínez, G.; Merinero, M.; Argüelles-Arias, F.; Alcudia, A. Polymeric Nanoparticles for Drug Delivery: Recent Developments and Future Prospects. *Nanomaterials (Basel)* **2020**, *10* (7). https://doi.org/10.3390/nano10071403.
- (47) Pérez-Herrero, E.; Fernández-Medarde, A. Advanced Targeted Therapies in Cancer: Drug Nanocarriers, the Future of Chemotherapy. *Eur J Pharm Biopharm* **2015**, *93*, 52–79. https://doi.org/10.1016/j.ejpb.2015.03.018.
- (48) Castro, K. C. de; Costa, J. M.; Campos, M. G. N. Drug-Loaded Polymeric Nanoparticles: A Review. *International Journal of Polymeric Materials and Polymeric Biomaterials* **2020**, 0 (0), 1–13. https://doi.org/10.1080/00914037.2020.1798436.
- (49) Ferrari, R.; Sponchioni, M.; Morbidelli, M.; Moscatelli, D. Polymer Nanoparticles for the Intravenous Delivery of Anticancer Drugs: The Checkpoints on the Road from the Synthesis to Clinical Translation. *Nanoscale* 2018, 10 (48), 22701–22719. https://doi.org/10.1039/C8NR05933K.
- (50) Kim, T. Y.; Kim, D. W.; Chung, J. Y.; Shin, S. G.; Kim, S. C.; Heo, D. S.; Kim, N. K.; Bang, Y. J. Phase I and Pharmacokinetic Study of Genexol-PM, a Cremophor-Free, Polymeric Micelle-Formulated Paclitaxel, in Patients with Advanced Malignancies. *Clinical Cancer Research* 2004, 10 (11), 3708–3716. https://doi.org/10.1158/1078-0432.CCR-03-0655.

- (51) Werner, M. E.; Cummings, N. D.; Sethi, M.; Wang, E. C.; Sukumar, R.; Moore, D. T.; Wang, A. Z. Preclinical Evaluation of Genexol-PM, a Nanoparticle Formulation of Paclitaxel, as a Novel Radiosensitizer for the Treatment of Non-Small Cell Lung Cancer. *Int J Radiat Oncol Biol Phys* 2013, 86 (3), 463–468. https://doi.org/10.1016/j.ijrobp.2013.02.009.
- (52) Etheridge, M. L.; Campbell, S. A.; Erdman, A. G.; Haynes, C. L.; Wolf, S. M.; McCullough, J. The Big Picture on Nanomedicine: The State of Investigational and Approved Nanomedicine Products. *Nanomedicine* **2013**, *9* (1), 1–14. https://doi.org/10.1016/j.nano.2012.05.013.
- (53) Fanciullino, R.; Ciccolini, J.; Milano, G. Challenges, Expectations and Limits for Nanoparticles-Based Therapeutics in Cancer: A Focus on Nano-Albumin-Bound Drugs. *Crit Rev Oncol Hematol* **2013**, 88 (3), 504–513. https://doi.org/10.1016/j.critrevonc.2013.06.010.
- (54) Sun, T.; Zhang, Y. S.; Pang, B.; Hyun, D. C.; Yang, M.; Xia, Y. Engineered Nanoparticles for Drug Delivery in Cancer Therapy. *Angew Chem Int Ed Engl* **2014**, *53* (46), 12320–12364. https://doi.org/10.1002/anie.201403036.
- (55) Maeda, H.; Sawa, T.; Konno, T. Mechanism of Tumor-Targeted Delivery of Macromolecular Drugs, Including the EPR Effect in Solid Tumor and Clinical Overview of the Prototype Polymeric Drug SMANCS. *J Control Release* 2001, 74 (1–3), 47–61. https://doi.org/10.1016/s0168-3659(01)00309-1.
- (56) Papa, S.; Rossi, F.; Ferrari, R.; Mariani, A.; De Paola, M.; Caron, I.; Fiordaliso, F.; Bisighini, C.; Sammali, E.; Colombo, C.; Gobbi, M.; Canovi, M.; Lucchetti, J.; Peviani, M.; Morbidelli, M.; Forloni, G.; Perale, G.; Moscatelli, D.; Veglianese, P. Selective Nanovector Mediated Treatment of Activated Proinflammatory Microglia/Macrophages in Spinal Cord Injury. ACS Nano 2013, 7 (11), 9881–9895. https://doi.org/10.1021/nn4036014.
- (57) Wicki, A.; Witzigmann, D.; Balasubramanian, V.; Huwyler, J. Nanomedicine in Cancer Therapy: Challenges, Opportunities, and Clinical Applications. *J Control Release* **2015**, *200*, 138–157. https://doi.org/10.1016/j.jconrel.2014.12.030.
- (58) Paramshetti, S.; Angolkar, M.; Al Fatease, A.; Alshahrani, S. M.; Hani, U.; Garg, A.; Ravi, G.; Osmani, R. A. M. Revolutionizing Drug Delivery and Therapeutics: The Biomedical Applications of Conductive Polymers and Composites-Based Systems. *Pharmaceutics* 2023, 15 (4), 1204. https://doi.org/10.3390/pharmaceutics15041204.

- (59) Miller, L. L.; Lau, A. N. K.; Miller, E. K. Electrically Stimulated Release of Neurotransmitters from a Surface. An Analog of the Presynaptic Terminal. *J. Am. Chem. Soc.* **1982**, *104* (19), 5242–5244. https://doi.org/10.1021/ja00383a048.
- (60) Zinger, B.; Miller, L. L. Timed Release of Chemicals from Polypyrrole Films. *J. Am. Chem. Soc.* **1984**, *106* (22), 6861–6863. https://doi.org/10.1021/ja00334a076.
- (61) Svirskis, D.; Travas-Sejdic, J.; Rodgers, A.; Garg, S. Electrochemically Controlled Drug Delivery Based on Intrinsically Conducting Polymers. *J Control Release* **2010**, *146* (1), 6–15. https://doi.org/10.1016/j.jconrel.2010.03.023.
- (62) Park, Y.; Jung, J.; Chang, M. Research Progress on Conducting Polymer-Based Biomedical Applications. *Applied Sciences* **2019**, *9* (6), 1070. https://doi.org/10.3390/app9061070.
- (63) Ge, J.; Neofytou, E.; Cahill, T. J.; Beygui, R. E.; Zare, R. N. Drug Release from Electric-Field-Responsive Nanoparticles. *ACS Nano* **2012**, *6* (1), 227–233. https://doi.org/10.1021/nn203430m.
- (64) Vaitkuviene, A.; Kašėta, V.; Voronovic, J.; Ramanauskaite, G.; Biziuleviciene, G.; Ramanaviciene, A. Evaluation of Cytotoxicity of Polypyrrole Nanoparticles Synthesized by Oxidative Polymerization. *Journal of hazardous materials* **2013**, 250–251, 167–174. https://doi.org/10.1016/j.jhazmat.2013.01.038.
- (65) Chapman, C. A. R.; Cuttaz, E. A.; Goding, J. A.; Green, R. A. Actively Controlled Local Drug Delivery Using Conductive Polymer-Based Devices. *Applied Physics Letters* **2020**, *116* (1), 010501. https://doi.org/10.1063/1.5138587.
- (66) Gomez, N.; Schmidt, C. E. Nerve Growth Factor-Immobilized Polypyrrole: Bioactive Electrically Conducting Polymer for Enhanced Neurite Extension. *Journal of Biomedical Materials Research Part A* **2007**, *81A* (1), 135–149. https://doi.org/10.1002/jbm.a.31047.
- (67) Sebaa, M.; Nguyen, T.; Dhillon, S.; Garcia, S.; Liu, H. The Effects of Poly(3, 4-Ethylenedioxythiophene) (PEDOT) Coating on Magnesium Degradation and Cytocompatibility with Human Embryonic Stem Cells for Potential Neural Applications. *Journal of biomedical materials research*. *Part A* **2015**, *103*. https://doi.org/10.1002/jbm.a.35142.
- (68) Luo, S.-C.; Mohamed Ali, E.; Tansil, N. C.; Yu, H.; Gao, S.; Kantchev, E. A. B.; Ying, J. Y. Poly(3,4-Ethylenedioxythiophene) (PEDOT) Nanobiointerfaces: Thin, Ultrasmooth, and Functionalized PEDOT Films with in Vitro and in Vivo

- Biocompatibility. *Langmuir* **2008**, *24* (15), 8071–8077. https://doi.org/10.1021/la800333g.
- (69) Liu, H.; Jian, R.; Chen, H.; Tian, X.; Sun, C.; Zhu, J.; Yang, Z.; Sun, J.; Wang, C. Application of Biodegradable and Biocompatible Nanocomposites in Electronics: Current Status and Future Directions. *Nanomaterials (Basel)* 2019, 9 (7). https://doi.org/10.3390/nano9070950.
- (70) Qin, C.; Yue, Z.; Chao, Y.; Forster, R. J.; Maolmhuaidh, F. Ó.; Huang, X.-F.; Beirne, S.; Wallace, G. G.; Chen, J. Bipolar Electroactive Conducting Polymers for Wireless Cell Stimulation. *Applied Materials Today* **2020**, *21*, 100804. https://doi.org/10.1016/j.apmt.2020.100804.
- (71) Backhurst, J. R.; Coulson, J. M.; Goodridge, F.; Plimley, R. E.; Fleischmann, M. A Preliminary Investigation of Fluidized Bed Electrodes. *J. Electrochem. Soc.* 1969, 116 (11), 1600. https://doi.org/10.1149/1.2411628.
- (72) Koefoed, L.; Pedersen, S. U.; Daasbjerg, K. Bipolar Electrochemistry—A Wireless Approach for Electrode Reactions. *Current Opinion in Electrochemistry* 2017, 2
 (1), 13–17. https://doi.org/10.1016/j.coelec.2017.02.001.
- (73) Shida, N.; Zhou, Y.; Inagi, S. Bipolar Electrochemistry: A Powerful Tool for Electrifying Functional Material Synthesis. *Acc. Chem. Res.* **2019**, *52* (9), 2598–2608. https://doi.org/10.1021/acs.accounts.9b00337.
- (74) Crooks, R. M. Principles of Bipolar Electrochemistry. *ChemElectroChem* **2016**, *3* (3), 357–359. https://doi.org/10.1002/celc.201500549.
- (75) Forster, R. J. Wirefree Electroceuticals: 3D Electrical and Electrochemical Stimulation of Biological Systems. *Current Opinion in Electrochemistry* **2023**, *39*, 101297. https://doi.org/10.1016/j.coelec.2023.101297.
- (76) Mavré, F.; Anand, R. K.; Laws, D. R.; Chow, K.-F.; Chang, B.-Y.; Crooks, J. A.; Crooks, R. M. Bipolar Electrodes: A Useful Tool for Concentration, Separation, and Detection of Analytes in Microelectrochemical Systems. *Anal. Chem.* 2010, 82 (21), 8766–8774. https://doi.org/10.1021/ac101262v.
- (77) Duval, J.; Kleijn, J. M.; van Leeuwen, H. P. Bipolar Electrode Behaviour of the Aluminium Surface in a Lateral Electric Field. *Journal of Electroanalytical Chemistry* **2001**, *505* (1), 1–11. https://doi.org/10.1016/S0022-0728(01)00461-2.
- (78) Wang, Y.-L.; Cao, J.-T.; Liu, Y.-M. Bipolar Electrochemistry A Powerful Tool for Micro/Nano-Electrochemistry. *ChemistryOpen* **2022**, *11* (12), e202200163. https://doi.org/10.1002/open.202200163.

- (79) Qin, C.; Yue, Z.; Forster, R. J.; Chen, J.; Wallace, G. G. On Demand, Wireless Electrochemical Release of Brain Derived Neurotrophic Factor. *Electrochemistry Communications* **2023**, *157*, 107626. https://doi.org/10.1016/j.elecom.2023.107626.
- (80) Mirvakili, S. M.; Langer, R. Wireless On-Demand Drug Delivery. *Nat Electron* **2021**, *4* (7), 464–477. https://doi.org/10.1038/s41928-021-00614-9.
- (81) Kagatani, S.; Shinoda, T.; Konno, Y.; Fukui, M.; Ohmura, T.; Osada, Y. Electroresponsive Pulsatile Depot Delivery of Insulin from Poly(Dimethylaminopropylacrylamide) Gel in Rats. *Journal of Pharmaceutical Sciences* 1997, 86 (11), 1273–1277. https://doi.org/10.1021/js9700762.
- (82) Qu, J.; Zhao, X.; Ma, P. X.; Guo, B. Injectable Antibacterial Conductive Hydrogels with Dual Response to an Electric Field and pH for Localized "Smart" Drug Release. *Acta Biomaterialia* **2018**, 72, 55–69. https://doi.org/10.1016/j.actbio.2018.03.018.
- (83) Bard, A. J.; Faulkner, L. R.; White, H. S. *Electrochemical Methods: Fundamentals and Applications*; John Wiley & Sons, 2022.
- (84) Elgrishi, N.; Rountree, K. J.; McCarthy, B. D.; Rountree, E. S.; Eisenhart, T. T.; Dempsey, J. L. A Practical Beginner's Guide to Cyclic Voltammetry. *J. Chem. Educ.* **2018**, *95* (2), 197–206. https://doi.org/10.1021/acs.jchemed.7b00361.
- (85) Seeber, R.; Zanardi, C.; Inzelt, G. Links between Electrochemical Thermodynamics and Kinetics. *ChemTexts* **2015**, *1* (4), 18. https://doi.org/10.1007/s40828-015-0018-9.
- (86) *Cyclic Voltammogram*; 2010. https://www.youtube.com/watch?app=desktop&v=1f92vGOridg (accessed 2024-01-21).
- (87) Savéant, J.-M. Elements of Molecular and Biomolecular Electrochemistry: An Electrochemical Approach to Electron Transfer Chemistry; John Wiley & Sons, 2006.
- (88) Bai, L.; Yuan, R.; Chai, Y.; Yuan, Y.; Wang, Y.; Xie, S. Direct Electrochemistry and Electrocatalysis of a Glucose Oxidase-Functionalized Bioconjugate as a Trace Label for Ultrasensitive Detection of Thrombin. *Chem Commun (Camb)* **2012**, *48* (89), 10972–10974. https://doi.org/10.1039/c2cc35295h.
- (89) Bruckenstein, S.; Robert Hillman, A.; Bandey, H. L. Chapter 13 Visualizing Ion and Solvent Transfer Processes in Electroactive Polymer Films. In *Comprehensive*

- Chemical Kinetics; Compton, R. G., Hancock, G., Eds.; Applications of Kinetic Modelling; Elsevier, 1999; Vol. 37, pp 489–521. https://doi.org/10.1016/S0069-8040(99)80018-1.
- (90) Mikhalovsky, S. V.; Gun'ko, V. M.; Pavey, K. D.; Tomlins, P. E.; James, S. L. 13
 Microgravimetry. In *Surfaces and Interfaces for Biomaterials*; Vadgama, P., Ed.; Woodhead Publishing Series in Biomaterials; Woodhead Publishing, 2005; pp 322–385. https://doi.org/10.1533/9781845690809.2.322.
- (91) Sauerbrey, G. Verwendung von Schwingquarzen zur Wägung dünner Schichten und zur Mikrowägung. *Z. Physik* **1959**, *155* (2), 206–222. https://doi.org/10.1007/BF01337937.
- (92) Ji, Y.; Yin, Z.-W.; Yang, Z.; Deng, Y.-P.; Chen, H.; Lin, C.; Yang, L.; Yang, K.; Zhang, M.; Xiao, Q.; Li, J.-T.; Chen, Z.; Sun, S.-G.; Pan, F. From Bulk to Interface: Electrochemical Phenomena and Mechanism Studies in Batteries via Electrochemical Quartz Crystal Microbalance. *Chem. Soc. Rev.* **2021**, *50* (19), 10743–10763. https://doi.org/10.1039/D1CS00629K.
- (93) Thambiratnam, K.; Reduan, S. A.; Tiu, Z. C.; Ahmad, H. Chapter 9 Application of Two-Dimensional Materials in Fiber Laser Systems. In *Nano-Optics*; Thomas, S., Grohens, Y., Vignaud, G., Kalarikkal, N., James, J., Eds.; Micro and Nano Technologies; Elsevier, 2020; pp 227–264. https://doi.org/10.1016/B978-0-12-818392-2.00009-3.
- (94) Edwards, A. A.; Alexander, B. D. UV-Visible Absorption Spectroscopy, Organic Applications. In *Encyclopedia of Spectroscopy and Spectrometry (Third Edition)*; Lindon, J. C., Tranter, G. E., Koppenaal, D. W., Eds.; Academic Press: Oxford, 2017; pp 511–519. https://doi.org/10.1016/B978-0-12-803224-4.00013-3.
- (95) Calloway, D. Beer-Lambert Law. *J. Chem. Educ.* **1997**, *74* (7), 744. https://doi.org/10.1021/ed074p744.3.
- (96) Ma, H.; Shieh, K.-J.; Qiao, T. Study of Transmission Electron Microscopy (TEM) and Scanning Electron Microscopy (SEM). *Nat Sci* **2006**, *4*.
- (97) Omidi, M.; Fatehinya, A.; Farahani, M.; Akbari, Z.; Shahmoradi, S.; Yazdian, F.; Tahriri, M.; Moharamzadeh, K.; Tayebi, L.; Vashaee, D. 7 Characterization of Biomaterials. In *Biomaterials for Oral and Dental Tissue Engineering*; Tayebi, L., Moharamzadeh, K., Eds.; Woodhead Publishing, 2017; pp 97–115. https://doi.org/10.1016/B978-0-08-100961-1.00007-4.

- (98) Administrator. *Looking at materials up close The Scanning Electron Microscope*. https://www.rrutc.msm.cam.ac.uk/outreach/articles/the-scanning-electron-microscope (accessed 2023-09-16).
- (99) Pendse, D. R.; Chin, A. K. Cathodoluminescence and Transmission Cathodoluminescence. In *Encyclopedia of Materials: Science and Technology*; Buschow, K. H. J., Cahn, R. W., Flemings, M. C., Ilschner, B., Kramer, E. J., Mahajan, S., Veyssière, P., Eds.; Elsevier: Oxford, 2001; pp 1–7. https://doi.org/10.1016/B0-08-043152-6/00190-X.
- (100) Guy, O. J.; Walker, K.-A. D. Chapter 4 Graphene Functionalization for Biosensor Applications. In *Silicon Carbide Biotechnology (Second Edition)*; Saddow, S. E., Ed.; Elsevier, 2016; pp 85–141. https://doi.org/10.1016/B978-0-12-802993-0.00004-6.
- (101) Mortimer, R. J. Spectroelectrochemistry, Methods and Instrumentation. In *Encyclopedia of Spectroscopy and Spectrometry (Third Edition)*; Lindon, J. C., Tranter, G. E., Koppenaal, D. W., Eds.; Academic Press: Oxford, 2017; pp 172–177. https://doi.org/10.1016/B978-0-12-803224-4.00289-2.
- (102) Baur, J. E. 19 Diffusion Coefficients. In *Handbook of Electrochemistry*; Zoski, C. G., Ed.; Elsevier: Amsterdam, 2007; pp 829–848. https://doi.org/10.1016/B978-044451958-0.50036-7.
- (103) Mei, B.-A.; Munteshari, O.; Lau, J.; Dunn, B.; Pilon, L. Physical Interpretations of Nyquist Plots for EDLC Electrodes and Devices. *J. Phys. Chem. C* **2018**, *122* (1), 194–206. https://doi.org/10.1021/acs.jpcc.7b10582.
- (104) Kötz, R.; Carlen, M. Principles and Applications of Electrochemical Capacitors. *Electrochimica Acta* **2000**, *45* (15), 2483–2498. https://doi.org/10.1016/S0013-4686(00)00354-6.
- (105) Lazanas, A. Ch.; Prodromidis, M. I. Electrochemical Impedance Spectroscopy—A Tutorial. *ACS Meas. Sci. Au* **2023**, *3* (3), 162–193. https://doi.org/10.1021/acsmeasuresciau.2c00070.
- (106) Yang, I.; Kim, S.-G.; Kwon, S. H.; Kim, M.-S.; Jung, J. C. Relationships between Pore Size and Charge Transfer Resistance of Carbon Aerogels for Organic Electric Double-Layer Capacitor Electrodes. *Electrochimica Acta* **2017**, *223*, 21–30. https://doi.org/10.1016/j.electacta.2016.11.177.

- (107) Lou, F.; Chen, D. Aligned Carbon Nanostructures Based 3D Electrodes for Energy Storage. *Journal of Energy Chemistry* **2015**, *24* (5), 559–586. https://doi.org/10.1016/j.jechem.2015.08.013.
- (108) Jow, T. R.; Marx, M. B.; Allen, J. L. Distinguishing Li+ Charge Transfer Kinetics at NCA/Electrolyte and Graphite/Electrolyte Interfaces, and NCA/Electrolyte and LFP/Electrolyte Interfaces in Li-Ion Cells. *J. Electrochem. Soc.* **2012**, *159* (5), A604. https://doi.org/10.1149/2.079205jes.

Chapter 2

Electrochemical and Surface Characterisation of Poly(3,4ethylenedioxythiophene) Dodecylbenzenesulfonate Layers

2. Electrochemical and Surface Characterisation of Poly(3,4-ethylenedioxythiophene) Dodecylbenzenesulfonate Layers

2.1. Introduction

Conducting polymers have been investigated for decades, gaining increasing interest due to their attractive chemical-physical properties. The first report on conducting polymers was the electrochemical synthesis of aniline, producing a blue/green layer on a platinum electrode discovered by Letheby in 1862.^{1–3} Since the 1970s, there has been considerable research progress, particularly regarding PANI, PPy, PT, and PEDOT.^{4–8} These systems, and in particular, PEDOT, are endowed with various attractive features, such as high conductivity, flexibility and mechanical stability, which render them attractive platforms for the fabrication of sensors, ^{9,10} photovoltaic cells, ¹¹ and drug delivery systems. ¹²

Polymer-based drug delivery provides a method which can control and target the release of therapeutics, providing a safer and more effective treatment for patients. ^{12,13} This phenomenon has been used in electrochemical environments, applying a specific voltage to release APIs in a matter of seconds. ¹² The purpose of this work is to replicate drug doping and de-doping procedures by using a bulky anion as an anionic drug substitute. This work provides an understanding of the doping and de-doping procedures that occur at varying potentials and how the size of a drug molecule can affect the electrochemical loading and release of the therapeutic. PEDOT exhibits *p*-type semiconducting behaviour upon oxidation, creating positive polarons and bipolarons which delocalise throughout the polymer chain, thus, generating electrical conductivity. ^{14,15} The dopant, whose function involves the withdrawal and replenishment of electrons from the polymer backbone, can modulate the system's properties. ^{14,16–18} Therefore, the presence of a bulky anion has the ability to change the doping and de-doping processes occuring in the PEDOT film. ¹⁹

In this work, PEDOT dodecylbenzenesulfonate (DBS) and PEDOT chloride films were explored to gain insights into the doping and de-doping processes of PEDOT while examining how the ion dopant size influences these procedures. DBS was selected as the bulky anion as cation exchange from a PEDOT/DBS film had not been seen in the literature. Cyclic voltammetry (CV) and Electrochemical Quartz Crystal Microbalance (EQCM) were employed to characterise the polymer characteristics on the electrode

surface. EQCM measurements provided quantitative results demonstrating the exchange of cations rather than the expected anion exchange for *p*-type doping polymers (this outcome was attributed to the presence of bulky anions). AC impedance examined the behaviour and state of the film at different reduction potentials while Scanning Electron Microscopy (SEM) and Atomic Force Microscopy (AFM) were used to investigate the film morphologies. Presented here is a viable conducting polymer, showing promising results for its use as a drug delivery vehicle. This study holds importance as it offers a comprehensive insight into the doping and de-doping processes of the conducting polymer PEDOT across various potentials. This chapter is essential for the advancement of this project, particularly in Chapter Three, where we delve into the examination of loading and releasing therapeutics from PEDOT.

2.2. Experimental

2.2.1. Chemicals

All chemicals used in this experimentation were of reagent grade and purchased from Merck and Fisher Scientific. 0.05, 0.3, and 1.0 μ m alumina powders were purchased from CH instruments. Purified water was acquired from the ELGA PURELAB milli-Q water purification system (option Q7), resistivity of 18.2 M Ω cm.

2.2.2. Electrochemical Characterisation

The electrochemical setup for cyclic voltammetry contained a three-electrode cell, including a glassy carbon electrode (GCE) (3 mm diameter), Ag/AgCl reference electrode (saturated KCl) and a platinum wire counter electrode. The GCE was polished with 0.05, 0.3 and 1.0 µm alumina powder. The electrode was rinsed and sonicated in deionised water after each polishing step and finally dried using nitrogen and capped with an Eppendorf tube. All solutions were deoxygenated and prepared at room temperature. PEDOT/DBS films were formed using chronocoulometry in a solution of 10 mM EDOT and 5 mM SDBS in DI water. PEDOT/Cl films were formed using chronocoulometry in a solution containing 10 mM EDOT and 0.1 M NaCl in DI water at 1.0 V for 10 mC. All experiments were performed using CHI-440a, CHI-660, and CHI-600 electrochemical workstations. The CHI-440a was used for electrochemical quartz crystal microbalance experiments. The AutoLab (Metrohm) systems potentiostat was used to perform the AC impedance spectroscopy. AC impedance was performed at different applied potentials

(vs. Ag/AgCl) from 0.01 to 1×10^5 Hz in a 1 M KCl solution. Impedance spectra were analysed by fitting equivalent electrical circuits using electrochemical impedance spectrum analyser software EISSA-1.

Surface coverage was calculated using the following equation (Eqt. 2.1):²⁰

$$\Gamma = Q/nFA$$
 Eqt.2.1

Where Γ is the surface coverage of the modified electrode in mol/cm², Q is the total electrode charge in C (obtained through CV integration in a consistent potential window), n is the number of transferred electrons (assuming 2.25),^{21,22} F is Faraday's constant, and A is the surface area of the electrode in cm².

The Randles-Sevcik equation was used to calculate the diffusion coefficient for the PEDOT/DBS film (Eqt. 1.3).^{23,24}

2.2.3. Electrochemical Quartz Crystal Microbalance

The electrochemical quartz crystal microbalance set up included an AT-cut quartz crystal with a diameter of 13.7 mm, a fundamental frequency of 7.995 MHz and a platinum working electrode area of 0.196 cm². An Ag/AgCl reference electrode (saturated KCl) and a platinum wire counter electrode were used to complete the electrochemical setup. All films were formed in 10 mM EDOT 5 mM SDBS solution for 15 cycles using cyclic voltammetry with a potential window from 0 to 1.05 V and a scan rate of 100 mV/s. The modified electrode was rinsed with DI water between experiments. The Sauerbrey Equation was used throughout this work to convert the frequency changes to mass changes (Eqt. 1.4):^{25,26}

$$\Delta f = -\frac{2f_0^2}{A\sqrt{\rho_q \mu_q}} \Delta m$$
 Eqt.1.4

Where Δf is the change in frequency, f_0 is the resonant frequency (7.995 MHz), A is the crystal area (0.196 cm²), ρ_q is the quartz density (2.648 g/cm³), μ_q is the quartz shear

modulus (2.947×10¹¹ g cm⁻¹ s⁻²) and Δm is the registered mass change. Based on these values, 1 Hz corresponds to 1.34 ng.cm⁻² Hz⁻¹. It is important to note that there are limitations to the Sauerbrey equation which are discussed in Section 1.6.4.

2.2.4. Morphological analysis

PEDOT/DBS and PEDOT/Cl films were formed using chronocoulometry as decribed in Section 2.2.2 on ITO slides for morphology analysis. Field emission-scanning electron microscopy (FE-SEM) images were recorded using a Zeiss SUPRA 40VP instrument, operating at a primary beam acceleration voltage of 10 kV and collecting electrons using an in-lens detector.

Atomic force microscopy (AFM) analyses were carried out in air, using a NT-MDT SPM Solver P47H-PRO instrument operated in semi-contact mode. After background subtraction and plane fitting, root-mean-square (RMS) roughness values were obtained from the height profiles of $5\times5~\mu\text{m}^2$ images according to the following relation (Eqt. 2.2): 27,28

RMS roughness =
$$[\Sigma(z_i - Z)^2 / n]^{1/2}$$
 Eqt.2.2

where z_i , Z and n represent the local height, the mean height and the data point number.

2.3. Results and Discussion

2.3.1. Cyclic Voltammetry

Figure 2.1 (a) displays the CV of the chloride doped PEDOT film in 0.1 M KCl. The resulting CV is scanned cathodically, initiating the reduction of the PEDOT polymer backbone through injecting electrons. Upon the initial reduction sweep, a sharp cathodic peak can be seen at -0.8 V, however upon continuous cycling this peak is no longer visible. It is possible that this peak could be associated with cation exchange as a result of charge compensation due to reduction, as observed by Tóth et al.²⁹ During the second and third cycles, this peak is not visible, meaning the film returns to its neutral 'undoped' state at -1.0 V. The PEDOT chains become neutral, eliminating the necessity for the presence of the dopant anion chloride within the polymer matrix. Hence, in order to achieve charge neutrality, the incorporated chloride is expelled from the PEDOT film.³⁰ This is evident

by the presence of a subtle, broad reduction peak, E_{pc} at -0.3 V (vs Ag/AgCl). Upon scan reversal, there is a broad reoxidation wave, E_{pa} at approximately -0.4 V (vs Ag/AgCl) which involves the injection of chloride anions from the supporting electrolyte for reasons of charge neutrality as the film is returned to its oxidised or doped conducting state.

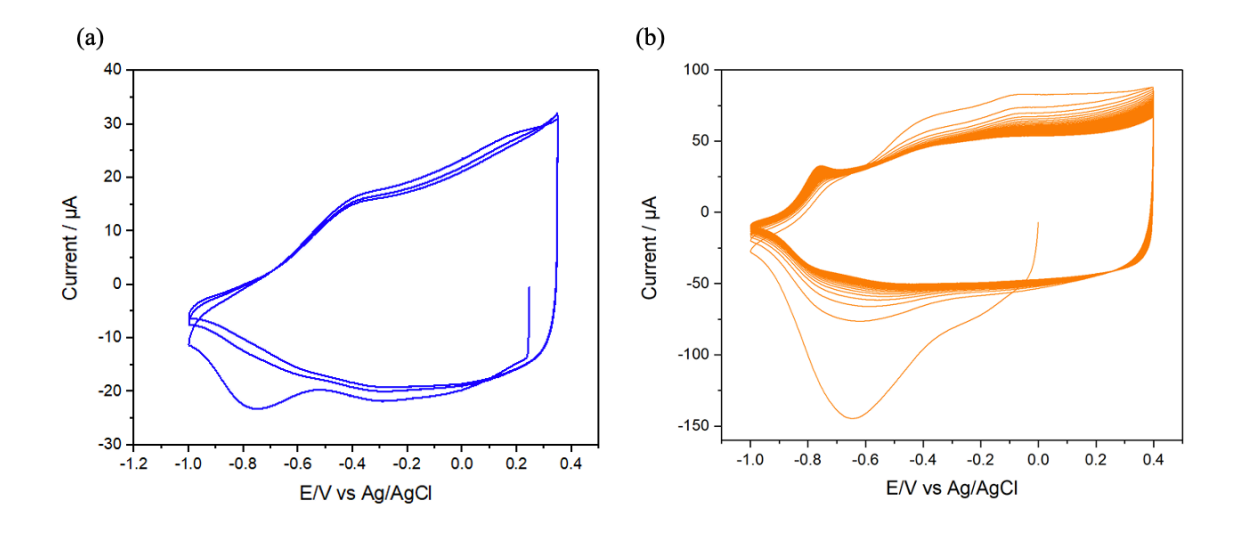


Figure 2. 1. (a) 10 mC PEDOT/Cl film cycled in 0.1 M KCl. Scan rate: 50 mV/s. (b) 10 mC PEDOT/DBS film (250 cycles) in 1 M KCl. Scan rate: 100 mV/s.

In contrast, the redox switching of the PEDOT/DBS film, as depicted in Figure 2.1 (b), shows an initial cathodic wave at a more positive potential, approximately, -0.65 V (vs Ag/AgCl), compared to the chloride-doped film discussed previously. The observation that both films undergo redox switching in identical electrolytes (i.e. KCl) but exhibit cathodic peaks with a close to 350 mV difference (comparing cycle 3), suggests a distinctly different doping/de-doping mechanisms during polymer redox switching between the two types of PEDOT films. The well-established understanding is that when bulky anions, such as DBS, are introduced into conducting polymer films as dopants, the bulky dopant remains within the film upon redox switching. This results in a process where cation insertion and expulsion from the supporting electrolyte takes place during polymer redox switching. ^{19,30,31}

The calculated surface coverage for the PEDOT/DBS film was 3.05×10^{-8} mol/cm² from the final redox cycle of the polymer film using equation (Eqt. 2.1) with an associated calculated diffusion coefficient of 1.52×10^{-12} cm² s⁻¹ assuming a 2.25 electron transfer (Eqt. 1.3). The surface coverage was calculated by integrating the CV to obtain charge using a consistent potential window to ensure consistency in comparing data. The

measured diffusion coefficient relates to the diffusion of ions to and from the polymer film during oxidation and reduction processes. This value is important for future work to understand the diffusing of the anionic drug to and from the polymer film. It can be seen that after 250 redox cycles, there is a decrease in the current which is likely due to the degradation of the PEDOT polymer at the electrode surface. From this work, we can see the direct influence that the type of doping ion can have on the redox switching properties of PEDOT.

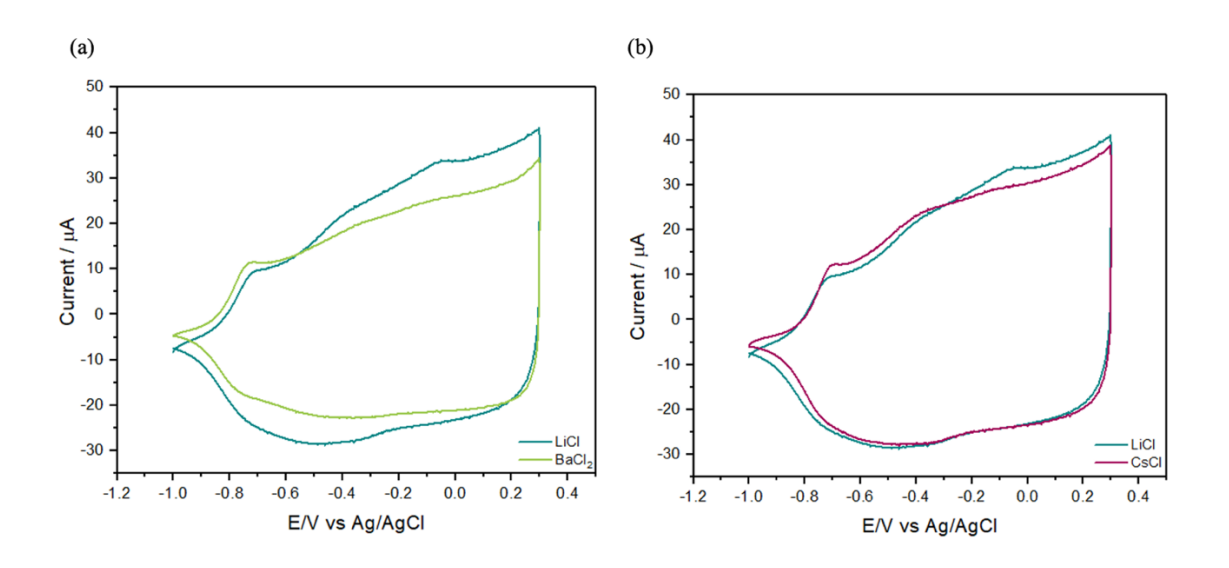


Figure 2.2. Overlay of 10 mC PEDOT/DBS film on GCE cycled in (a) 1M LiCl and 1M BaCl₂ (b) 1M LiCl and 1M CsCl. Scan rate 50 mV/s.

Table 2.1. Table of hydrated radii of ions extracted from literature.

Cation	Ion radius (nm)	Hydrated radius (nm)	Ref.
Li ⁺	0.068	0.38	32
Na ⁺	0.095	0.36	32
\mathbf{K}^{+}	0.133	0.33	32
Cs ⁺	0.169	0.33	32
Ba ²⁺	0.135	0.40	33

Based on work performed by Gruia et al.,³⁴ the presence of a bulky anion influences the doping procedures of the polymer matrix. After incorporating the bulky anion DBS into the PEDOT film, additional experimentation was conducted to explore the influence of

DBS on ion exchange. CVs were performed in various electrolytes altering only the positive ion (eg. NaCl, KCl, CsCl). The reason for this was to ensure that any changes in the CVs were solely due to the presence of a different cation upon doping and de-doping. Table 2.1 displays the ion radii and hydrated radii of cations which have been extracted from the literature. From the CVs shown in Figure 2.2, there are extremely subtle changes in the cathodic peak potentials (E_{pc}) upon changing the electrolyte. As a result of this, it is not possible to clearly identify which cation is being incorporated into the film easier based on size. Performing this experiment using cations with greater variations in sizes would have resulted in a more conclusive experiment. As a result of the similarities in the CVs presented in Figure 2.2, EQCM was used to investigate the mass changed that occur upon changing the doping cation.

2.3.2. Electrochemical Quartz Crystal Microbalance Measurement

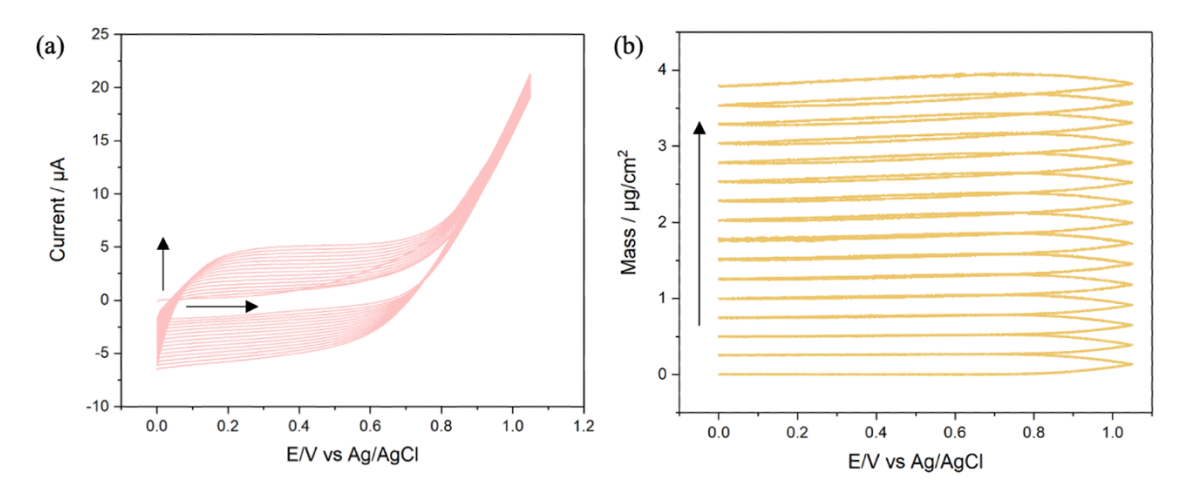


Figure 2.3. (a) Electropolymerisation of PEDOT/DBS by cyclic voltammetry in 10 mM EDOT 5 mM SDBS in aqueous solution on Pt quartz crystal electrode. Scan rate 100 mV/s. (b) Mass changes obtained simultaneously during electropolymerisation of PEDOT/DBS film using QCM.

EQCM measurements were conducted to delve deeper into the electrodeposition of the DBS doped PEDOT film and the dynamics of cation insertion and expulsion during the redox switching of the film between its conducting and insulating states post-formation. Figure 2.3 (a) depicts the resulting cyclic voltammogram obtained for the

electrodeposition of the PEDOT/DBS. It is apparent that the current steadily increases with each cycle, demonstrating the ongoing growth of the conducting polymer film on the electrode surface.³⁵ The accompanying EQCM data shown in Figure 2.3 (b) demonstrates a rise in mass on the surface of the electrode as the continuous cycling progresses, oxidising the monomer. A total mass increase of 3.8 μ g/cm² or 2.7x10⁻⁸ mol/cm² was calculated using Eqt. 2.1 after the PEDOT DBS formation.

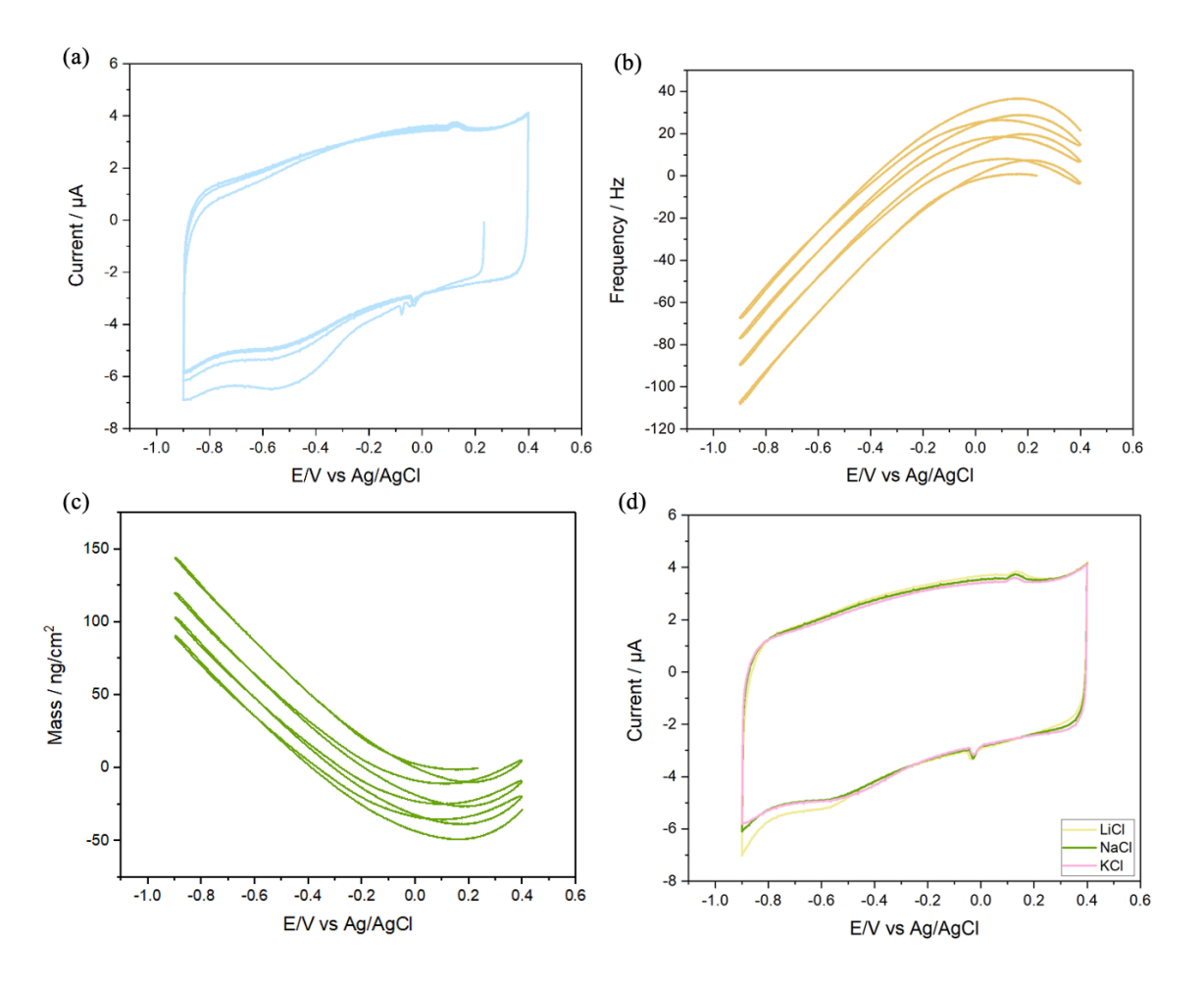


Figure 2.4. (a) PEDOT/DBS film cycled in 0.1M KCl on Pt quartz crystal electrode (b) EQCM frequency response of PEDOT/DBS cycled in 0.1 M KCl (c) EQCM mass response of PEDOT/DBS cycled in 0.1 M KCl (d) PEDOT/DBS film cycled in 0.1 M LiCl, 0.1 M NaCl and 0.1 M KCl (third cycle). Scan rate 50 mV/s.

EQCM was specifically chosen for this study as it enables simultaneous mass measurements during cyclic voltammetry, providing a means to confirm cation exchange. Figures 2.4 (a) and (b) show the resulting CV and accompanying EQCM frequency curve of the PEDOT/DBS film. The EQCM data illustrates that during cathodic scanning of the deposited film, there is a decrease in frequency, followed by an associated increase in

frequency during anodic scanning. As described by the Sauerbrey equation (Eqt. 1.4),²⁵ frequency is inversely proportional to mass, thereby a frequency decrease in the film corresponds to a mass increase at the surface of the modified electrode.³⁴ An increase of mass occurs within the film during reduction, validating that the DBS ion has changed the overall net charge of the film, leading to cation exchange.

The frequency changes shown in Figure 2.4 (b) are translated to their corresponding mass values through the employment of the Sauerbrey equation (Eqt. 1.4), as illustrated in Figure 2.4 (c). As the reduction scan approaches the switching potential of -0.9 V, there is a notable mass increase during the initial cycle of the PEDOT DBS film. This substantiates that the cathodic wave of the CV corresponds to the insertion of cations from the supporting electrolyte into the polymer film, which is attributed to the hindered ability of the bulky DBS moiety to be expelled from the polymer film. During redox cycling the film in an anodic direction (-0.9 V to +0.2 V), a mass decrease is noticeable during this reoxidation process. This occurs as the incorporated cations are removed from the film to maintain charge neutrality.²⁹ For a more in-depth investigation of the impact of cation exchange, Figure 2.4 (d) illustrates the CVs obtained for the PEDOT/DBS film in a range of alkali metal chloride electrolytes including LiCl, NaCl and KCl. Only subtle changes were observed on the polymer's cathodic wave for Li⁺, Na⁺, and K⁺ electrolytes in Figure 2.4 (d), which was expected as per results in Figure 2.2. As a continuation of the hydrated radii experimentation, the mass measurements upon cation exchange were calculated to further delve into the effects of these cations on doping. The mass calculated at -0.9 V (using Eqt. 1.4) for the first polymeric cycle for lithium ions was 199.39 ng/cm² or 2.87x10⁻⁸ mol/cm² (obtained by dividing the mass by the molecular weight), 171.39 ng/cm² or 7.46x10⁻⁹ mol/cm² for sodium and 143.92 ng/cm² or 3.68x10⁻⁹ mol/cm² for potassium. The theoretical apparent molar masses follow: Li⁺ (6.94 g/mol), Na⁺ (22.98 g/mol) and K⁺ (39.07 g/mol). It is important to note that this is not an entirely accurate measurement of the number of cations migrating to the film as other ions within the solvent will be drawn into and expelled from the film simultaneously, however for this calculation only cations were considered.³⁶ From these results it is clear that lithium had the most moles of material deposited upon cation insertion, with sodium and potassium following suit with slightly less.

2.3.3. AC Impedance

In order to get a better understanding of the modified electrode-electrolyte interface during the reduction of the polymer film, the electrochemical impedance spectrum was recorded at different potentials where the PEDOT/DBS film went from oxidised to reduced (Figure 2.5). Several circuit elements are related to the different transport and capacitive mechanisms involved in polymer oxidation (doping) and polymer reduction (de-doping). All spectra were fitted using the equivalent circuit shown in insert of Figure 2.5 which consist of a series of resistances for the electrolyte and contact contribution R_s, a capacitance C_{dl} usually modelled with a constant phase element (CPE) for the double layer at the electrode-electrolyte interface, a charge transfer resistance R_{ct}, and finally a diffusion element accounting for the charging of the film.

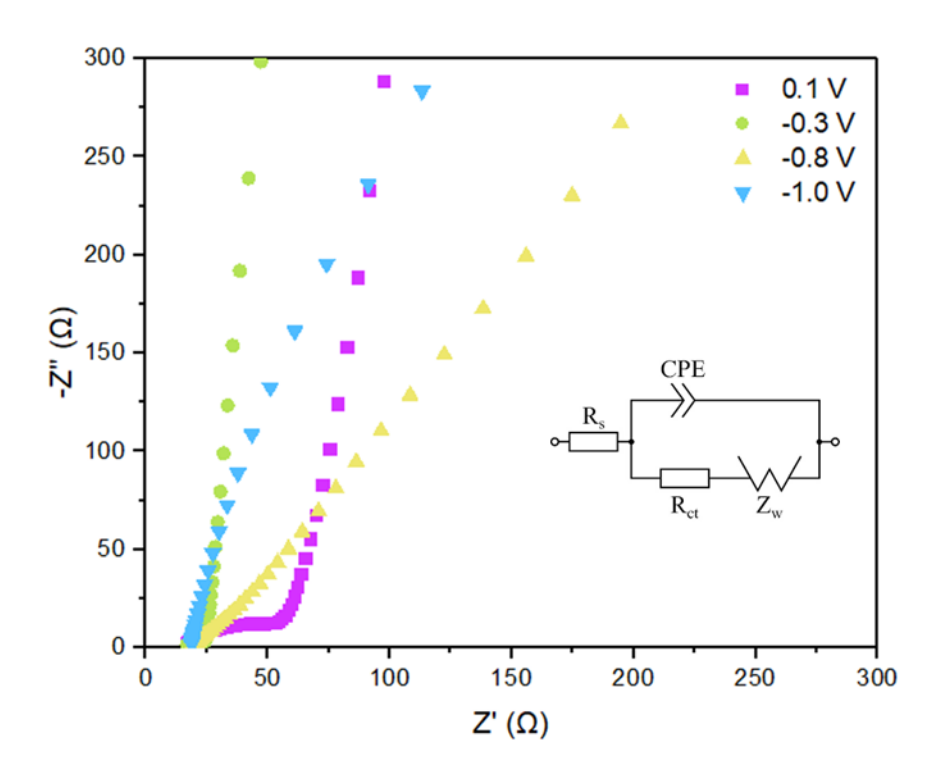


Figure 2.5. Nyquist plot of 10 mC PEDOT/DBS film in 1 M KCl on GCE. AC impedance was performed at different applied potentials (0.1 V, -0.3 V, -0.8 V, -1.0 V) (vs. Ag/AgCl) from 0.01 to 1×10^5 Hz.

The solution resistances were similar across all applied potentials. However, when the potential became more negative, the charge transfer resistance increased, indicating that the film was likely neutral and non-conductive. The film's charge transfer resistances were low where it was conductive (oxidation and reduction).³⁷ Moreover, the cation

migration towards the interface of the electrode compensating the negative charge of the film will also have an influence on the doping state of the polymer further influencing the charge transfer. At mid to low frequency ranges, all potentials show typical capacitive behaviour that is expected for PEDOT. The Warburg impedance was described as an open-circuit finite Warburg element with a diffusion resistance (Z_w). It is the resistance caused by the diffusion of doped species (cation) to and from the modified electrode. At lower frequencies, the capacitive behaviour is found, and it can be related to the film charging mechanism. The increase in CPE indicates that more ions are accommodated in the double layer at higher potentials, most likely due to the higher polarization material. 39

Table 2.2. Numerical values of solution resistance (R_s), capacitance (C), charge transfer resistance (R_{ct}), and Warburg diffusion (A_w). Data obtained by fitting to the circuit in Figure 2.5.

\mathbf{V}	CPE (µF)	$R_s(\Omega)$	$R_{CT}(\Omega)$	$W(\Omega/s^{1/2})$
0.1	113	15.2	36.30	324.91
-0.3	105	15.9	6.36	149.70
-0.8	240	22.04	31	199.49
-1.0	240	22.04	6998.20	266.25

2.3.4. Characterisation of PEDOT/Cl and PEDOT/DBS Films

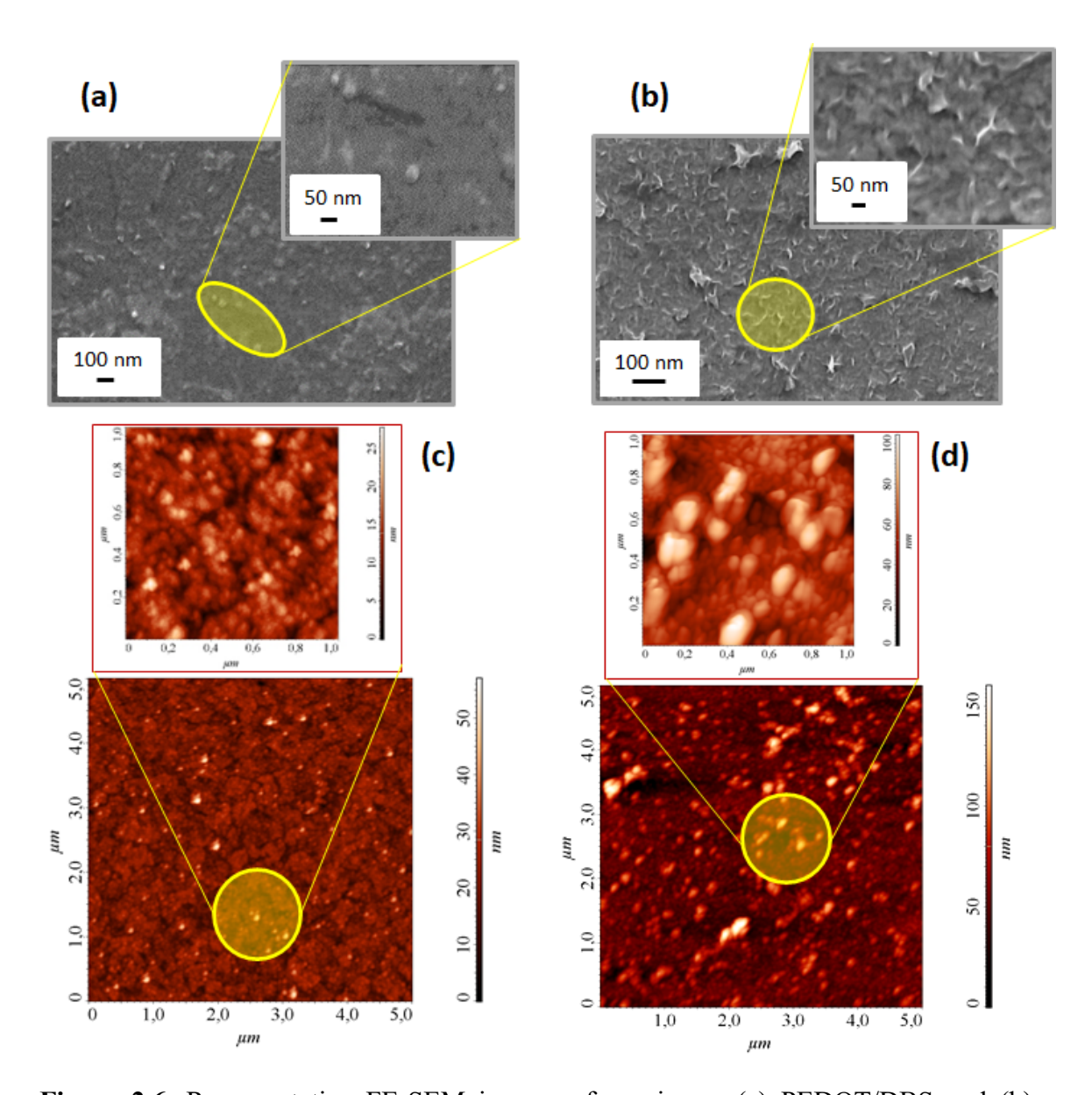


Figure 2.6. Representative FE-SEM images of specimens (a) PEDOT/DBS and (b) PEDOT/Cl. AFM micrographs of samples (c) PEDOT/DBS and (d) PEDOT/Cl.

The system morphology was investigated by the combined use of AFM and FE-SEM. Figures 2.6 (a) and (b) display selected FE-SEM images of samples PEDOT/DBS and PEDOT/Cl, respectively. PEDOT/DBS featured a rather compact morphology, whereas for the latter, the occurrence of evenly distributed protruding aggregates suggested an increase in the overall specimen area. In this regard, additional important information was obtained by AFM analyses. Images of both PEDOT/DBS and PEDOT/Cl recorded at different magnification levels (Figures 2.6 (c)-(d)) evidenced a globular morphology for both specimens, with aggregate dimensions undergoing an appreciable increase upon

going from PEDOT/DBS to PEDOT/Cl. The corresponding RMS roughness values (4.0 and 16.0 nm, respectively) indicated a higher roughness in the latter case. Since an enhancement of RMS data typically indicates an increase in surface area,²⁸ this feature could have potential advantages for functional applications, thanks to the high contact area with the reaction medium.

2.4. Conclusion

In this work, PEDOT/Cl and PEDOT/DBS films were investigated to understand their doping properties. PEDOT/Cl exhibits typical doping expected for *p*-type doping polymers, which is anion insertion upon oxidation and anion expulsion during reduction.⁴⁰ During electropolymerisation, PEDOT is doped with the bulky anion DBS. From this work it is clear that DBS becomes immobilised, also resulting in the insertion of cations upon reduction and expelling cations while oxidation occurs. Cation exchange behaviour has been investigated for PPy/DBS films, as well as PEDOT/DS films; however to the best of the author's knowledge, the cation exchange behaviour of PEDOT/DBS has yet to be described.^{19,36} From EQCM data, during the cyclic voltammogram, a mass increase during reduction and a mass decrease consequent to oxidation was observed. This work demonstrates that PEDOT can act as an anion and cation exchanger and provides a fundamental understanding of the doping and de-doping procedures. The work completed in this chapter assists in the design and development of the drug delivery system in Chapter 3.

2.5. References

- (1) Visakh, P. M. Chapter 1 Polyaniline-Based Blends, Composites, and Nanocomposites: State of the Art, New Challenges, and Opportunities. In *Polyaniline Blends, Composites, and Nanocomposites*; Visakh, P. M., Pina, C. D., Falletta, E., Eds.; Elsevier, 2018; pp 1–22. https://doi.org/10.1016/B978-0-12-809551-5.00001-1.
- (2) Fomo, G.; Waryo, T.; Feleni, U.; Baker, P.; Iwuoha, E. Electrochemical Polymerization. In *Functional Polymers*; Jafar Mazumder, M. A., Sheardown, H., Al-Ahmed, A., Eds.; Polymers and Polymeric Composites: A Reference Series; Springer International Publishing: Cham, 2019; pp 105–131. https://doi.org/10.1007/978-3-319-95987-0_3.
- (3) Bockris, J. O.; Miller, D. The Electrochemistry of Electronically Conducting Polymers. In *Conducting Polymers*; Alcácer, L., Ed.; Springer Netherlands: Dordrecht, 1987; pp 1–36. https://doi.org/10.1007/978-94-009-3907-3 1.
- (4) K, N.; Sekhar Rout, C. Conducting Polymers: A Comprehensive Review on Recent Advances in Synthesis, Properties and Applications. *RSC Advances* **2021**, *11* (10), 5659–5697. https://doi.org/10.1039/D0RA07800J.
- (5) Qazi, T. H.; Rai, R.; Boccaccini, A. R. Tissue Engineering of Electrically Responsive Tissues Using Polyaniline Based Polymers: A Review. *Biomaterials* **2014**, *35* (33), 9068–9086. https://doi.org/10.1016/j.biomaterials.2014.07.020.
- (6) Kisiel, A.; Korol, D.; Michalska, A.; Maksymiuk, K. Polypyrrole Nanoparticles of High Electroactivity. Simple Synthesis Methods and Studies on Electrochemical Properties. *Electrochimica Acta* 2021, 390, 138787. https://doi.org/10.1016/j.electacta.2021.138787.
- (7) Hu, L.; Song, J.; Yin, X.; Su, Z.; Li, Z. Research Progress on Polymer Solar Cells Based on PEDOT:PSS Electrodes. *Polymers* **2020**, *12* (1), 145. https://doi.org/10.3390/polym12010145.
- (8) Kaloni, T. P.; Giesbrecht, P. K.; Schreckenbach, G.; Freund, M. S. Polythiophene: From Fundamental Perspectives to Applications. *Chem. Mater.* **2017**, *29* (24), 10248–10283. https://doi.org/10.1021/acs.chemmater.7b03035.
- (9) Ramanavicius, S.; Ramanavicius, A. Conducting Polymers in the Design of Biosensors and Biofuel Cells. *Polymers (Basel)* **2020**, *13* (1), 49. https://doi.org/10.3390/polym13010049.

- (10) Zhao, Y.; Cao, L.; Li, L.; Cheng, W.; Xu, L.; Ping, X.; Pan, L.; Shi, Y. Conducting Polymers and Their Applications in Diabetes Management. *Sensors (Basel)* **2016**, *16* (11), 1787. https://doi.org/10.3390/s16111787.
- (11) Hou, W.; Xiao, Y.; Han, G.; Lin, J.-Y. The Applications of Polymers in Solar Cells:

 A Review. *Polymers (Basel)* **2019**, *11* (1), 143. https://doi.org/10.3390/polym11010143.
- (12) Krukiewicz, K.; Kruk, A.; Turczyn, R. Evaluation of Drug Loading Capacity and Release Characteristics of PEDOT/Naproxen System: Effect of Doping Ions. *Electrochimica Acta* **2018**, 289, 218–227. https://doi.org/10.1016/j.electacta.2018.09.011.
- (13) Macha, I. J.; Ben-Nissan, B.; Vilchevskaya, E. N.; Morozova, A. S.; Abali, B. E.; Müller, W. H.; Rickert, W. Drug Delivery From Polymer-Based Nanopharmaceuticals—An Experimental Study Complemented by Simulations of Selected Diffusion Processes. Frontiers in Bioengineering and Biotechnology 2019, 7.
- (14) Le, T.-H.; Kim, Y.; Yoon, H. Electrical and Electrochemical Properties of Conducting Polymers. *Polymers* **2017**, *9* (4), 150. https://doi.org/10.3390/polym9040150.
- (15) Inzelt, G. Charge Transport in Conducting Polymer Film Electrodes. *Chemical & Biochemical Engineering Quarterly (cabeq@pbf.hr); Vol.21 No.1* **2007**, *21*.
- (16) Jacobs, I. E.; Lin, Y.; Huang, Y.; Ren, X.; Simatos, D.; Chen, C.; Tjhe, D.; Statz, M.; Lai, L.; Finn, P. A.; Neal, W. G.; D'Avino, G.; Lemaur, V.; Fratini, S.; Beljonne, D.; Strzalka, J.; Nielsen, C. B.; Barlow, S.; Marder, S. R.; McCulloch, I.; Sirringhaus, H. High-Efficiency Ion-Exchange Doping of Conducting Polymers. *Advanced Materials n/a* (n/a), 2102988. https://doi.org/10.1002/adma.202102988.
- (17) Gueye, M. N.; Carella, A.; Faure-Vincent, J.; Demadrille, R.; Simonato, J.-P. Progress in Understanding Structure and Transport Properties of PEDOT-Based Materials: A Critical Review. *Progress in Materials Science* 2020, 108, 100616. https://doi.org/10.1016/j.pmatsci.2019.100616.
- (18) MacDiarmid, A. G.; Mammone, R. J.; Kaner, R. B.; Porter, S. J.; Pethig, R.; Heeger, A. J.; Rosseinsky, D. R. The Concept of 'Doping' of Conducting Polymers: The Role of Reduction Potentials [and Discussion]. *Philosophical*

- Transactions of the Royal Society of London. Series A, Mathematical and Physical Sciences **1985**, 314 (1528), 3–15.
- (19) McCormac, T.; Breen, W.; McGee, A.; Cassidy, J. F.; Lyons, M. E. G. Cyclic Voltammetry of Polypyrroledodecylbenzenesulfonate Layers. *Electroanalysis* 1995, 7 (3), 287–289. https://doi.org/10.1002/elan.1140070317.
- (20) Nasirizadeh, N.; Shekari, Z.; Nazari, A.; Tabatabaee, M. Fabrication of a Novel Electrochemical Sensor for Determination of Hydrogen Peroxide in Different Fruit Juice Samples. *Journal of Food and Drug Analysis* **2016**, *24* (1), 72–82. https://doi.org/10.1016/j.jfda.2015.06.006.
- (21) Wagner, M.; Lisak, G.; Ivaska, A.; Bobacka, J. Durable PEDOT:PSS Films Obtained from Modified Water-Based Inks for Electrochemical Sensors. *Sensors and Actuators B: Chemical* **2013**, *181*, 694–701. https://doi.org/10.1016/j.snb.2013.02.051.
- (22) Sundfors, F.; Bobacka, J.; Ivaska, A.; Lewenstam, A. Kinetics of Electron Transfer between Fe(CN)63-/4- and Poly(3,4-Ethylenedioxythiophene) Studied by Electrochemical Impedance Spectroscopy. *Electrochimica Acta* **2002**, *47* (13), 2245–2251. https://doi.org/10.1016/S0013-4686(02)00063-4.
- (23) Bard, A. J.; Faulkner, L. R.; White, H. S. *Electrochemical Methods: Fundamentals and Applications*; John Wiley & Sons, 2022.
- (24) Bai, L.; Yuan, R.; Chai, Y.; Yuan, Y.; Wang, Y.; Xie, S. Direct Electrochemistry and Electrocatalysis of a Glucose Oxidase-Functionalized Bioconjugate as a Trace Label for Ultrasensitive Detection of Thrombin. *Chem Commun (Camb)* **2012**, *48* (89), 10972–10974. https://doi.org/10.1039/c2cc35295h.
- (25) Sauerbrey, G. Verwendung von Schwingquarzen zur Wägung dünner Schichten und zur Mikrowägung. Z. Physik 1959, 155 (2), 206–222. https://doi.org/10.1007/BF01337937.
- (26) Niu, L.; Yang, L.; Yang, J.; Chen, M.; Zeng, L.; Duan, P.; Wu, T.; Pameté, E.; Presser, V.; Feng, G. Understanding the Charging of Supercapacitors by Electrochemical Quartz Crystal Microbalance. *Industrial Chemistry & Materials* **2023**, *I* (2), 175–187. https://doi.org/10.1039/D2IM00038E.
- (27) Barreca, D.; Carraro, G.; Warwick, M. E. A.; Kaunisto, K.; Gasparotto, A.; Gombac, V.; Sada, C.; Turner, S.; Tendeloo, G. V.; Maccato, C.; Fornasiero, P. Fe2O3–TiO2 Nanosystems by a Hybrid PE-CVD/ALD Approach: Controllable

- Synthesis, Growth Mechanism, and Photocatalytic Properties. *CrystEngComm* **2015**, *17* (32), 6219–6226. https://doi.org/10.1039/C5CE00883B.
- (28) Benedet, M.; Andrea Rizzi, G.; Gasparotto, A.; Lebedev, O. I.; Girardi, L.; Maccato, C.; Barreca, D. Tailoring Oxygen Evolution Performances of Carbon Nitride Systems Fabricated by Electrophoresis through Ag and Au Plasma Functionalization. *Chemical Engineering Journal* 2022, 448, 137645. https://doi.org/10.1016/j.cej.2022.137645.
- (29) Tóth, P. S.; Janáky, C.; Berkesi, O.; Tamm, T.; Visy, C. On the Unexpected Cation Exchange Behavior, Caused by Covalent Bond Formation between PEDOT and Cl– Ions: Extending the Conception for the Polymer–Dopant Interactions. *J. Phys. Chem. B* **2012**, *116* (18), 5491–5500. https://doi.org/10.1021/jp2107268.
- (30) Tan, P.; Lu, F.; Han, Y. In-Depth Exploration of the Mechanism by Which Various Dopant Ions Affect the Infrared Electrochromic Characteristics of Poly(3,4-Ethylenedioxythiophene) Conducting Polymers. *Chem. Mater.* **2023**. https://doi.org/10.1021/acs.chemmater.3c01093.
- (31) Petroffe, G.; Beouch, L.; Cantin, S.; Aubert, P.-H.; Plesse, C.; Dudon, J.-P.; Vidal, F.; Chevrot, C. Investigations of Ionic Liquids on the Infrared Electroreflective Properties of Poly(3,4-Ethylenedioxythiophene). *Solar Energy Materials and Solar Cells* **2018**, *177*, 23–31. https://doi.org/10.1016/j.solmat.2017.07.018.
- (32) Israelachvili, J. N. 4 Interactions Involving Polar Molecules. In *Intermolecular* and Surface Forces (Third Edition); Israelachvili, J. N., Ed.; Academic Press: San Diego, 2011; pp 71–90. https://doi.org/10.1016/B978-0-12-375182-9.10004-1.
- (33) Zhong, C.; Yida, D.; Hu, W.; Qiao, J.; Zhang, L.; Zhang, J. A Review of Electrolyte Materials and Compositions for Electrochemical Supercapacitors. *Chemical Society reviews* **2015**, *44*, 7431–7920. https://doi.org/10.1039/c5cs00303b.
- (34) Gruia, V.-T.; Ispas, A.; Efimov, I.; Bund, A. Cation Exchange Behavior during the Redox Switching of Poly (3,4-Ethylenedioxythiophene) Films. *J Solid State Electrochem* **2020**, *24* (11), 3231–3244. https://doi.org/10.1007/s10008-020-04809-6.
- (35) Daideche, K.; Hasniou, L.; Lerari, D. Electro Synthesis and Characterization of PANI and PANI/ZnO Composites Films. *Chemistry Proceedings* **2020**, *3* (1), 110. https://doi.org/10.3390/ecsoc-24-08328.

- (36) Hillman, A. R.; Daisley, S. J.; Bruckenstein, S. Solvent Effects on the Electrochemical P-Doping of PEDOT. *Phys. Chem. Chem. Phys.* **2007**, *9* (19), 2379–2388. https://doi.org/10.1039/B618786B.
- (37) Hass, R.; García-Cañadas, J.; Garcia-Belmonte, G. Electrochemical Impedance Analysis of the Redox Switching Hysteresis of Poly(3,4-Ethylenedioxythiophene) Films. *Journal of Electroanalytical Chemistry* **2005**, *577* (1), 99–105. https://doi.org/10.1016/j.jelechem.2004.11.020.
- (38) Mei, B.-A.; Munteshari, O.; Lau, J.; Dunn, B.; Pilon, L. Physical Interpretations of Nyquist Plots for EDLC Electrodes and Devices. *J. Phys. Chem. C* **2018**, *122* (1), 194–206. https://doi.org/10.1021/acs.jpcc.7b10582.
- (39) Bobacka, J. Potential Stability of All-Solid-State Ion-Selective Electrodes Using Conducting Polymers as Ion-to-Electron Transducers. *Anal. Chem.* **1999**, *71* (21), 4932–4937. https://doi.org/10.1021/ac990497z.

Chapter 3

Electrochemical Doping and De-doping of Therapeutics

3. Electrochemical Doping and De-doping of Therapeutics

3.1. Introduction

The objective of this work was to create an 'on demand' drug delivery system with the use of biocompatible, multifunctional, electronically conducting polymers so as to enable a more effective therapy for cancer patients while reducing side effects. In recent years, conducting polymers have demonstrated potential for their use in drug delivery systems (DDS). ^{1,2} Indubitably, these materials must portray two important characteristics which are conductivity and biocompatibility. Based on the redox switching of conducting polymers, a conducting polymer-based drug delivery system was successfully developed, which was used for the release of the therapeutics shown in Figure 3.1. This work showed promising application for a targeted and controlled drug delivery system, having the ability to switch on or off when necessary.

Figure 3.1. Chemical structure of (a) naproxen sodium salt (b) mitoxantrone dihydrochloride.

In the first part of this work two primary doping agents are investigated to compare the efficiency of drug loading and release characteristics of the anti-inflammatory drug naproxen. The ionic radii of NO₃⁻ and ClO₄⁻ are 0.179 nm and 0.240 nm respectively.³ The different molecular sizes of the PEDOT/NO₃ and PEDOT/ClO₄ films result in changes to the structure of the polymer matrix upon formation, which in turn affects the doping and de-doping effects of the film.^{4,5} Naproxen is used in the treatment of diseases such as osteoarthritis and rheumatoid arthritis, as well as muscle and joint pains. Additionally, this work sees poly(3,4 – ethylenedioxythiophene), PEDOT, as a drug delivery vehicle for the electrochemical release of anti-cancer drug mitoxantrone. Using

techniques such as chronocoulometry, cyclic voltammetry and electrochemical quartz crystal microbalance (EQCM), the effects of drug loading and release were investigated based on the PEDOT film thickness. The effects were examined using PEDOT films of 5, 10 and 20 mC. This work demonstrates the loading and release of a metastatic breast cancer drug, addressing the challenge of maintaining the optimum systemic concentration of drugs for effective therapy and to minimise side effects, so as to improve patient's lives.

3.2. Materials and Methods

3.2.1. Preparation of the Working Electrode

Cyclic Voltammetry

All electrochemical experiments were performed using the CHI-440a electrochemical workstation. A standard three-electrode set-up was used to perform all electrochemical experiments including an Au quartz crystal working electrode, Ag/AgCl (saturated KCl) reference electrode, and a platinum wire counter electrode. PEDOT films were formed by cyclic voltammetry in a solution of 10 mM EDOT in 0.1 M LiClO₄ or 0.1 M KNO₃. The monomer was electrochemically oxidised using a potential window of +1.1 V to -0.5 V for 25 cycles at a scan rate of 0.1 V/s. The Randles-Sevcik equation was used to calculate the diffusion coefficients for the PEDOT/ClO₄ and PEDOT/NO₃ films. The Randles-Sevcik equation is as follows (Eqt. 1.3):^{6,7}

$$i_p = 2.69x10^5$$
. A. $D^{1/2}$. $n^{3/2}$. $v^{1/2}$. C Eqt.1.3

Where i_p is the peak current in A, A is the area of the working electrode in cm², D is the diffusion coefficient of the drug in cm²/s, n is the number of electrons transferred, v is the scan rate in V/s, and C is the concentration of electrolyte in mol/cm³.

Chronocoulometry

Chronocoulometry was used for the effect of film thickness experimentation (Section 3.4). A standard three-electrode set-up was used to perform all electrochemical experiments including an Au quartz crystal working electrode, Ag/AgCl reference electrode, and a platinum wire counter electrode. Film formation was performed upon

application of +1.0 V until the desired charge was reached (5 mC, 10 mC, and 20 mC). A 10 mM EDOT 0.1 M LiClO₄ solution was used to perform the polymerisation.

3.2.2. Electrochemical Quartz Crystal Microbalance

All electrochemical experiments were performed using the CHI-440a electrochemical workstation. An AT-cut gold quartz crystal with area 0.196 cm², fundamental frequency 7.995 MHz was used as the working electrode, Ag/AgCl (saturated KCl) reference electrode, and a platinum wire counter electrode. The CH Instruments electrochemical quartz crystal microbalance was used for all experiments. The relationship between both frequency and mass changes were calculated using the Sauerbrey equation (Eqt. 1.4):⁸

$$\Delta f = \frac{-2f_0^2}{A(\mu\rho)^{1/2}} \Delta m$$
 Eqt.1.4

Where Δf is the change in frequency, f_0 is the resonant frequency of the fundamental mode of the crystal, A is the area of the Au disk on the crystal (0.196 cm²), μ is the shear modulus of quartz (2.947 x 10^{11} g/cm s²), ρ is the density of quartz (2.684 g/cm³) and Δ m is the change in mass. A 1 Hz change in frequency corresponds to a mass change (adsorbed or desorbed) of 1.34 ng.

3.2.3. Doping and De-Doping Procedures

Naproxen

PEDOT/ClO₄ and PEDOT/NO₃ films were prepared by cyclic voltammetry. Both films were de-doped in their respective electrolytes (ie. PEDOT/NO₃ de-doped in 0.1 M KNO₃) for 600 seconds at -0.5 V for PEDOT/ClO₄ and -0.2 V for PEDOT/NO₃. The specific reduction potentials were chosen based on trialled EQCM experimentation, that resulted in mass decreases upon reduction. The films were then doped with 10 mM naproxen sodium salt in DI water for 600 seconds at +0.5 V for both films. The naproxen solution was made with DI water to prevent the incorporation of other ions into the film. Both films then went under spontaneous release which was achieved by applying open circuit potential (occurred at 0.2 V). Both films performed controlled release by applying -0.5 V

to PEDOT/ClO₄ and -0.2 V to PEDOT/NO₃. The working electrode and electrochemical cell were rinsed with deionised water three times between experiments to ensure all ions at the surface of the film were removed.

Mitoxantrone

For the effect of film thickness work, all films (5 mC, 10 mC, and 20 mC) were formed using chronocoulometry until the desired charge was reached. All films were initially dedoped in 0.1 M LiClO₄ at -0.5 V for 300 seconds which was established from the naproxen drug experimentation. The films were then doped using a 5 mM mitoxantrone dihydrochloride DI water solution for 300 seconds at +0.5 V for both films. A 5 mM mitoxantrone solution was chosen due to the cost of the drug. Spontaneous release was performed by applying open circuit potential for 300 seconds in 0.1 M LiClO₄. Re-doping was achieved by applying +0.5 V to the 5 mM mitoxantrone dihydrochloride solution for 300 seconds. Controlled release was performed by initially applying -0.5 V for 300 seconds in 0.1 M LiClO₄.

Drug Release Kinetics

Avrami's equation is used to describe recrystallisation kinetics, however, it is commonly used to describe drug release kinetics (Eqt. 3.1) (Eqt. 3.2).^{5,8,10}

$$X = 1 - exp(-kt^n)$$
 Eqt. 3.1

$$X = \frac{M_t}{M_{\infty}}$$
 Eqt. 3.2

The equation can be re-written as follows (Eqt. 3.3):

$$\ln(-\ln(1-X)) = \ln k + n \ln (t)$$
 Eqt. 3.3

Where M_t is the mass of drug released at any time t in ng cm², M_{∞} is the total mass of the drug in the matrix in ng cm², k is the rate constant in s⁻¹, and n is the kinetic exponent.

The rate constant and kinetic exponent were calculated by plotting ln(-ln(1-X)) versus ln(t). Both k and n were obtained from the intercept and slope respectively.¹¹

3.3. Results and Discussion

3.3.1. Characterisation of the Effects of Dopants on Naproxen Loading and Release

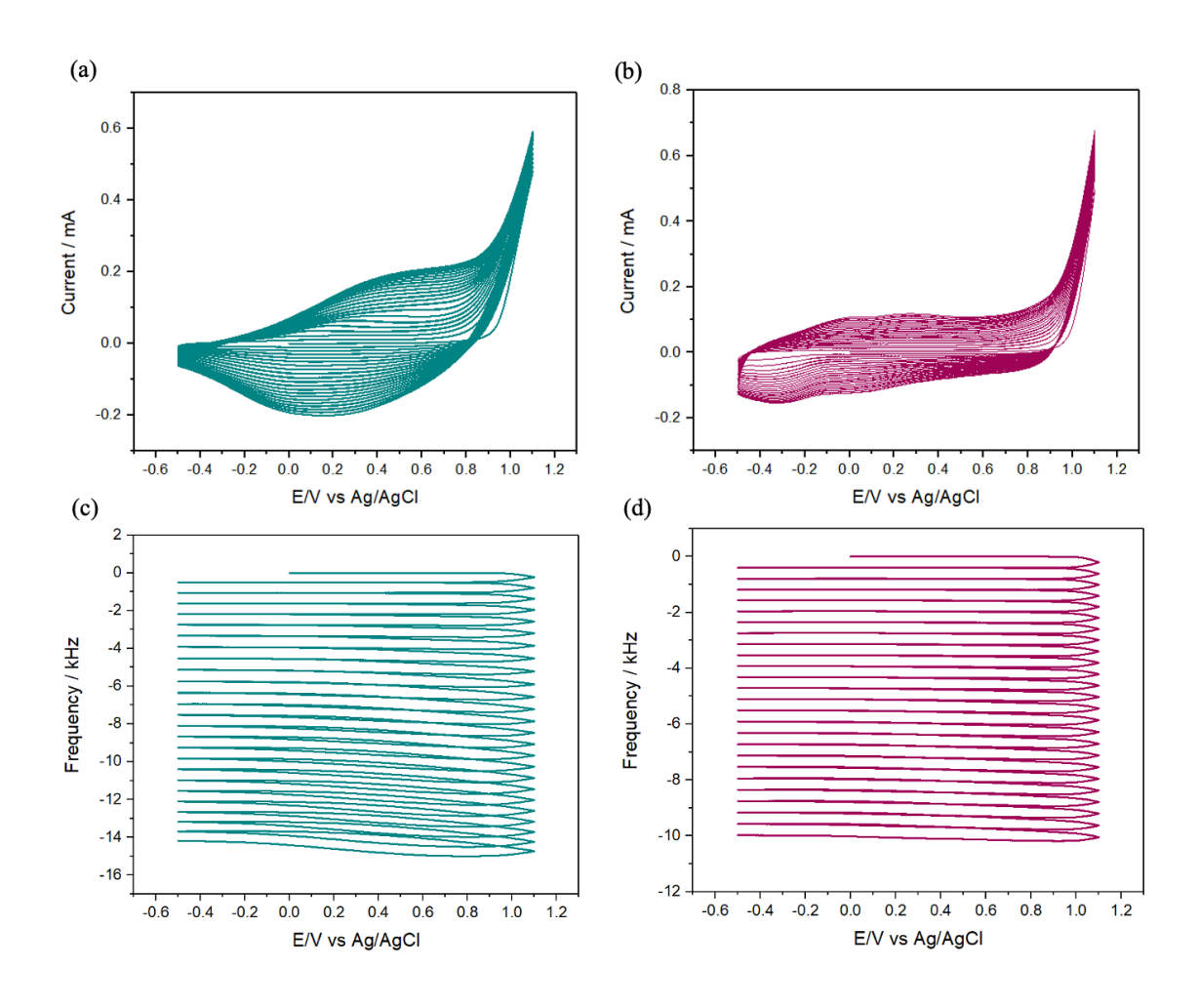


Figure 3.2. (a) Electrochemical polymerisation of PEDOT/ClO₄ by cyclic voltammetry for 25 cycles in 10 mM EDOT 0.1 M LiClO₄ solution on an Au quartz crystal at 100 mV/s (b) Electropolymerisation of PEDOT/NO₃ by cyclic voltammetry for 25 cycles in 10 mM EDOT 0.1 M KNO₃ solution on an Au quartz crystal (c) EQCM frequency response for PEDOT/ClO₄ film formation (d) EQCM frequency response for PEDOT/NO₃ film formation.

Figure 3.2 (a) and (b) display the cyclic voltammograms for the electropolymerisation of the PEDOT/ClO₄ and PEDOT/NO₃ films respectively. At a minimum, + 0.85 V (versus Ag/AgCl) is required to initiate the oxidation of the PEDOT monomer, therefore, a positive voltage of 1.1 V was applied to begin the polymerisation. Both CVs are commenced by a positive scan, initiating the electron loss which results in the formation

of cationic radicals.¹⁴ The growth in current upon increasing cycling suggests the deposition of the film on the electrode surface. This is typical of electropolymerisation as the surface area increases due to the three-dimensional structure of the polymer, causing an increase in the size of the double layer due to charging, and consequently an increase in capacitive current which can be seen in Figure 3.2 (a) and (b). 15 Figure 3.2 (c) and (d) presents the EQCM frequency data for both film formations. As per Sauerbrey's equation (Eqt. 1.4), frequency is inversely proportional to mass, therefore, as frequency decreases, mass is increasing. This is caused by the dampening of the resonating crystal due to the deposition of the polymer, resulting in a frequency decrease. ¹⁶ From the frequency data in Figure 3.2 (c) and (d) frequency is decreasing, signifying a mass increase and therefore demonstrating that the film layers are being deposited on the surface of the electrode. Using the Sauerbrey equation, the overall mass of the polymer deposited on the electrode surface was calculated to be 19 µg/cm² for PEDOT/ClO₄ and 13.4 µg/cm² for PEDOT/NO₃ (Table 3.1). The mass changes were calculated at -0.5 V, as the films are in the 'un-doped' state at this potential, meaning that all current observed is solely due to the charging of the polymer film.¹⁵ The moles of deposited EDOT were calculated for both films (Table 3.2), with PEDOT/ClO₄ depositing 1.33×10^{-7} mol/cm² and PEDOT/NO₃ depositing 9.42×10⁻⁸ mol/cm². From these values, it is fair to suggest that approximately the same quantity of polymer is being deposited for both complexes.

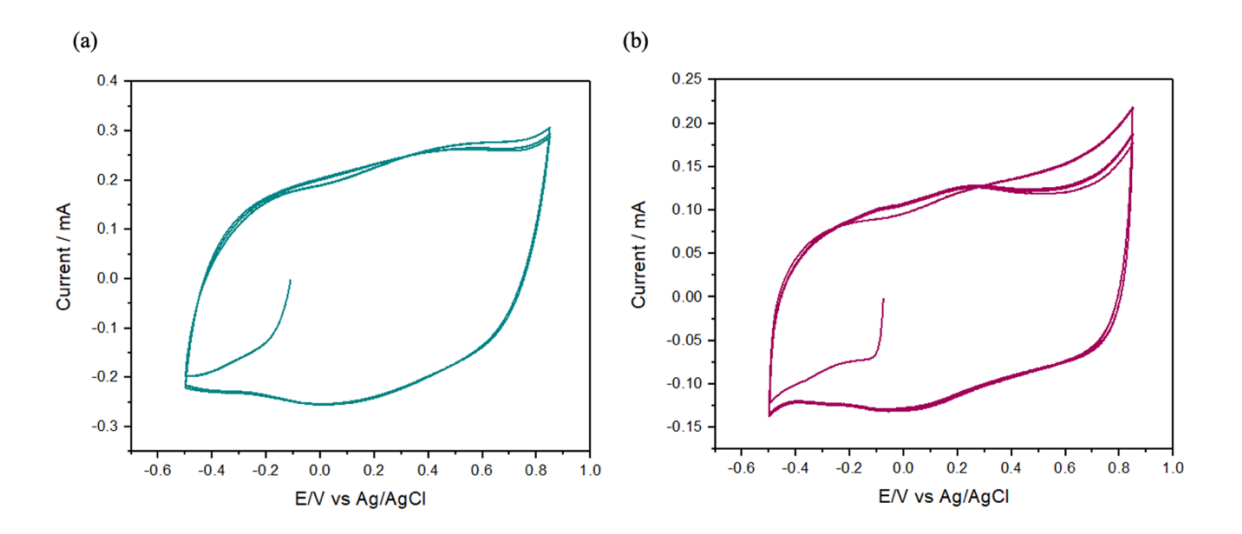


Figure 3.3. (a) Cyclic voltammogram of PEDOT/ClO₄ film cycled in 0.1 M LiClO₄ at 0.1 V/s (b) Cyclic voltammogram of PEDOT/NO₃ film cycled in 0.1 KNO₃ at 0.1 V/s. Both cyclic voltammograms were started at open circuit potential.

In order to determine the potentials at which doping and de-doping of anions occurred for each film, cyclic voltammograms were performed of both perchlorate and nitrate films. From this data the ion exchange processes which occur during the oxidation and reduction cycles can be seen, switching the polymer between conducting and non-conducting states. PEDOT exhibits p-type doping, thus, generating a positive charge upon oxidation. This positive charge is in the form of polarons and bipolarons which are delocalised across the polymer, generating conductivity.¹⁷ As a result of this net positive charge, anions from the supporting electrolyte will reside near the positively charged polarons and bipolarons for charge compensation.¹⁷ Figure 3.3 (a) displays the PEDOT/ClO₄ film cycled in LiClO₄. Upon oxidation, the film is becoming positively charged as a result of the formation of positively charged polarons and bipolarons. This charge is then compensated by the incorporation of perchlorate ions into the film at 0.4 V. Conversely, when the film is being reduced, the film becomes increasingly negatively charged, expelling the perchlorate ions from the film at 0 V, and returning it to its neutral non-conducting form. Similarly in Figure 3.3 (b), upon oxidation, nitrate ions are incorporated into the film at 0.2 V, while nitrate ions are then expelled from the film at 0 V. These experiments were necessary for the determination of potentials required for the doping and de-doping procedures for both individual systems. The diffusion coefficients for both perchlorate and nitrate species were calculated using the Randles-Sevcik equation (Eqt. 1.3) to investigate the rate at which the ions diffuse from the modified electrode to solution, and vice versa. The diffusion coefficients were calculated at the oxidation and reduction potentials that were used for the doping and de-doping procedures. The PEDOT/ClO₄ film had a diffusion coefficient of 1.9×10^{-8} cm² s⁻¹ at 0.5 V and 1.4×10^{-8} cm² s⁻¹ at -0.5 V. The PEDOT/KNO₃ film had a diffusion coefficient of 4.1×10⁻⁹ cm² s⁻¹ at 0.5 V and 4.5×10⁻⁹ cm² s⁻¹ at -0.2 V. From these values, the perchlorate ions diffuse to and from the polymer film at a faster rate than that of the nitrate ions. In comparison with the PEDOT/DBS film in Chapter 2, both perchlorate and nitrate ions diffuse at a faster rate than that of the potassium diffusing into the PEDOT/DBS film (diffusion coefficient of $1.52 \times 10^{-12} \text{ cm}^2 \text{ s}^{-1}$).

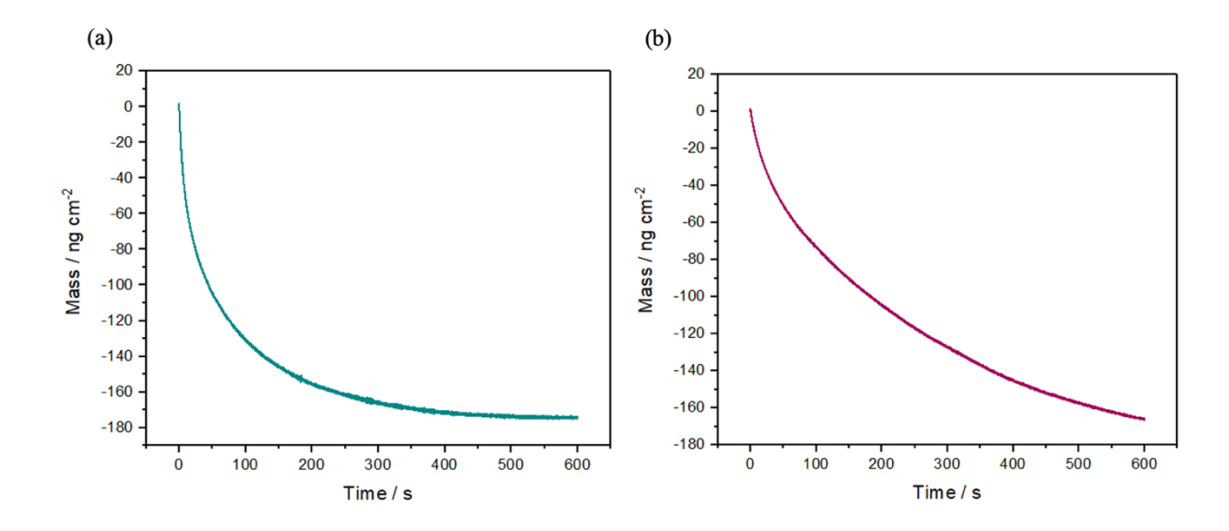


Figure 3.4. Mass change versus time graph of (a) ClO₄⁻ de-doping at -0.5 V for 600 seconds in 0.1 M LiClO₄ by chronoamperometry (b) NO₃⁻ de-doping at -0.2 V for 600 seconds in 0.1 M KNO₃ by chronoamperometry.

The idea of incorporating a primary dopant was established after the attempt to electropolymerise EDOT in the presence of naproxen resulted in no polymerisation. Reasons for this could be due to the lack of conductivity in the solution (low electrolyte concentration) resulting in a high solution resistance or perhaps the charge of the drug (not sufficiently negatively charged), preventing doping from occurring. Similar results were seen by Krukiewicz et al. as their group failed to initially polymerise EDOT with the drug. Chronoamperometry was used for the doping and de-doping procedures as it allowed for a specific voltage to be applied whilst a current versus time response was obtained. Sauerbrey's equation (Eqt. 1.4) was used to calculate the mass changes from the frequency results. It is important to note that there are limitations to the Sauerbrey equation, such as; (1) The equation assumes a thin, rigid film (2) The equation does not consider viscoelastic effects. ¹⁸ In Figure 3.4 (a), the initial primary dopant perchlorate is de-doped from the PEDOT/ClO₄ film upon the application of a negative voltage of -0.5 V for 600s. A reduction potential of -0.5 V was selected based on literature. Also, in the CV in Figure 3.3 (a), the reduction peak occurs at approximately 0 V, therefore a reduction potential of -0.5 V allows sufficient voltage for the removal of any dopants during chronoamperometry. After 600 seconds, the chronoamperometric mass results begin to plateau, evidently removing perchlorate from the film. The quantity of perchlorate removed was calculated to be 174 ng/cm². Similarly, the anionic dopant nitrate was expelled from the film by applying a negative potential of -0.2 V for 600 seconds in 0.1 M KNO₃. The value of -0.2 V was selected from the cyclic voltammogram results in Figure 3.3 (b), as the cathodic peak potential occurred at 0 V. -0.5 V was not used for the PEDOT/NO₃ film as a mass increase was observed at this potential. From the mass versus time graph in Figure 3.4 (b), there is a mass decrease as the negative potential is applied. An overall mass decrease of 166 ng cm⁻² was calculated, accounting for the removal of nitrate. The quantity of perchlorate de-doped from the film was calculated to be 1.75×10⁻⁹ mol/cm², while 2.67×10⁻⁹ mol/cm² of nitrate was removed from the film. The PEDOT/NO₃ film released more dopant than that of the PEDOT/ClO₄ film which could be due to the nitrate ion being more hydrophilic than the perchlorate ion.¹⁹

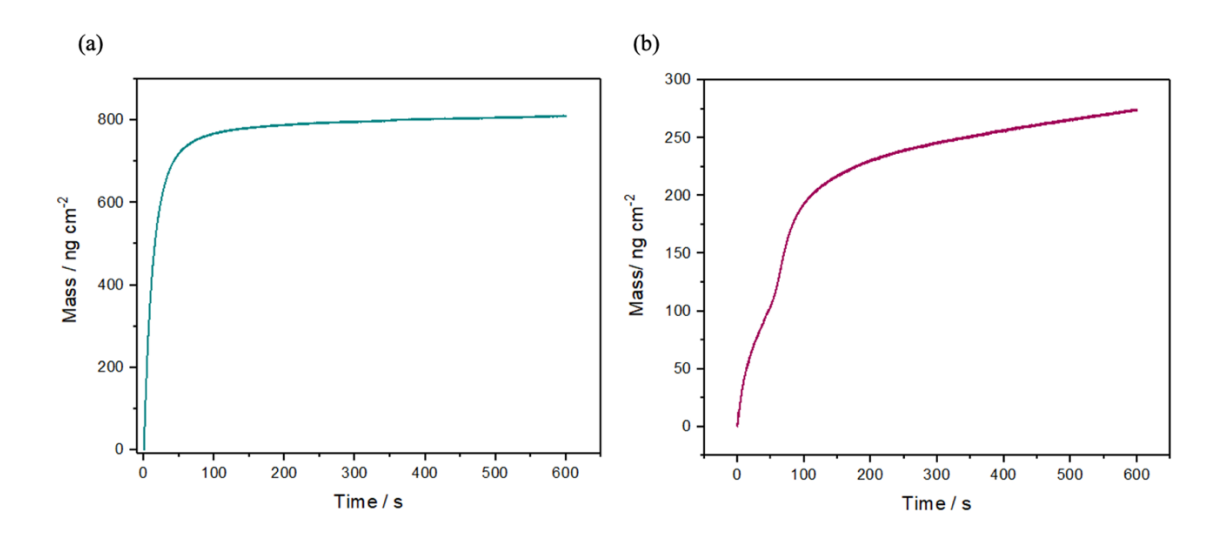


Figure 3.5. (a) PEDOT/ClO₄ film naproxen loading for 600 seconds at +0.5 V using chronoamperometry in 10 mM naproxen sodium salt (b) PEDOT/NO₃ film naproxen loading for 600 seconds at +0.5 V using chronoamperometry in 10 mM naproxen sodium salt.

Figure 3.5 (a) and (b) correspond to the drug loading of the anti-inflammatory drug naproxen. The drug was loaded by applying a potential of +0.5 V which was also selected based on the anodic peak potentials of the cyclic voltammograms in Figure 3.3 (a) and (b). Upon application of the positive potential in a naproxen DI water solution, the mass response obtained from the EQCM data suggests a mass increase with increasing time for 600 seconds. It appears as an exponential increase for both films with an initial steep

incline, followed by a plateau. As the positive charge is created on the PEDOT backbone, the naproxen in solution is compensating the charge due to its negative charge at a neutral pH. As time increases, the strength of the positive charge is being compensated, thus, no longer requiring the same quantity of naproxen to dope into the film, hence the mass tapering off between 300 and 600 seconds. 811 ng/cm² of naproxen was calculated to enter the PEDOT/ClO4 film. 274 ng/cm² was calculated to be incorporated into the PEDOT/NO3 film. The quantity of naproxen was also calculated, resulting in 3.22×10-9 mol/cm² of drug entering the PEDOT/ClO4 film and 1.09×10-9 mol/cm² of drug entering PEDOT/NO3 film. Interestingly, three times the amount of drug enters the PEDOT/ClO4 film which is likely due to the primary dopant having a hydrated radius bigger than the nitrate ion (0.24 nm and 0.18 nm respectively).

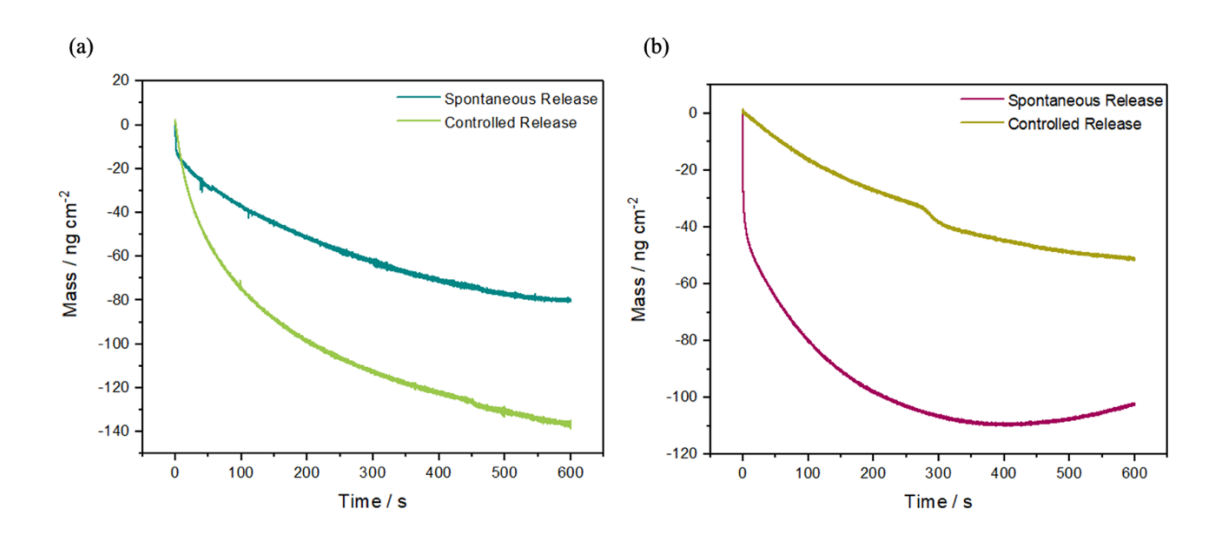


Figure 3.6. Mass versus time graph of (a) PEDOT/ClO₄ spontaneous release using open circuit potential for 600 seconds and controlled release at -0.5 V for 600 seconds (b) PEDOT/NO₃ spontaneous release using open circuit potential for 600 seconds and controlled release at -0.2 V for 600 seconds.

Spontaneous and controlled release of naproxen were calculated to understand the ability of the film to retain and distribute its contents when necessary. This process was essential in the on/off switch strategy that was proposed for the drug delivery system (i.e. releasing the drug upon electrochemical stimulation only). Spontaneous release was achieved by using open circuit potential as no current is flowing in the cell. 80.3 ng/cm² of drug was released spontaneously from the PEDOT/ClO₄ film which accounted for 9.9% of the

overall drug quantity removed. 102 ng/cm² of naproxen was released under OCP conditions (at 0.2 V) for PEDOT/NO₃. This accounts for 37.2 % of the drug that was initially incorporated into the film. When compared to the 80.3 ng cm⁻² of naproxen spontaneously released from the PEDOT/ClO₄ film, this shows that PEDOT/ClO₄ film has superior drug entrapment qualities. The removal of the drug during spontaneous release is not of upmost importance as the quantity release is miniscule in comparison to therapeutic ranges. When comparing these results with that performed by Krukiewicz et al., their PEDOT/ClO₄ film spontaneously released 2.19 µg/ cm² of naproxen after loading 5.57 µg/cm².⁴ The quantity of drug released (ng/cm²) by controlled release was achieved by applying a potential of -0.5 V for the PEDOT/ClO₄ film and -0.2 V for the PEDOT/NO₃ film (vs Ag/AgCl) for 600 seconds (Table 3.1). The quantity of drug released from the controlled release procedure for PEDOT/ClO₄ was calculated to be 136 ng/cm². Controlled release of the PEDOT/NO₃ film resulted in a mass decrease of 51 ng/ cm². The quantity (mol/cm²) of controlled drug release was also calculated for both films and is displayed in Table 3.2. The PEDOT/ClO₄ film demonstrates superior controlled release, releasing over double the amount of naproxen than that of the PEDOT/NO₃ film.

Table 3.1. Drug loading and release of naproxen from ClO₄ and NO₃ films. Mass calculated in ng cm⁻² unless stated otherwise. Mass calculated using Eqt 1.4. Note that this is a one-time experiment.

	PEDOT/CIO ₄	PEDOT/NO ₃
Polymer Film	19.0 μg cm ⁻²	13.4 μg cm ⁻²
Primary Dopant Removal	174.0	166.0
Naproxen Loading	811.0	274.0
Spontaneous Release	80.6	102.0
Naproxen Re-Loading	543	153.6
Controlled Release	136	51

Table 3.2. Calculated quantity of polymer film, drug loading and drug release from PEDOT/ClO₄ and PEDOT/NO3 films. Note that this is a one-time experiment.

	PEDOT/ClO ₄ (mol/cm ²)	PEDOT/NO ₃ (mol/cm ²)
Polymer Film	1.33×10 ⁻⁷	9.42×10 ⁻⁸
Primary Dopant Removal	1.75×10 ⁻⁹	2.67×10 ⁻⁹
Naproxen Loading	3.22×10 ⁻⁹	1.09×10 ⁻⁹
Spontaneous Release	3.18×10^{-10}	4.04×10^{-10}
Controlled Release	5.39×10 ⁻¹⁰	2.02×10 ⁻¹⁰

Table 3.3. Release kinetics of both PEDOT/ClO₄ and PEDOT/NO₃ films for both spontaneous and controlled release. The Avrami equation was used to calculate the rate constants and kinetic exponents (Eqt. 3.3). Note that these are a one-time experiment.

		Rate Constant k, s ⁻¹	Kinetic Exponent
PEDOT/CIO ₄	Spontaneous Release	5.83×10 ⁻³	0.457
	Controlled Release	1.84×10^{-2}	0.365
PEDOT/NO ₃	Spontaneous Release	0.160	0.184
	Controlled Release	2.782×10^{-3}	0.687

The rate constants and kinetic exponents for both release mechanisms were calculated using Avrami's equation (Eqt. 3.3). The Avrami equation is generally used to describe recrystallisation kinetics, however, it has been adapted and is frequently used to describe drug release kinetics.^{20,21} Firstly, the kinetic exponent calculated using the Avrami equation relates to the drug release mechanism, with values of 0.5 or less corresponding to Fickian diffusion, which is the diffusion of species from an area of higher concentration to an area of low concentration.²²⁻²³ Values ranging between 0.5 and 1.0 are referred to as anomalous transport, which includes a range of transport processes including polymer degradation, polymer swelling and drug diffusion.²⁴ Based on these values, the

PEDOT/ClO₄ controlled release mechanism is dominated by Fickian diffusion whilst the PEDOT/NO₃ film controlled release is a result of anomalous transport. With regard to release rates, the PEDOT/ClO₄ spontaneous release occurs at a slower rate than that of the controlled release which is expected as it would be assumed that upon application of a potential, the drug would be released at a faster rate. The PEDOT/ClO₄ controlled release also releases at a faster rate than the PEDOT/NO₃ controlled release. Interestingly, the PEDOT/NO₃ spontaneous release has the fastest release rate which is likely due to leaching of the drug from the film.

3.3.2. The Effects of Film Thickness on Drug Loading and Release

Building on the findings outlined in Section 3.3, the optimal primary dopant chosen was perchlorate, considering its drug loading and release capabilities. Three PEDOT/ClO₄ films of different thicknesses were investigated to understand the effects of varying thicknesses on the drug loading and release capacities. Films of varying sizes were investigated to understand the linearity of drug loading with film thickness. Mitoxantrone was used in this experimentation in the dihydrochloride form to improve its ability to dissolve in aqueous solutions. Mitoxantrone is a neutrally charged drug with a pka value of between 8.27 and 9.36, meaning that the compound is a weak acid and can donate a proton under certain conditions.²⁵ However, in the chosen electrolyte of approximately pH 7, it is likely that the drug will stay in the neutral or slightly positively charged form. As a result of this it is important to note that the PEDOT film is likely being doped with the negatively charge chloride ion with the possibility that the anti-cancer drug is being drawn into solution with solvent and ions during oxidation due to polymer swelling.

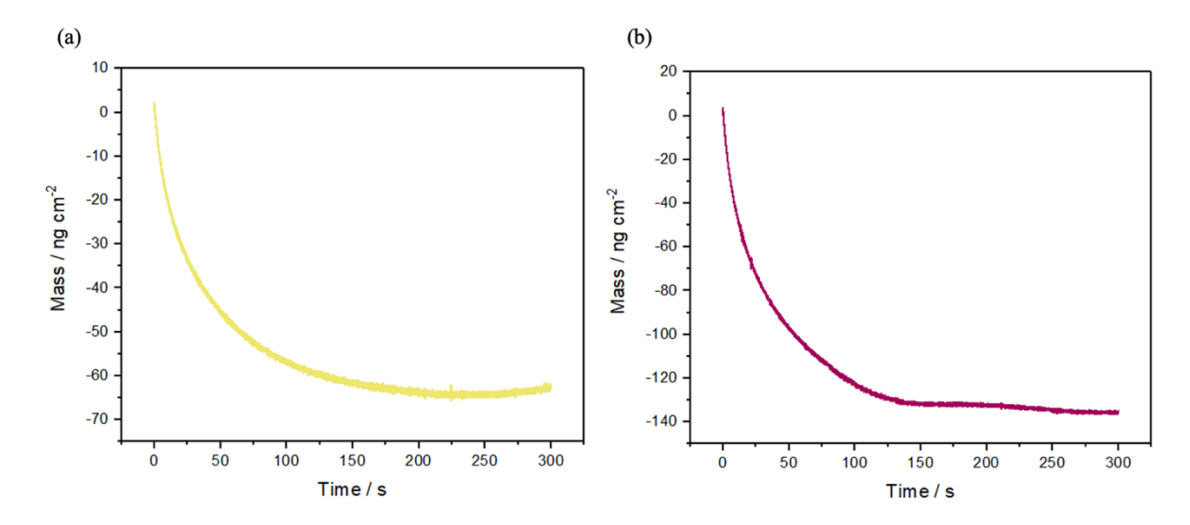


Figure 3.7. Mass versus time response of PEDOT/ ClO₄ film de-doping ClO₄ in 0.1 M LiClO₄ for 300 seconds at –0.5 V using chronoamperometry. Film thicknesses include (a) 10 mC and (b) 20 mC. Film formation was performed in 10 mM EDOT 0.1 M LiClO₄ solution using chronocoulometry.

PEDOT films of varying thicknesses (5, 10, 20 mC) were electrochemically polymerised using chronocoulometry. This technique involves the application of a potential in return for a charge versus time response. At a minimum, +0.85 V (versus Ag/AgCl) is required to initiate the oxidation of the PEDOT monomer, therefore, a positive voltage of 1.0 V was applied to begin the polymerisation. ^{12,13} Upon application of the positive voltage, the loss of an electron is initiated which results in the formation of cationic radicals. ¹⁴ As the PEDOT film grows, the charge increases as it is consumed by the electropolymerisation reaction. ²⁶ Perchlorate was then de-doped from the film by applying a cathodic potential of -0.5 V which was established from cyclic voltammogram performed in Figure 3.3 (a). The mass versus time graphs in Figure 3.7, show the removal of the perchlorate ion as the mass decreases upon application of the negative potential. As expected, the greatest quantity of perchlorate ion de-doping was performed by the 20 mC film, with a mass decrease of 136.0 ng cm⁻². From the calculated moles (Table 3.5) of perchlorate de-doped from the film, the quantity of primary dopant released linearly with film thickness.

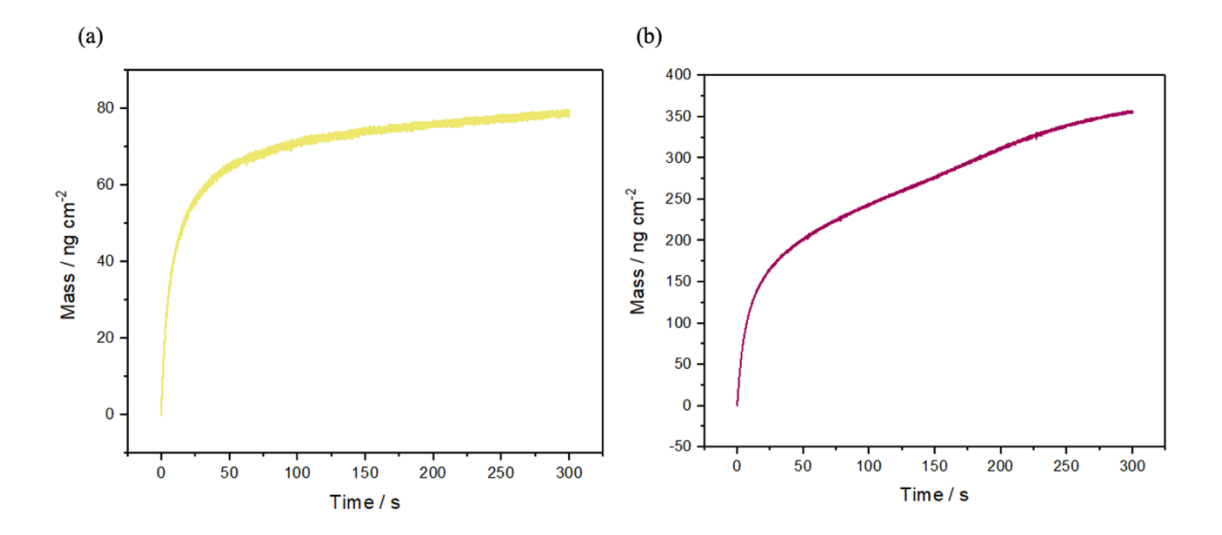


Figure 3.8. Mass versus time response of PEDOT/ClO₄ film loading with 5 mM anticancer drug mitoxantrone in DI water for 300 seconds at + 0.5 V using chronoamperometry. (a) 10 mC and (b) 20 mC.

Drug loading was performed for 300 seconds at a positive potential of +0.5 V for the incorporation of the drug into the film. Upon further investigation of the pka values for the mitoxantrone complex and the pH of the electrolyte solution (pH 6-7.5), it is likely that the drug would stay in the neutral or even slightly positively charged form.²⁷ As a result of this, the possibility of the chloride entering the film must be considered; however, it is possible that the drug is entering the film as a result of polymer swelling upon oxidation.²⁸ Ideally, further characterisation such as EDX would be performed on the film to confirm the presence of the drug through elemental analysis. Drug loading capacities were calculated using the Sauerbrey equation (Eqt. 1.4) and are displayed in Table 3.4. From the mass versus time graphs, the mass in each graph increased with increasing time, showing the loading of the drug into the film. Again, the 20 mC showed greatest loading, with the quantity (mol/cm²) increasing linearly with increasing film thickness.

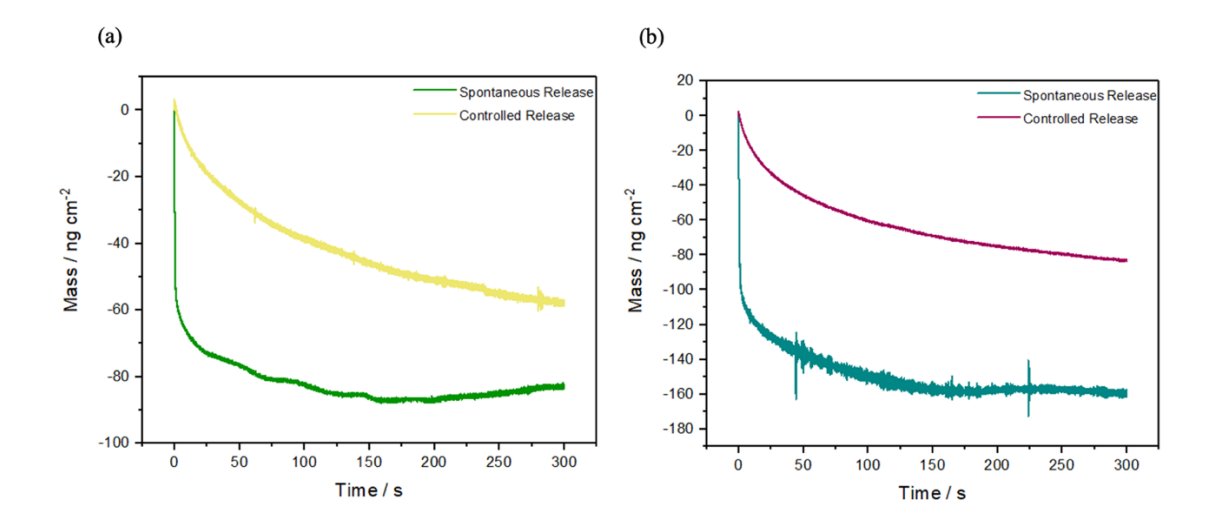


Figure 3.9. Mass versus time response of (a) 10 mC PEDOT/ClO₄ film spontaneous and controlled release of mitoxantrone (b) 20 mC PEDOT/ClO₄ film spontaneous and controlled release of mitoxantrone.

Spontaneous release was achieved by applying open circuit potential whilst using chronoamperometry. In each of the three films, spontaneous release released a higher concentration of drug than controlled release. This could be due to the size of the drug molecule, inhibiting its incorporation into the polymer film. In all of the spontaneous release graphs, there is an immediate mass loss in the first 10 seconds. This immediate mass decrease is likely due to an excess of drug located on the outside of the film, or possibly due to poor adherence of the species which would correlate with the neutral or slightly positive charge of the drug based on the pka values. Table 3.5 displays the quantity (mol/cm²) of material released upon controlled release (-0.5 V for 300 s) which demonstrates a linear increase in drug release with increasing film thickness. From this, the thickness of the film has a direct effect on the drug loading and release capabilities of polymer films.

Table 3.4. Mass changes of PEDOT/ClO₄ films of varying thicknesses at 300 seconds. Mass calculated using Eqt 1.4.

	5 mC	10 mC	20 mC
	(ng/cm ²)	(ng/cm ²)	(ng/cm ²)
ClO ₄ De-Doping	39.8	63.1	136.0
MDC Loading	64.6	78.3	356.0
MDC Spontaneous Release	38.7	83.5	162.0
MDC Re-Loading	63.8	20.5	134.0
MDC Controlled Release	36.2	58.7	83.4

Table 3.5. Calculated quantity of mitoxantrone for PEDOT/ClO₄ films of varying thicknesses after 300 seconds.

	5 mC	10 mC	20 mC
	(mol / cm ²)	(mol / cm ²)	(mol / cm ²)
ClO ₄ De-Doping	4.0×10 ⁻¹⁰	6.3×10 ⁻¹⁰	1.3×10 ⁻⁹
MDC Loading	1.2×10 ⁻¹⁰	1.5×10 ⁻¹⁰	6.8×10 ⁻¹⁰
MDC Spontaneous Release	7.4×10 ⁻¹¹	1.6×10 ⁻¹⁰	3.1×10 ⁻¹⁰
MDC Controlled Release	6.9×10^{-11}	1.1×10^{-10}	1.6×10^{-10}

3.4. Conclusion

In conclusion to the effects of primary dopants on the release of the anti-inflammatory drug naproxen (negatively charged drug at neutral pH), both polymer films demonstrate the ability to create a polymer-based drug delivery system based on redox switching. Overall, the PEDOT/ClO₄ film showed optimal results for both drug loading and release which is likely due to the larger size of the doping ion. The most successful drug loading was performed by the PEDOT/ClO₄ film, with an increased weight of 811 ng/cm² while PEDOT/NO₃ had a mass increase of 274 ng/cm². Interestingly, the significant difference in drug loading does not correlate with the quantity of primary ions removed from the films, proving that the size of the primary dopant has a direct effect on the quantity of material being doped into the film. PEDOT/ClO₄ had the most efficient controlled release, releasing 136 ng/cm² of naproxen. From the calculated rate constants, PEDOT/ClO₄ releases the drug via controlled release at a faster rate than that of PEDOT/NO₃ which was calculated using the Avrami equation. Overall, the data suggests that the primary dopant does have a substantial effect on the doping capabilities of the polymer system. The effects of varying film thicknesses were investigated to understand the influence of film thickness on drug loading and release. As expected, the film thickness has a direct correlation with the quantity of material loaded and released. In terms of loading and spontaneous release, the quantity of material increases linearly with increasing film thickness. From this work, it is clear that the drug loading and release mechanism using conducting polymers is achievable, having the ability to dope and de-dope the polymer film upon the application of a potential. Overall, this work effectively demonstrates the influence of the primary doping ion and film thickness on the drug loading and release capabilities of a polymer-based drug delivery system. This Chapter acts as a stepping stone to Chapter 4 where the fundamental of bipolar electrochemistry is discussed for the future work (Chapter 7) of creating a wireless drug delivery system.

3.5. References

- (1) Park, Y.; Jung, J.; Chang, M. Research Progress on Conducting Polymer-Based Biomedical Applications. *Applied Sciences* **2019**, *9* (6), 1070. https://doi.org/10.3390/app9061070.
- (2) Smith, J. Conducting Polymers as Drug Release Systems. In Nano- and Microfabrication Techniques in Drug Delivery; Lamprou, D., Ed.; Advanced Clinical Pharmacy - Research, Development and Practical Applications; Springer Nature, 2022.
- (3) Marcus, Y. Ionic Radii in Aqueous Solutions. *Chem. Rev.* **1988**, *88* (8), 1475–1498. https://doi.org/10.1021/cr00090a003.
- (4) Krukiewicz, K.; Kruk, A.; Turczyn, R. Evaluation of Drug Loading Capacity and Release Characteristics of PEDOT/Naproxen System: Effect of Doping Ions. *Electrochimica Acta* 2018, 289, 218–227. https://doi.org/10.1016/j.electacta.2018.09.011.
- (5) Krukiewicz, K.; Kowalik, A.; Turczyn, R.; Biggs, M. J. P. In Vitro Attenuation of Astrocyte Activation and Neuroinflammation through Ibuprofen-Doping of Poly(3,4-Ethylenedioxypyrrole) Formulations. *Bioelectrochemistry* **2020**, *134*, 107528. https://doi.org/10.1016/j.bioelechem.2020.107528.
- (6) Bard, A. J.; Faulkner, L. R.; White, H. S. *Electrochemical Methods: Fundamentals and Applications*; John Wiley & Sons, 2022.
- (7) Bai, L.; Yuan, R.; Chai, Y.; Yuan, Y.; Wang, Y.; Xie, S. Direct Electrochemistry and Electrocatalysis of a Glucose Oxidase-Functionalized Bioconjugate as a Trace Label for Ultrasensitive Detection of Thrombin. *Chem Commun (Camb)* **2012**, *48* (89), 10972–10974. https://doi.org/10.1039/c2cc35295h.
- (8) Sauerbrey, G. Verwendung von Schwingquarzen zur Wägung dünner Schichten und zur Mikrowägung. *Z. Physik* **1959**, *155* (2), 206–222. https://doi.org/10.1007/BF01337937.
- (9) Otgonbayar, Z.; Yang, S.; Kim, I.-J.; Oh, W.-C. Surface Modification Effect and Electrochemical Performance of LiOH-High Surface Activated Carbon as a Cathode Material in EDLC. *Molecules* **2021**, *26* (8), 2187.
- (10) Jokanović, V.; Čolović, B.; Dutour Sikirić, M.; Trajković, V. A New Approach to the Drug Release Kinetics of a Discrete System: SiO2 System Obtained by

- Ultrasonic Dry Spraying. *Ultrasonics Sonochemistry* **2013**, *20* (1), 535–545. https://doi.org/10.1016/j.ultsonch.2012.08.015.
- (11) Sun, X. S. 11 PLASTICS DERIVED FROM STARCH AND POLY (LACTIC ACIDS). In *Bio-Based Polymers and Composites*; Wool, R. P., Sun, X. S., Eds.; Academic Press: Burlington, 2005; pp 369–410. https://doi.org/10.1016/B978-012763952-9/50012-5.
- (12) Pigani, L.; Heras, A.; Colina, Á.; Seeber, R.; López-Palacios, J. Electropolymerisation of 3,4-Ethylenedioxythiophene in Aqueous Solutions. *Electrochemistry Communications* **2004**, *6* (11), 1192–1198. https://doi.org/10.1016/j.elecom.2004.09.021.
- (13) Lupu, S.; Lakard, B.; Hihn, J.-Y.; Dejeu, J. Novel in Situ Electrochemical Deposition of Platinum Nanoparticles by Sinusoidal Voltages on Conducting Polymer Films. *Synthetic Metals* **2012**, *162* (1), 193–198. https://doi.org/10.1016/j.synthmet.2011.11.031.
- (14) Nie, S.; Li, Z.; Yao, Y.; Jin, Y. Progress in Synthesis of Conductive Polymer Poly(3,4-Ethylenedioxythiophene). *Front Chem* **2021**, *9*, 803509. https://doi.org/10.3389/fchem.2021.803509.
- (15) Peerce, P. J.; Bard, A. J. Polymer Films on Electrodes: Part II. Film Structure and Mechanism of Electron Transfer with Electrodeposited Poly(Vinylferrocene). *Journal of Electroanalytical Chemistry and Interfacial Electrochemistry* 1980, 112 (1), 97–115. https://doi.org/10.1016/S0022-0728(80)80011-8.
- (16) Gruia, V.-T.; Ispas, A.; Efimov, I.; Bund, A. Cation Exchange Behavior during the Redox Switching of Poly (3,4-Ethylenedioxythiophene) Films. *J Solid State Electrochem* **2020**, *24* (11), 3231–3244. https://doi.org/10.1007/s10008-020-04809-6.
- (17) Le, T.-H.; Kim, Y.; Yoon, H. Electrical and Electrochemical Properties of Conducting Polymers. *Polymers* **2017**, *9* (4), 150. https://doi.org/10.3390/polym9040150.
- (18) Vogt, B. D.; Lin, E. K.; Wu, W.; White, C. C. Effect of Film Thickness on the Validity of the Sauerbrey Equation for Hydrated Polyelectrolyte Films. *J. Phys. Chem. B* **2004**, *108* (34), 12685–12690. https://doi.org/10.1021/jp0481005.
- (19) Urbansky, E. T. Perchlorate Chemistry: Implications for Analysis and Remediation. *Bioremediation Journal* **1998**, 2 (2), 81–95. https://doi.org/10.1080/10889869891214231.

- (20) Alshammary, B.; Casillas, N.; Cook, R. B.; Swingler, J.; Ponce de León, C.; Walsh, F. C. The Importance of the Film Structure during Self-Powered Ibuprofen Salicylate Drug Release from Polypyrrole Electrodeposited on AZ31 Mg. *J Solid State Electrochem* 2016, 20 (12), 3375–3382. https://doi.org/10.1007/s10008-016-3288-2.
- (21) Shamaeli, E.; Alizadeh, N. Nanostructured Biocompatible Thermal/Electrical Stimuli-Responsive Biopolymer-Doped Polypyrrole for Controlled Release of Chlorpromazine: Kinetics Studies. *International Journal of Pharmaceutics* **2014**, 472 (1), 327–338. https://doi.org/10.1016/j.ijpharm.2014.06.036.
- (22) Ritger, P. L.; Peppas, N. A. A Simple Equation for Description of Solute Release I. Fickian and Non-Fickian Release from Non-Swellable Devices in the Form of Slabs, Spheres, Cylinders or Discs. *Journal of Controlled Release* **1987**, *5* (1), 23–36. https://doi.org/10.1016/0168-3659(87)90034-4.
- (23) Fu, Y.; Kao, W. J. Drug Release Kinetics and Transport Mechanisms of Non-Degradable and Degradable Polymeric Delivery Systems. *Expert Opin Drug Deliv* 2010, 7 (4), 429–444. https://doi.org/10.1517/17425241003602259.
- (24) Siepmann, J.; Siepmann, F. Mathematical Modeling of Drug Delivery. International Journal of Pharmaceutics 2008, 364 (2), 328–343. https://doi.org/10.1016/j.ijpharm.2008.09.004.
- (25) Manallack, D. T. The pKa Distribution of Drugs: Application to Drug Discovery. *Perspect Medicin Chem* **2007**, *1*, 25–38.
- (26) Martinez, J. G.; Mehraeen, S.; Jager, E. W. H. Electrochemical Considerations for the Electropolymerization of PPy on PEDOT:PSS for Yarn Actuator Applications. *ChemElectroChem* 2023, 10 (15), e202300188. https://doi.org/10.1002/celc.202300188.
- (27) Beranek, R. (Photo)Electrochemical Methods for the Determination of the Band Edge Positions of TiO₂-Based Nanomaterials. *Advances in Physical Chemistry* **2012**, *2011*, e786759. https://doi.org/10.1155/2011/786759.
- (28) Otero, T.; Romero, M. Poly (3, 4-Ethylendioxithiophene) (PEDOT) Oxidation: Activation Energy and Conformational Energy. *Journal of Physics: Conference Series* **2008**, *127*, 012016. https://doi.org/10.1088/1742-6596/127/1/012016.

Chapter 4

Wirefree and Conventional Electrodeposition of PEDOT Films

4. Wirefree and Conventional Electrodeposition of PEDOT Films

4.1. Introduction

Bipolar or wireless electrochemistry (BPE) allows redox processes, such as the electrodeposition of a conducting polymer film, to occur without any physical wire between a power source and the working electrode.^{1,2} This system has been known for some time with Fleischmann et al. recording the 'electrical conduction of spherical particles fluidised by electrolyte flow' in the late 1960s.³ At least two driving or feeder electrodes, which have no direct contact to the bipolar electrode, are connected to a power supply resulting in the generation of an electric field. ^{1,4,5} The strength of the electric field is determined by the voltage applied to the feeders that ultimately induces potentials in the BPE that can drive anodic reduction and oxidation processes.⁶

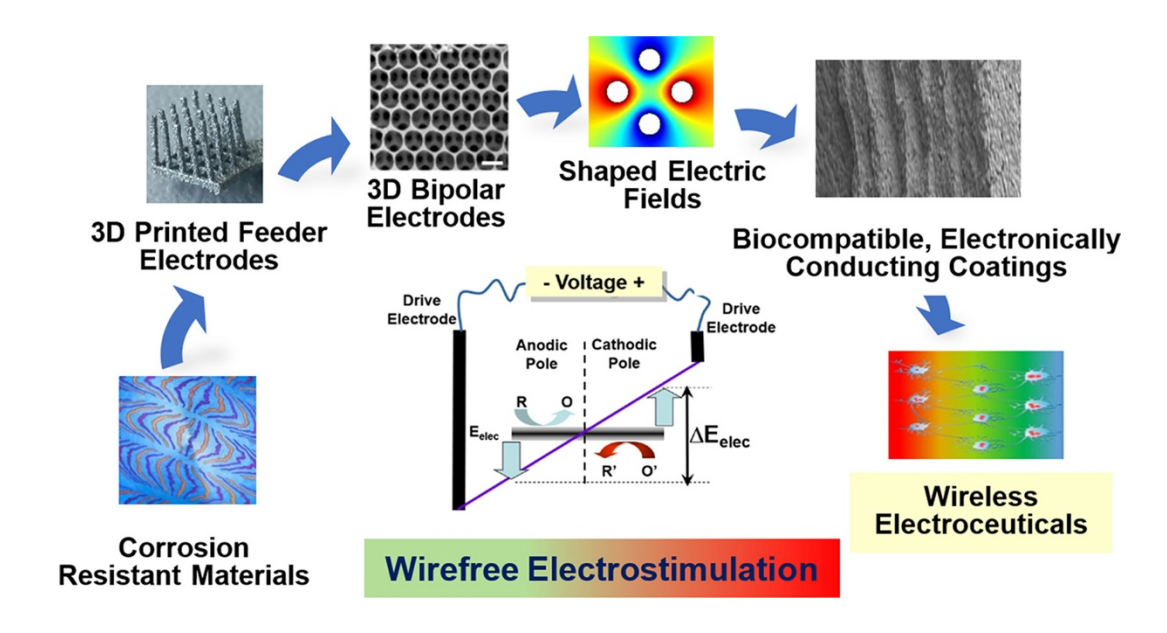


Figure 4. 1. Diagram depicting the diverse applications for wireless electrostimulation. Extracted from Forster.²

As illustrated in Figure 4.1, wireless electrochemistry has many possible applications, from elucidating the initiation and development of disease, to the treatment of diseases through electroceuticals.² The purpose of this work is to develop a deep understanding of the electric field generated in a bipolar (BP) cell to enable future applications such as the electrostimulation of biological cells.^{1,7} The approach is to wirelessly polymerise

poly(3,4-ethylenedioxythiophene) (PEDOT) which should reflect the voltage distribution across the bipolar electrode (BPE). By adjusting different variables such as concentration, voltage, and time, a more in-depth understanding of the electric field distribution can be achieved. In this work, bipolar PEDOT films and conventional PEDOT films have been compared based on film thicknesses, electronic structure, homogeneity, morphology, and surface free energy. The wireless polymerisation is carried out in electrolyte free Milli-Q water and is expected to be in an 'un-doped' state as no doping anion was deliberately added to the solution, whereas the conventional deposition is carried out with 0.1 M LiClO₄ as electrolyte. The BP experimentation was performed in an electrolyte free medium as electrolyte distorts the electric field distribution.⁸ The structure and spectroscopic properties of both films were analysed by UV-vis spectroscopy. These results suggest that both bipolar and conventional deposition methods yield the same PEDOT material. These results give a promising insight into the possibilities of conducting polymers in bipolar electrochemistry for application in water treatment,⁹ cell stimulation¹ and drug delivery.¹⁰

4.2. Materials and Methods

4.2.1. Materials

All materials used throughout this experimentation were of reagent grade and were obtained from Merck. Fluorine doped tin oxide glass (10 cm x 10 cm x 2.3 mm) was purchased from Merck and cut using a diamond glass cutter purchased from Amazon. Purified water was used throughout and had a resistivity of $18.2 \text{ M}\Omega$ cm.

4.2.2. Bipolar Setup

The bipolar electrochemical cell was designed in house using FreeCAD and printed in acrylonitrile butadiene styrene (ABS) filament using an Ultimaker S5 3D printer. The cell was designed with a 3 cm separation between feeder electrodes that precisely accommodates a 2 cm x 1 cm internal cavity for the BPE, to ensure alignment. A well and tweezer slot were placed below and to the side of the (FTO) for easy removal without damaging the polymer film. The objects were unified and cut out using the Boolean operation on FreeCAD, and then exported as an stl file. Cura software was used to adjust specific parameters (resolution, infill density, temperature) for 3D printing. The cell was printed with ABS filament using normal resolution of 0.15 mm with an infill density of 20%, and was printed at a temperature of 230°C. The BP cell was powered using the EA-

PS 5200-02A power supply. FTO glass was used as the BPE and titanium as the feeder electrodes. FTO electrodes of approximately $2\pm 0.2\,$ cm $\times 1\pm 0.2\,$ cm were sonicated in an alcohol (ethanol/ isopropanol) and dried using nitrogen gas prior to use. A multimeter was used to determine which side of the glass had the FTO layer by measuring the resistance. The titanium electrodes were sanded using 1600 grit sandpaper between experiments and were approximately 2cm x 1cm x 2mm in size. Bipolar polymerisation was achieved using 3 ml of 10 mM EDOT in deionised water solution. The voltage induced across the BPE was calculated using the following equation (Eqt.1.1):

$$\Delta E_{elec} = E_{tot} \left(\frac{l_{elec}}{l_{channel}} \right)$$
 Eqt. 1.1

where $l_{channel}$ is the distance between driving electrodes, l_{elec} is the length of the BPE, and E_{tot} is the total voltage applied to the system.

4.2.3. Electrochemical Setup

Cyclic voltammetry was performed using AutoLab (Metrohm) systems potentiostat. FTO electrode (2 cm × 1 cm) with a working surface area of 1 cm² was used as the working electrode by covering the remaining slide with teflon tape. This was performed to provide a consistent surface area between experiments, and to allow sufficient space for the crocodile clip to attach to the electrode. An Ag/AgCl (saturated KCl) was used as the reference electrode, and coiled platinum wire counter electrode with area of ≈3.62 cm² completed the three-electrode setup. For conventional polymerisation, galvanostatic polymerisation was performed using a current of 0.0002 A. All films were cycled in 0.1 M LiClO₄ solutions. Film thickness was calculated using the following equation (Eqt. 4.1):¹¹

$$l_f = \frac{Q_p M_w}{\eta_e F \rho_f A}$$
 Eqt. 4.1

where Q_p polymerisation charge (t x I), M_w molecular weight of the monomer, η_e number of electrons (2.25), F faraday's constant, ρ_f film density (assume 1 g/cm³) and A area (1 cm²).

Surface coverage was calculated using the following (Eqt. 2.1):12

$$\Gamma = Q/nFA$$
 Eqt. 2.1

where Γ is the surface coverage of the modified electrode in mol/cm², Q is the total charge of the electrode in C, n is the number of transferred electrons (assuming 2.25), 13,14 F is Faraday's constant, and A is the surface area of the electrode in cm².

4.2.4. Profilometry

Profilometry was performed on the Bruker DektakXT profilometer. BP samples that were polymerised at 30 V for 20 minutes in 10 mM EDOT in DIW were prepared by removing half of the polymer on the horizontal axis of the BPE. This was achieved by placing a ruler on the horizontal axis of the BPE and wiping off the polymer with forceps and a lint free tissue that was dampened with milli-Q water. This was performed as it provided an accurate step from the bare FTO to the polymerised area. The stylus was moved from the bare FTO side to the polymerised side. Five runs of each sample were performed at 0.05 cm, 0.1 cm, 0.2 cm, 0.3 cm and 0.4 cm from the edge of the BPE anode.

4.2.5. UV-Vis Spectroscopy

UV-Vis spectroscopy was performed using the Agilent Cary UV-Vis spectrometer. Samples included conventional PEDOT/Cl and PEDOT/ClO₄ films, as well as BP PEDOT films which were polymerised at 30V for 20, 30 and 40 minutes on FTO. The PEDOT films on FTO were loaded into an inhouse 3D printed sample holder within the spectrometer which allowed the sample height to be adjusted as well as keeping the sample vertical. The blank used for UV-vis spectroscopy included a clean FTO BPE that was exposed to BP conditions at 30 V for 20 minutes in Milli-Q water. Gaussian

deconvolutions of the conventional and bipolar PEDOT films were performed to gain an understanding of the electronic states of the materials.

4.2.6. Microscopy

A Nikon eclipse ME600 microscope was used to visualise the polymerisation profile on the BPE electrode. This was achieved by measuring the distance from the edge of the anode of the BPE to the location where there is no polymer film deposited. This method does not have the sensitivity to detect very thin layers/monolayers. The microscope images were captured using a camera inserted into the microscope and were displayed using S-EYE software. The percentage surface coverage was calculated by dividing the measured polymerisation distance by the length of the BPE. This number shows approximately how much of the FTO BPE is covered in polymer (cm²).

4.2.7. Scanning Electron Microscopy

The Jeol JSM-IT 100 InTouchScope electron microscope was used to image the BP PEDOT films on FTO using an accelerating voltage of 2.0 kV and a secondary electron detector. BP films were polymerised in 10 mM EDOT in DI water at 30 V for 20 minutes. The positive side of the BPE (where PEDOT was polymerised) was visible using the microscope. This was used as a reference point for the imaging location on the BPE.

4.2.8. Surface Free Energy

Contact angle measurements were performed using an FTA200 Dynamic Contact Angle analyser. A single droplet of deionised water was deposited on the bare FTO, modified BPE, and conventional films, and the resulting contact angle was measured. PEDOT films formed using the bipolar setup were polymerised in a 10 mM EDOT in Mill-Q water solution at 30 V for 20 minutes. The droplet of deionised water was located across the gradient bipolar polymerised PEDOT film. Conventional polymerisation was achieved by polymerising EDOT in a standard three electrode set up using an FTO (1cm² working area) working electrode, Ag/AgCl reference electrode (saturated KCl) and a coiled platinum wire counter electrode ($\approx 3.62~\rm cm^2$). Conventional polymerisation was performed by applying 200 μA for 300 seconds in 10 mM EDOT 0.1 M LiClO4 solution as this setup produced the same quantity of PEDOT as the 30 V 20 minute BP experiments.

4.3. Results and Discussion

4.3.1. Computer Aided Design (CAD) and 3D Printing

FreeCAD was used to design the in house bipolar electrochemical cell. Cura software was used to convert CAD files into stl files for compatibility with the 3D printer. As illustrated in Figure 4.2, the cell was based on a two, 2 mm, feeder electrodes and one bipolar electrode located between the feeders. After troubleshooting various designs, the following design was used for all experiments. The titanium feeder electrodes were separated by a distance of 3 cm. A 2 cm x 1 cm BPE slot was incorporated in the design to ensure accurate alignment of the BPE and consistency in FTO sizes. A 1 cm x 1 cm well was also incorporated in the design to prevent the FTO suctioning to the base of the cell. A tweezer slot was placed perpendicular to the FTO slot for ease of FTO removal after polymerisation. Prior to selecting a 3D printing material, the stability of each material towards dissolution in EDOT and pyrrole was tested. The materials tested included acrylonitrile butadiene styrene (ABS), tough polylactic acid (PLA), and composite conductive PLA. A droplet of concentrated EDOT monomer was dropped onto each material and was checked every thirty minutes for two hours. ABS showed the best results as the monomer did not interact with the material within the first hour.

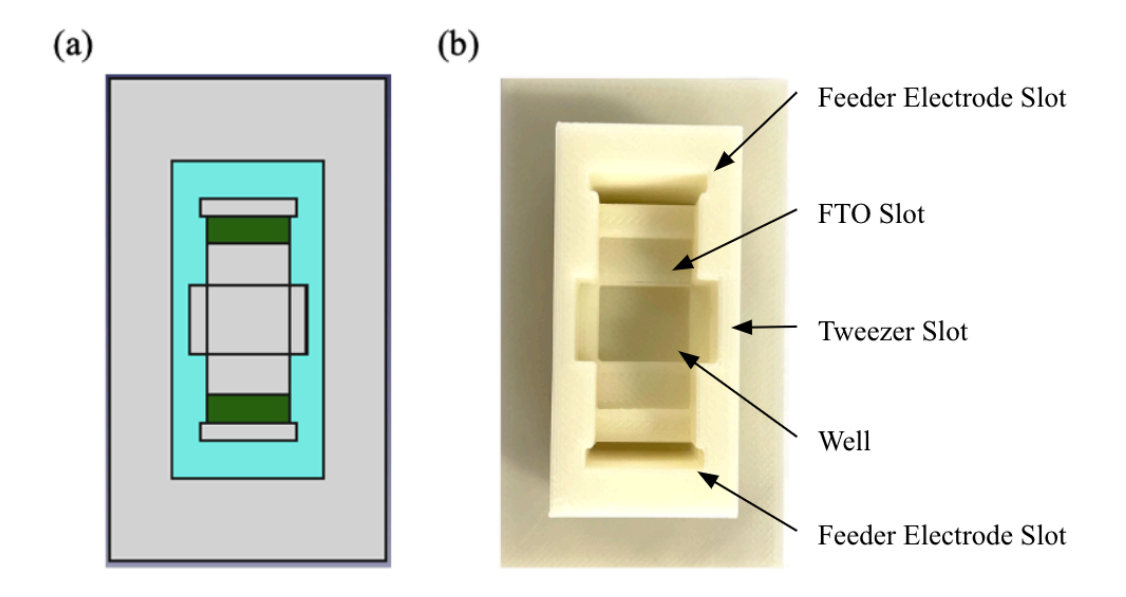


Figure 4. 2. (a) FreeCAD design of the in house bipolar electrochemical cell with two feeder electrodes, FTO slot, and tweezer slot (b) 3D printed bipolar electrochemical cell printed in acrylonitrile butadiene styrene (ABS).

4.3.2. Bipolar Polymerisation

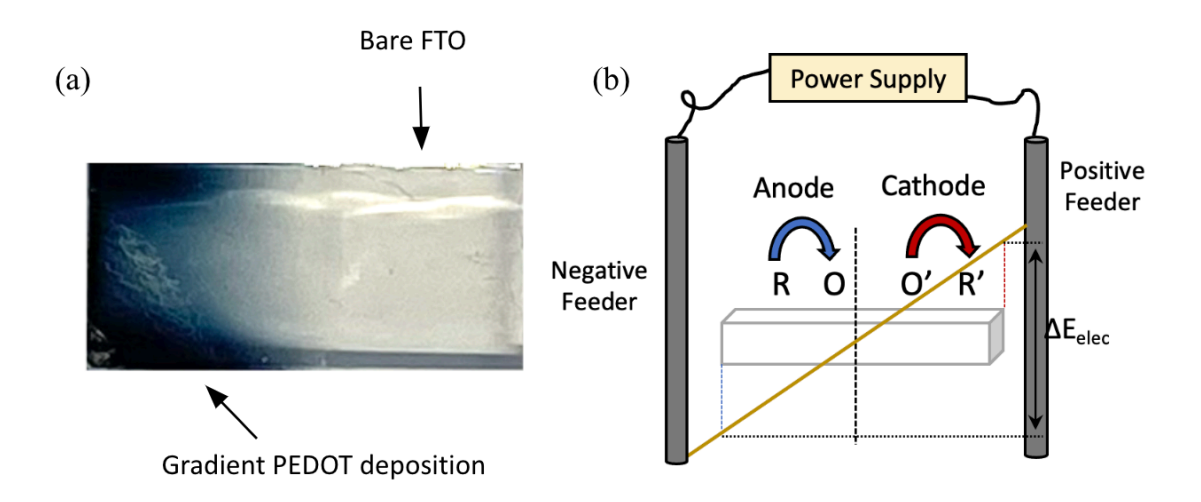


Figure 4. 3. (a) Bipolar electrode (BPE) after bipolar polymerisation in a two-feeder set up as shown in Figure 4.2. BP polymerisation was performed in a 10 mM EDOT DI water solution at 30 V for 20 minutes on FTO glass (BPE) (b) linear potential decay model currently used to describe the bipolar system.

Polymerisation using bipolar electrochemistry was performed in a two-feeder electrode system using a 30 V potential difference between the two feeder electrodes (10 V cm⁻¹) for 20 minutes in Milli-Q water without deliberately added electrolyte. Figure 4.3 (a) shows the corresponding PEDOT deposition on the FTO glass BPE, resulting in a 'U' shaped deposition. Using Eqt. 1.1, the voltage experienced at the edges of the BP anode and cathode were calculated to be +10 V and -10 V respectively. CV in a conventional electrode cell indicates EDOT polymerises at 0.85 V, therefore the BP system is expected to provide ample voltage for the polymerisation processes across much of its surface. 15 The polymerisation of EDOT is initiated through the oxidation of the monomer, resulting in two polymer growth pathways; (1) cationic radical coupling (2) reactions between the cationic radicals and the neutral monomer, resulting in polymer formation. ¹⁶ In Figure 4.3 (a), it is clear that PEDOT is deposited on the BPE, forming a gradient blue layer on the substrate surface as a result of the potential difference across the BPE. The unexpected 'U' shaped deposition of the BP polymerised PEDOT has been recorded by other research groups, and is likely to be a result of the distortion of the electric field once the BPE is inserted, resulting in thicker PEDOT deposition at the edges of the BPE.8 Conducting polymers are renowned for their conductivity, which is derived in part from the 'doping' process. PEDOT exhibits p-type doping, meaning that positively charged polarons and bipolarons form upon oxidation, resulting in anions from the electrolyte solution entering the PEDOT film to maintain electroneutrality.¹⁷ However, in the bipolar system, no electrolyte is intentionally added, and the BP film could be in the un-doped state, and therefore less conductive than a doped PEDOT film. Doped PEDOT shows conductivity levels of 5400 S/cm, whereas conductivity levels of PEDOT are 0.1 S/cm in the undoped form. 18,19 Sheet resistance measurements were performed using four point probe; however, due to interactions with the FTO substrate the results were not included as they were not conclusive.

4.3.3. Conventional Electropolymerisation

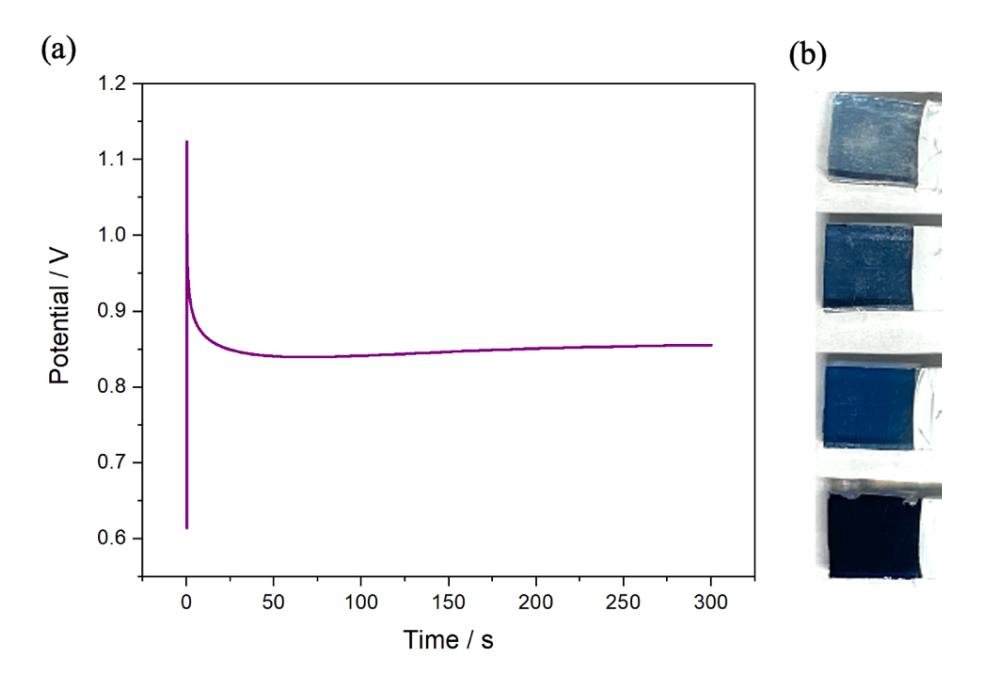


Figure 4. 4. (a) Galvanostatic polymerisation of EDOT for 300 s at 200 μ A in 10 mM EDOT 0.1 M LiClO₄ on FTO glass (b) Images from top to bottom of PEDOT polymerised at 200 μ A for 100, 200, 300 and 600 seconds in 10 mM EDOT 0.1 M LiClO₄ solution on FTO glass.

Conventional polymerisation was carried out using galvanostatic polymerisation of EDOT for 100, 200, 300 and 600 seconds in LiClO₄, as seen in Figure 4.4 (b). The galvanostatic polymerisation method involves the application of a constant current, resulting in a potential versus time response. As seen in Figure 4.4 (a), to support a current of 200 μA,²⁰ the potential initially shifts to approximately 1.12 V, providing sufficient voltage to oxidise the monomer at the bare electrode.¹⁵ The potential then decreases to approximately 0.85 V after 25 seconds due to the presence of oligomers on the electrode surface, which reduces the potential required for monomer oxidation.²¹ This steady state potential of 0.85 V is maintained for the remainder of the polymerisation as PEDOT continues to be deposited on the underlying PEDOT film.²⁰ As illustrated in Figure 4.4 (b), the conventional PEDOT/ClO₄ polymerisation produced films with a uniform coverage across the electrode, unlike the BP films shown in Figure 4.3 that show differences in coverage across the positive pole of the bipolar electrode. As shown in Figure 4.4 (b), as polymerisation time increases, the film becomes darker in colour,

indicating an increase in material being deposited on the FTO surface. The conventional PEDOT films are intentionally doped with ClO₄⁻ while the films produced using bipolar electrochemistry do not contain perchlorate and may not be doped.

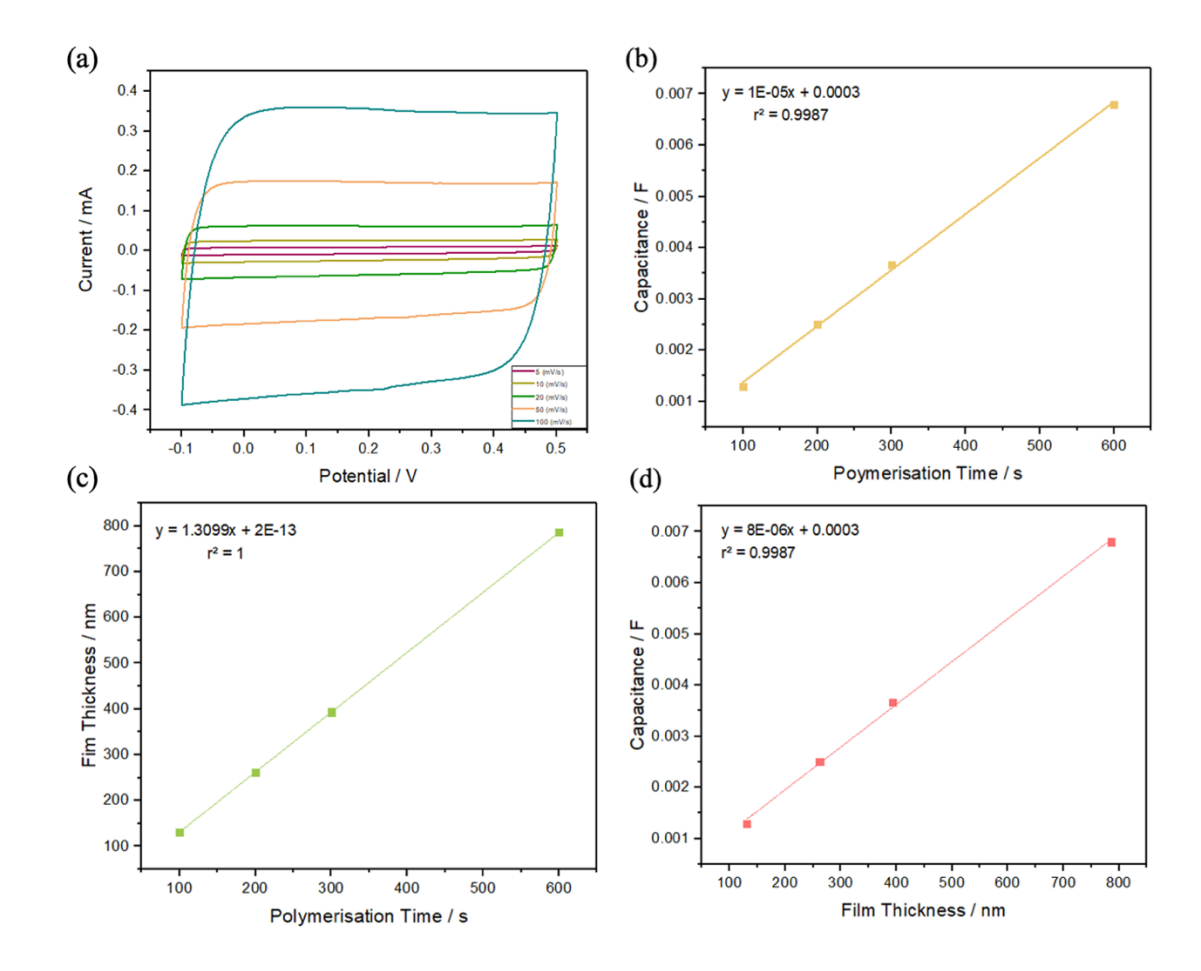


Figure 4. 5. (a) Scan rate study of the PEDOT/ClO₄ film in 0.1 M LiClO₄ from 5 mV/s to 100 mV/s (b) Conventional film capacitance versus polymerisation time (c) Film thickness versus polymerisation time calculated using Eqt. 4.1 (d) Capacitance versus film thickness for the conventional PEDOT film.

The film capacitance depends on its thickness and composition/physicochemical properties. Therefore, the capacitance of the conventional film was determined so that is could be compared with the values obtained for the films produced using BPE. Film capacitance was calculated by measuring the scan rate dependent current at 0.2 V as seen in Figure 4.5 (a). At 0.2 V the current is dominated by film charging and no faradaic processes are occurring. Capacitance values were required to determine a conventional

polymerisation time that deposited the same amount of material as the optimised BP 30 V 20 minutes film. An increased polymerisation time increases the quantity of material deposited linearly which is illustrated in Figure 4.5 (b). Using the polymerisation charge, the film thicknesses of the conventionally deposited films were calculated using Eqt. 4.1. From this, the film thickness was plotted against the capacitance values obtained in Figure 4.5 (b) and the equation of the line was used to calculate the amount of time required by conventional polymerisation to produce a film with the same amount of deposited PEDOT as the BPE. The 30 V 20 minute bipolar film equated to 294 s of galvanostatic polymerisation at 200 μA . The film thickness for the BP film was calculated at an average of $\approx\!385$ nm, while the film thickness for a 294 s conventional polymerisation was $\approx\!377$ nm.

4.3.4. UV-vis of Conventional and Bipolar Films

UV-Vis spectroscopy can provide useful insights into the chemical composition and band gaps of electronically conducting polymers both of which can be influenced by the conditions used to electrodeposit CP films, e.g., applied potential, deposition rate, electrolyte etc.^{22,23} Moreover, UV-Vis can be used to determine the oxidation and doping states of the material. For example, doped PEDOT shows conductivity levels of 5400 S/cm, and 0.1 S/cm in the undoped form which is reflected in the UV-Vis spectrum.^{18,19} Understanding the extent of doping is especially important in the case of wirefree deposition since polymerisation can be achieved even in "electrolyte free" media, perhaps allowing the relative importance of electronic and ionic conductivity to be uniquely investigated. Figure 4.6 shows the UV-Vis spectra for a PEDOT film deposited using a 2 cm long FTO bipolar electrode and an electric field of 10 V cm⁻¹ in Milli-Q water in the absence of deliberately added electrolyte. Figure 4.6 also shows the UV-Vis spectrum for a PEDOT film that was electrodeposited in 10 mM EDOT in 0.1 M LiClO₄ at a current of 200 µA for 300 seconds.

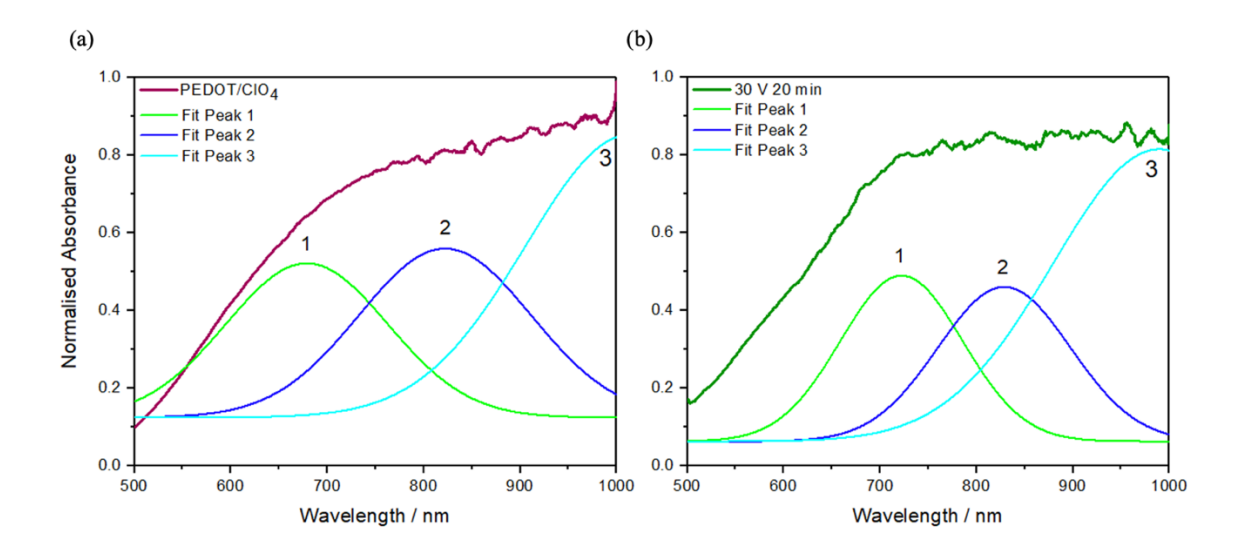


Figure 4. 6. Normalised absorbance of 400 nm – 1000 nm wavelength light through (a) conventionally deposited PEDOT/ClO₄ on FTO by applying 200 μA for 300 seconds in 10 mM EDOT 0.1 M LiClO₄ (purple) and (b) bipolar deposited PEDOT on FTO polymerised at 30 V for 20 minutes in 10 mM EDOT Milli-Q water (green).

Figure 4.6 shows that the material deposited using bipolar and conventional approaches are similar with both absorbing strongly from 650 nm to 1200 nm which is consistent with both films being in the polaronic state.²⁴ This is an interesting observation as the BP polymerisation of EDOT was performed in Milli-Q water, with no intentionally added electrolyte which would have led to the assumption that the BP film would be un-doped. Gaussian deconvolution was performed on both data sets to reveal the peak positions within the spectra. From this, information regarding electronic states can be further investigated through the gaussian peak locations. Three peaks were identified in the PEDOT/ClO₄ film, which corresponds to three transition states of the polymer. The initial peak at 680 nm (PEDOT/ClO₄ film) and 710 nm (BP film) corresponds to the transition of a lower polaronic band to a higher polaronic band while the second peak which is occurring at approximately 850 nm for both films also corresponds to polaronic and bipolaronic transitions of the PEDOT film. The third gaussian peak which occurs at 1000 nm is a result of both polaron and bipolaron absorption. ^{25,26} From this it can be concluded that both the BP and conventional films possess similar electronic states and possibly similar doping levels, suggesting that these materials are analogous. This is a significant result due to the absence of electrolyte during the bipolar polymerisation process as well as the substantially different voltages used to polymerise the monomer.

4.3.5. Influence of Deposition Time on PEDOT Film Formation

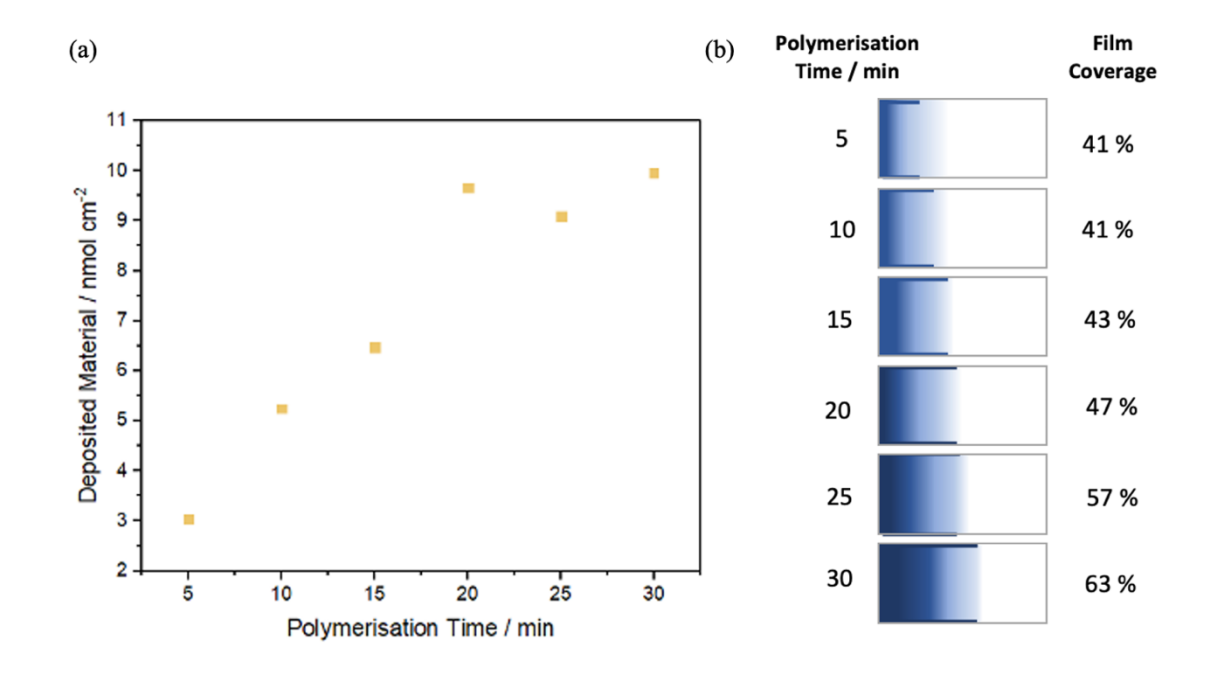


Figure 4. 7. The influence of time on BP polymerisation (a) The quantity of PEDOT deposited at constant 30 V for 5 to 30 minutes in a 10 mM EDOT DI water solution (b) Film surface coverage across the length of the BPE. Polymerisation was performed at a constant 30 V for varying times of 5 to 30 minutes.

The effect of polymerisation time on BP polymerisation was investigated by applying a constant potential of 30 V for 5, 10, 15, 20, 25 and 30 minutes. A scan rate study was then performed for each BPE in 0.1 M LiClO₄ using a traditional three-electrode cell. Film capacitance was calculated by measuring the scan rate dependent current at 0.2 V. In order to calculate the quantity (mol/cm²) of deposited EDOT using Eqt. 2.1, charge was obtained by multiplying capacitance by the potential window of 0.6 V. The film coverage was calculated by measuring the polymerisation distance across the length of the BPE using a microscope. The distance was calculated from the edge of the FTO, to a point where no blue film could be observed on the electrode surface. This method does not take thin films/monolayers into consideration. Figure 4.7 displays the amount of EDOT material deposited on the BPE surface per polymerisation time, which follows a linear incline followed by a plateau at higher polymerisation times. The first observation to be made regarding the samples in Figure 4.7 (b) is that they do not follow the linear model

in Figure 4.3 (b). The well-known linear model that is used to describe BP processes, suggests a zero potential in the centre of the BPE with the rest of the BPE having an incremental potential increase/decrease. An observation that confirms the inaccuracy of the linear potential decay model is the polymerisation distance. At higher polymerisation times, 25 and 30 minutes, polymerisation is occurring on more than 50% of the BPE, showing that zero potential is not in the centre of the BPE as previously thought. From this work, it is clear that time has a significant influence on the processes occurring at the BPE, and possibly impacts the movement of zero potential from what was initially thought to occur at the centre of the BPE.

4.3.6. Influence of Voltage on Linear Potential Decay

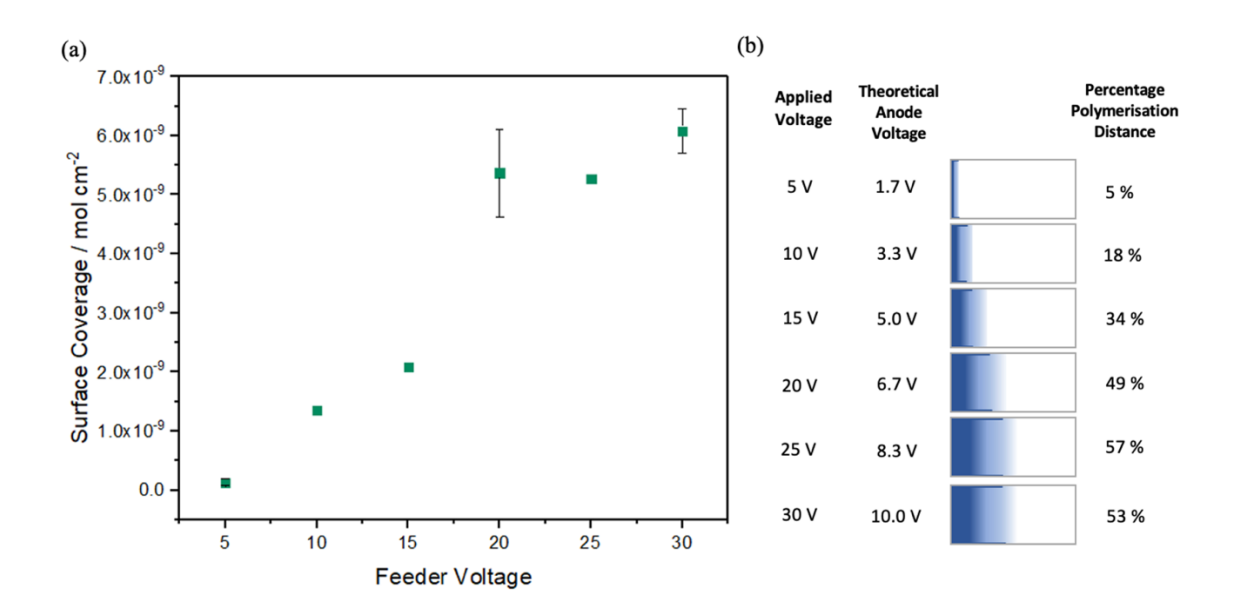


Figure 4. 8. The influence of the voltage applied to the feeder electrodes on BP polymerisation. (a) Dependence of the quantity of PEDOT deposited on the BPE as the voltage dropped across the two feeder electrodes is varied. The deposition time is 15 minutes. Diagram of the bipolar polymerised PEDOT on the FTO surface at varying voltages for constant time 15 minutes. BP polymerisation was performed in 10 mM EDOT Milli-Q water solution from 5 V to 30 V.

The effects of voltage on the deposition of EDOT was investigated by applying voltages of 5, 10, 15, 20, 25, and 30 V to the bipolar system while keeping time constant at 15 minutes. This experimentation was performed to understand the potential distribution across the BPE. Theoretically, the BPE experiences a linear decay across entire BPE as shown in Figure 4.3 (b),^{6,27} thus, the centre of the BPE theoretically experiences a potential of zero volts. The potential distribution across the BPE was calculated using Eqt. 1.1. Film capacitance was calculated by measuring the scan rate dependent current at 0.2 V. Bare FTO capacitance was also calculated (1x10⁻⁶ F) and subtracted from all BPE polymerisation results. The film capacitance was then converted to charge by multiplying the capacitance by the potential window of 0.6 V. From this, Eqt. 2.1 was used to calculate the surface coverage (mol/cm²). This work demonstrates that the applied voltage has a direct effect on the quantity of PEDOT material deposited on the BPE. As

shown in Figure 4.8 (a), as the voltage increases, the quantity of deposited PEDOT is also increasing, demonstrating a directly proportional relationship, aligning with the findings presented in Figure 4.8 (b). Based on Figure 4.8 (b), as the voltage rises, the length of the deposition also increases due to the heightened voltage being experienced across the BPE. For example, when a voltage of 10 V is applied, the BP anode theoretically experiences 3.3 V, while the cathode experiences -3.3 V. Whereas when 30 V is applied to the system, 10 V is theoretically experienced at the edge of the BP anode, hence the increased deposition of PEDOT. In comparison to the bipolar system schematic in Figure 4.3 (b), the experimental results show that the BPE does not experience a linear potential effect, which is evident when viewing the 25 V and 30 V samples in Figure 4.8. These samples show polymerisation beyond the centre of the BPE which is not expected based on the current bipolar theory that the centre of the BPE equates to 0 V. This phenomenon has not been seen in the literature to the best of the authors knowledge.

4.3.7. Profilometry

Profilometry was performed on the optimised PEDOT BP (polymerised at 30 V for 20 minutes in 10 mM EDOT in Milli-Q water) films to understand the height steps due to the electric field distribution. In these measurements, the PEDOT film was mechanically removed across the horizontal axis as shown in Figure 4.9 (a). This created a step from which the stylus could measure the thickness of the deposited film. Profilometric experiments were only performed to a distance of 0.4 cm (from the edge of the BP anode to the centre of the BPE) since beyond this distance the film thickness was less than approximately 25 nm. As illustrated in the diagram in Figure 4.9, the quantity of deposition varies across the BPE as a result of changing potentials. Consequently, thicker deposition occurs at the end close to the feeder which generates a more positive potential, while deposition becomes thinner toward the centre of the BPE. These values are quantitatively shown in Figure 4.9 (b) with the BP positive pole averaging a maximum thickness of ≈280 nm at the edge parallel to the feeder, which decreases to 125 nm within a distance of 0.15 cm from the edge. These results correlate with the potential distribution studies shown in Figure 4.8, confirming that a potential decay is occurring across the BPE, consequently resulting in a gradient quantity of material being deposited from the edge of the positive BP pole to the opposing end of the BPE.

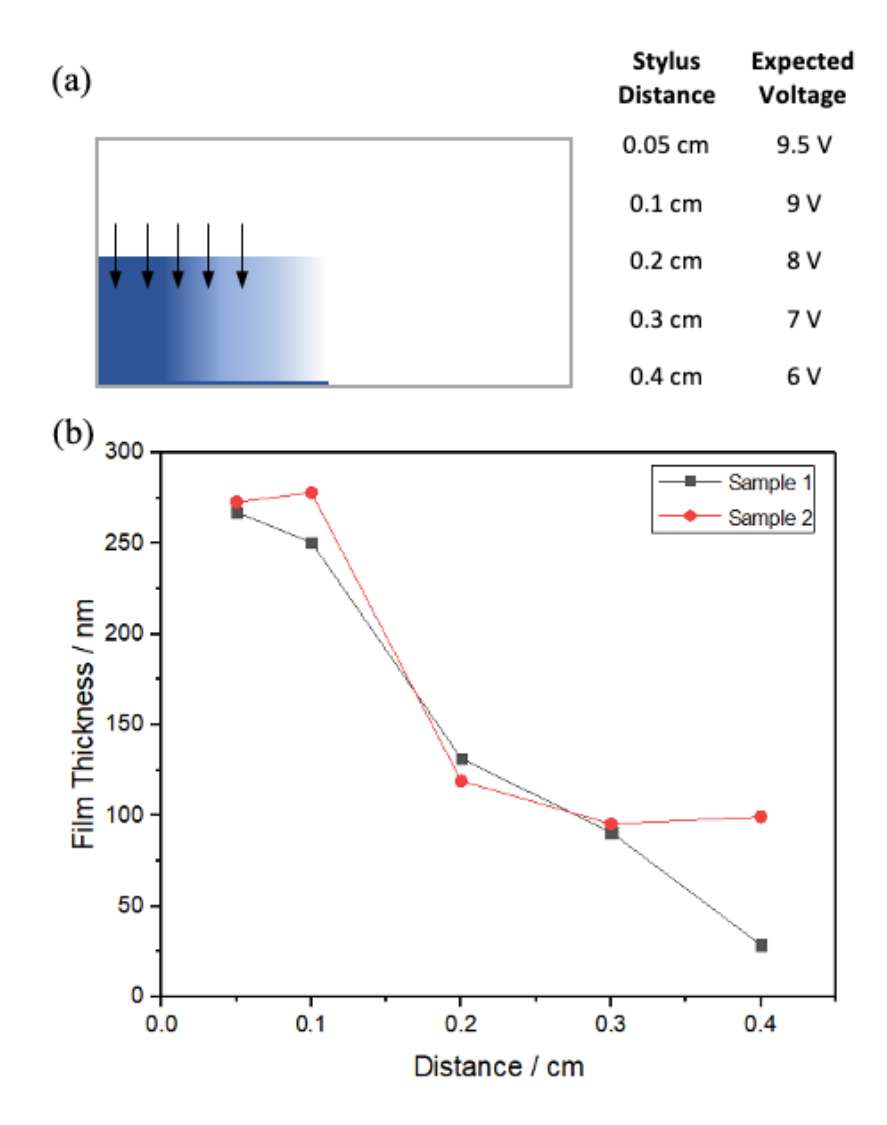


Figure 4. 9. (a) Diagram of a BP PEDOT film deposited on FTO using a feeder voltage drop of 30 V for 20 minutes in 10 mM EDOT Milli-Q water solution. Half of the deposited film was removed to create a clean step for the stylus, as described in Section 4.2.4. The arrows show the stylus paths. The stylus distance represents the location across the length of the BP. (b) Dependence of the film thickness with increasing distance from edge of the BPE anode towards the centre of the BPE.

The profilometry data indicates that the film is thicker on the edge that sits parallel to the feeder electrode to which the negative potential is applied which induces a positive potential in the BPE thus driving PEDOT deposition. These results also demonstrate that the magnitude of the voltage induced in the BPE (if the electric field strength is uniform as assumed in the classical model of Figure 4.3 (b)) affects the quantity of PEDOT deposited, showing that as voltage decreases, film thickness and therefore quantity of material, also decreases.

Significantly, thicker PEDOT deposition was also observed at the edges of the FTO that are perpendicular to the feeder electrodes. This behaviour could arise because of a) the BPE is distorting the shape of the electric field b) the edges of the FTO are rougher than the centre of the FTO after cutting or c) an inhomogeneous field at the edges of the BPE because the feeder and BP electrodes are the same width.

4.3.8. Influence of Mass Transport Effects

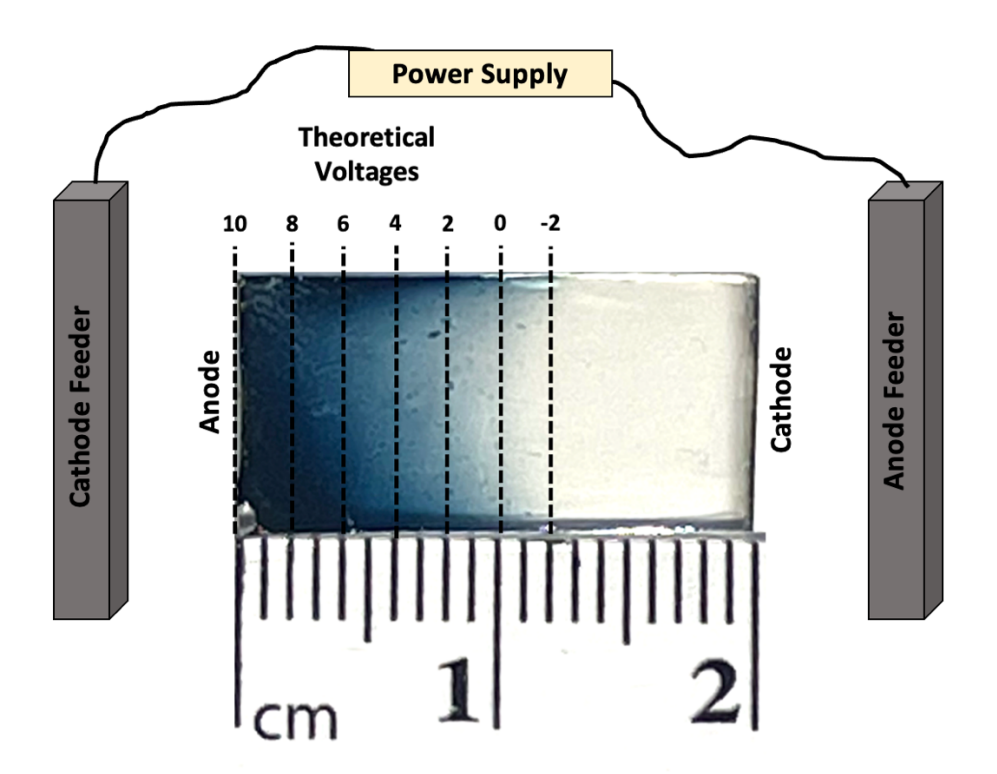


Figure 4. 10. Schematic representation of a 30 V 30 minute bipolar polymerisation in 10 mM EDOT Milli-Q water solution. The maximum possible voltages, calculated using Eqt. 1.1, are indicated along the length of the BPE.

Voltages were calculated at different distances along the bipolar electrode to identify and compare the areas of polymerisation with the induced voltage. Interestingly, PEDOT can be seen to have deposited in areas which is not expected when compared to the well-known linear potential decay model shown in Figure 4.3 (b). Since the BPE is 2 cm in length, zero volts occurs at 1 cm, so any polymerisation beyond this point is occurring at an electrode surface that has a negative induced potential. Since EDOT polymerisation involves the formation of cation radicals and commences at approximately 0.85 V vs. Ag/AgCl,²⁸ polymerisation beyond the mid-point is not expected. However, as shown in Figure 4.10 for a 30 V 30 minute BP polymerisation, the film is seen as far as 2.6 mm beyond the mid-point of the BPE. The main reason for this being that bipolar electrochemistry involves an electric field through the solution which drives electrophoresis.²⁹ The effects of the electric field result in the movement of charged particles, which in this case come in the form of cationic radicals and oligomers and the

effects may be especially pronounced since the deposition is carried out in the absence of deliberately added electrolyte. From the experimental results, it is possible that EDOT cation radicals migrate in the electric field beyond the point where they were generated, oligomerise in solution and then deposit on the BPE at a location where the induced potential is insufficient for direct electropolymerisation. In fact, oligomers could be seen swirling in solution during the bipolar experimentation, leading to the conclusion that stirring as a result of the electric field has a significant influence on where deposition occurs. As a note, an important requirement for a significant electric field is the presence of a low concentration electrolyte.^{5,30}

4.3.9. Scanning Electron Microscopy

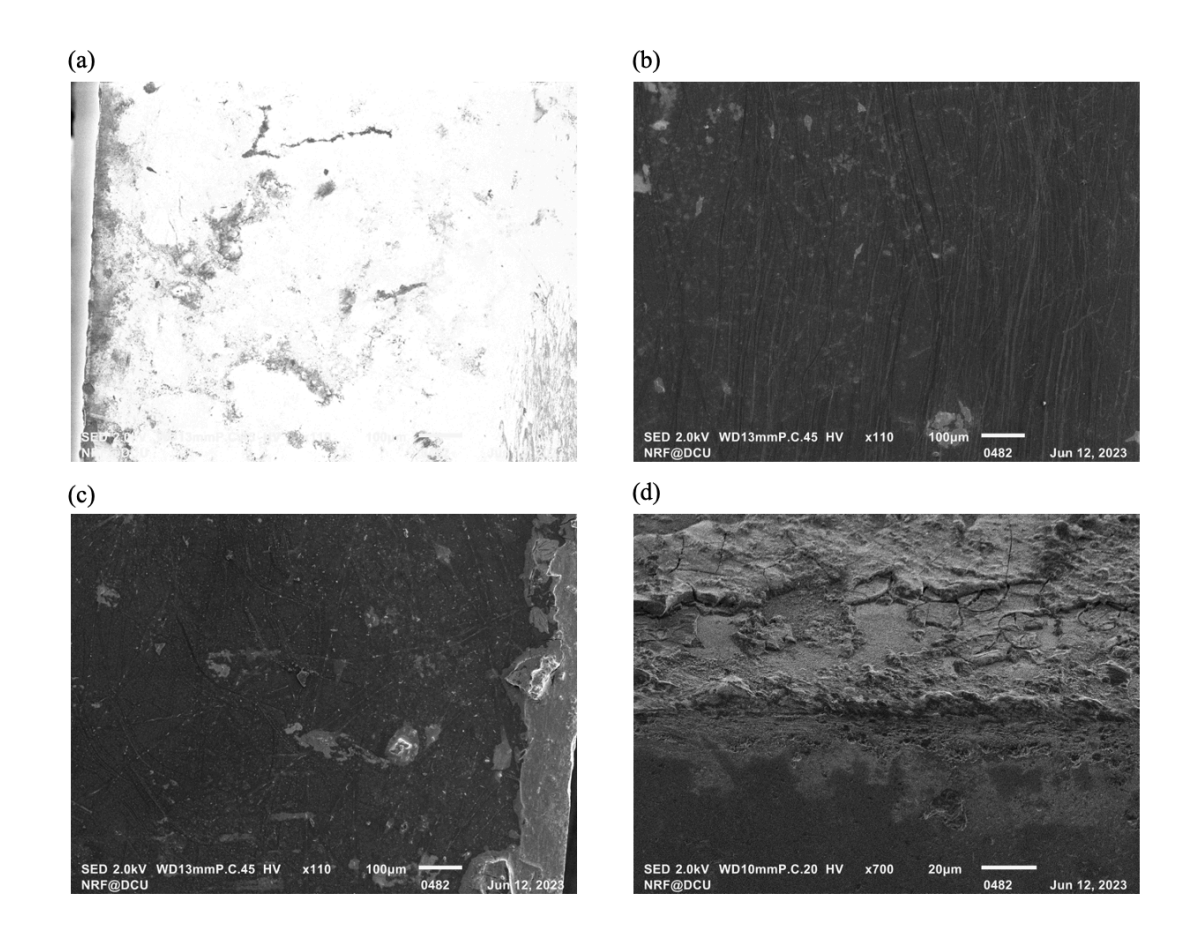


Figure 4. 11. SEM images of (a) bipolar electrode negative pole after polymerisation at 30 V for 20 minutes in 10 mM EDOT Milli-Q water (b) bipolar electrode positive pole after polymerisation at 30 V for 20 minutes in 10 mM EDOT in Milli-Q water (c) edge of the bipolar electrode positive pole after 30 V 20 minute polymerisation of 10 mM EDOT in Milli-Q water film (d) Horizontal edge (2 cm side) of the bipolar positive pole after 30 V 20 minute polymerisation of 10 mM EDOT in Milli-Q water.

Figure 4.11 (a) shows the BP negative pole after polymerisation at 30 V for 20 minutes in a 10 mM EDOT Mill-Q water solution which shows no PEDOT polymerisation. The FTO surface appears polymer free, however, there is noticeable deposition at the edge of the BP cathode which was seen visually upon bipolar polymerisation. At this moment it is unclear what this material is, however, this will be characterised in future work. Figure 4.11 (b) showcases the optimised PEDOT film (polymerisation at 30 V for 20 minutes) which has a smooth morphology. An interesting observation involves the vertical lines evident in this image, which may arise from the electric field or potentially from scratches on the thick FTO layer on the glass prior to polymerisation. Figure 4.11 (c) also displays

the BP deposited PEDOT at the anode of the BPE. The image shows a network of ridges in the PEDOT film which is most likely due to the polymer formation in the electric field. Figure 4.11 (d) presents a side view of the PEDOT film, revealing the rough, thick film on the FTO substrate. The rough texture of the film would promote stable biological cell adhesion, which could broaden the uses of this substrate for applications such as cell stimulation, which has .^{1,31}

4.3.10. Surface Free Energy

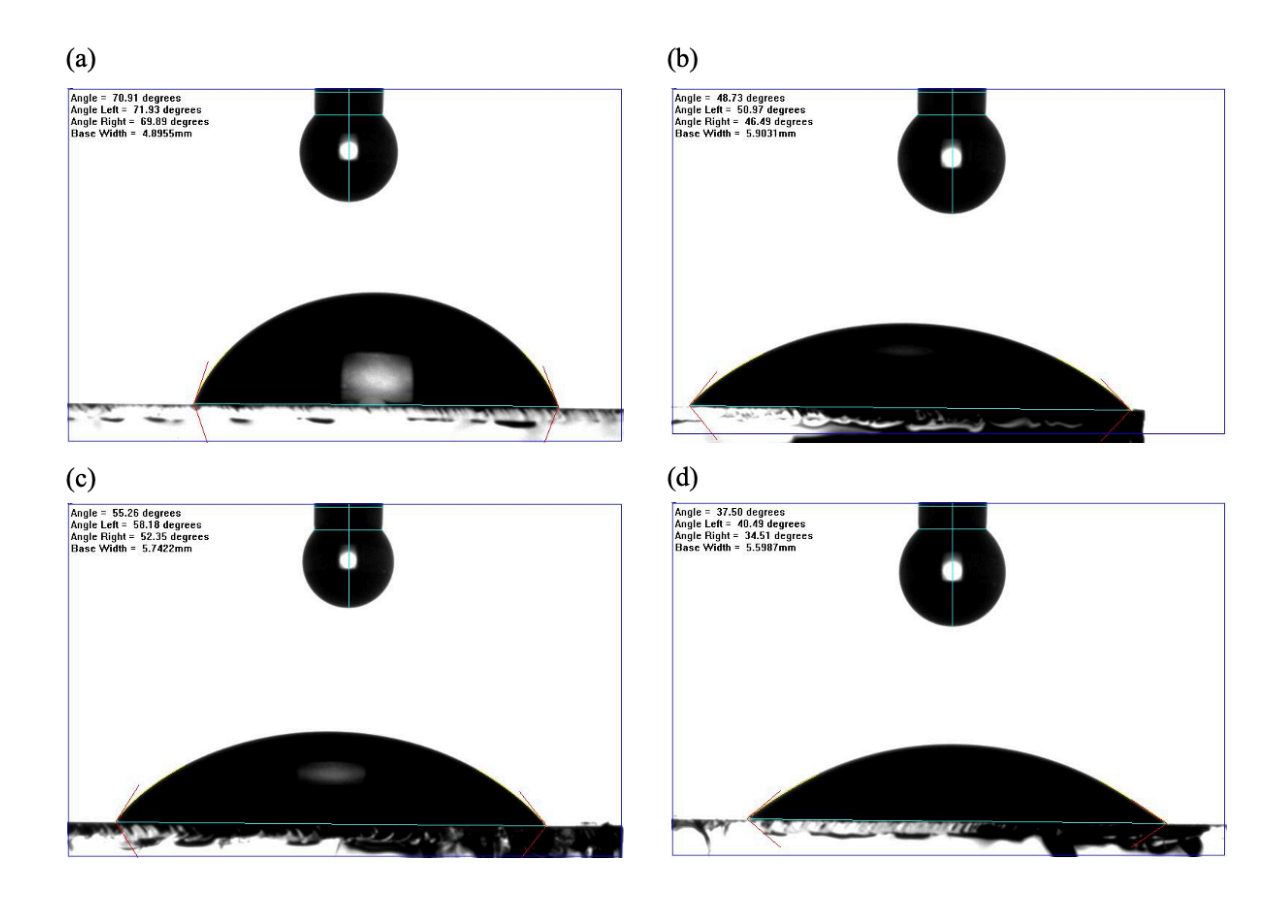


Figure 4. 12. Contact angle measurement of (a) bare FTO, (b) and (c) BP PEDOT film polymerised at 30 V for 20 min in a 10 mM EDOT Milli-Q solution on an FTO slide (d) conventionally deposited PEDOT on an FTO electrode (2 cm x 1 cm) at 200 μA for 300 seconds in 10 mM EDOT 0.1 M LiClO₄.

Contact angle was used to probe the hydrophobic or hydrophilic nature of both the BP and conventional PEDOT films, given that the surface free energy significantly influences

cell adhesion. Surface energy is an important element of a solid surface and its interactions at the solid interface, such as adhesion. Hydrophilic materials have a high surface energy and a contact angle $< 90^{\circ}$, promoting cell adhesion, which favours surfaces with contact angles ranging between 40° and 70° . To measure the contact angle, the sessile drop method was used with deionised water. The relationship between surface free energy and contact angle are described by the following Young equation: 34°

$$\gamma_L \cos\theta = \gamma_S - \gamma_{SL}$$

where γ_L is the surface energy, θ is the contact angle, γ_S is the surface energy of the solid and γ_{SL} is the surface energy of the solid/liquid interface.

Figure 4.12 show that both the BP PEDOT film and the conventionally deposited PEDOT film have a moderately hydrophilic surface with angles of 49° and 55° (Figure 4.12 inset), making them a potentially useful substrate for the adhesion of cells. The contact angle for the conventional PEDOT/ClO₄ film measured 38°, also acting as a favourable substrate for cell adhesion. However, the BP films might be slight preferred for cell adhesion, given that the ideal contact angle ranges between 40° and 70°. Overall based on the measured contact angles, the BP and conventional films are only slightly different in terms of hydrophilicity with a difference of over 11° between them. Interestingly, the BP contact angles (Figure 4.12 (b) and (c) inset) show that the positive side (right) of the BPE that is coated in polymer is more hydrophilic than the left angle measurement, which corresponds to the gradient polymer deposition. This shows that the polymer increases the hydrophilicity of the FTO substrate.

4.4. Conclusion

UV-Vis and electrochemistry indicate that the composition of the polymers deposited by the bipolar polymerisation and conventional methods and their band gaps are indistinguishable. This is a significant and surprising result given the potentially significant difference in voltages used to drive polymerisation and the fact that the BP polymerisation is carried out in the absence of deliberately added electrolyte. A key component of this work is the characterisation of the bipolar polymerisation process by investigating the effects of voltage and time. From this it is clear that an increase in the voltage difference between the two feeder electrodes results in an increased amount of deposition on the bipolar electrode (Figure 4.8), while an increase in deposition time shows a consistent increase in the fraction of the BP electrode that becomes coated with at least some PEDOT increase for deposition times between 20 and 30 minutes (Figure 4.7). This experimentation also allowed for a more in depth understanding of the electric field distribution which we now have sufficient evidence to believe that it is not a linear potential decay across the BPE, as polymerisation beyond zero volts has been demonstrated. From these results, it is clear that time has a significant influence on the fraction of BP electrode that is coated in polymer, further reiterating that the BP model is not simply a linear potential decay. Profilometry was used to investigate the height steps in film growth from the centre of the BPE to the positively charged pole on the BPE. The results from this correlated with the influence of applied voltage on deposition (Figure 4.8), resulting in increased deposition toward the positively charged end of the BPE, with decreasing film thickness toward the centre of the FTO, as a result of decreasing voltages (+10 V to -10 V) being experienced from the BP anode to the BP cathode. This work also shows the potential of the BP PEDOT films as platforms for cell stimulation as the films showed a hydrophilic behaviour with a contact angle between 49° and 55°, which is ideal for the adhesion of cells. The slightly rough morphology of the films as shown by SEM images also demonstrate a promising platform for cell adhesion. Overall, both BP and conventionally deposited films are indistinguishable materials, with the only differentiating factor being the gradient deposition shown through the BP method. The findings of this chapter lead seamlessly to Chapter 5, where the influence of electrode length and multiple feeder electrodes on the electric field distribution will be investigated.

4.5. References

- (1) Qin, C.; Yue, Z.; Chao, Y.; Forster, R. J.; Maolmhuaidh, F. Ó.; Huang, X.-F.; Beirne, S.; Wallace, G. G.; Chen, J. Bipolar Electroactive Conducting Polymers for Wireless Cell Stimulation. *Applied Materials Today* **2020**, *21*, 100804. https://doi.org/10.1016/j.apmt.2020.100804.
- (2) Forster, R. J. Wirefree Electroceuticals: 3D Electrical and Electrochemical Stimulation of Biological Systems. *Current Opinion in Electrochemistry* **2023**, *39*, 101297. https://doi.org/10.1016/j.coelec.2023.101297.
- (3) Backhurst, J. R.; Coulson, J. M.; Goodridge, F.; Plimley, R. E.; Fleischmann, M. A Preliminary Investigation of Fluidized Bed Electrodes. *J. Electrochem. Soc.* **1969**, *116* (11), 1600. https://doi.org/10.1149/1.2411628.
- (4) Koefoed, L.; Pedersen, S. U.; Daasbjerg, K. Bipolar Electrochemistry—A Wireless Approach for Electrode Reactions. *Current Opinion in Electrochemistry* **2017**, *2* (1), 13–17. https://doi.org/10.1016/j.coelec.2017.02.001.
- (5) Shida, N.; Zhou, Y.; Inagi, S. Bipolar Electrochemistry: A Powerful Tool for Electrifying Functional Material Synthesis. *Acc. Chem. Res.* **2019**, *52* (9), 2598–2608. https://doi.org/10.1021/acs.accounts.9b00337.
- (6) Crooks, R. M. Principles of Bipolar Electrochemistry. *ChemElectroChem* **2016**, *3* (3), 357–359. https://doi.org/10.1002/celc.201500549.
- (7) Qin, C.; Yue, Z.; Chao, Y.; Forster, R. J.; Maolmhuaidh, F. Ó.; Huang, X.-F.; Beirne, S.; Wallace, G. G.; Chen, J. Data on the Bipolar Electroactive Conducting Polymers for Wireless Cell Stimulation. *Data in Brief* **2020**, *33*, 106406. https://doi.org/10.1016/j.dib.2020.106406.
- (8) Zhou, Y.; Shida, N.; Tomita, I.; Inagi, S. Fabrication of Gradient and Patterned Organic Thin Films by Bipolar Electrolytic Micelle Disruption Using Redox-Active Surfactants. *Angew Chem Int Ed* **2021**, *60* (26), 14620–14629. https://doi.org/10.1002/anie.202103233.
- (9) Qi, Z.; You, S.; Ren, N. Wireless Electrocoagulation in Water Treatment Based on Bipolar Electrochemistry. *Electrochimica Acta* **2017**, *229*, 96–101. https://doi.org/10.1016/j.electacta.2017.01.151.
- (10) Kiran Raj, G.; Singh, E.; Hani, U.; Ramesh, K. V. R. N. S.; Talath, S.; Garg, A.; Savadatti, K.; Bhatt, T.; Madhuchandra, K.; Osmani, R. A. M. Conductive Polymers and Composites-Based Systems: An Incipient Stride in Drug Delivery

- and Therapeutics Realm. *Journal of Controlled Release* **2023**, *355*, 709–729. https://doi.org/10.1016/j.jconrel.2023.02.017.
- (11) Peerce, P. J.; Bard, A. J. Polymer Films on Electrodes: Part II. Film Structure and Mechanism of Electron Transfer with Electrodeposited Poly(Vinylferrocene). *Journal of Electroanalytical Chemistry and Interfacial Electrochemistry* **1980**, *112* (1), 97–115. https://doi.org/10.1016/S0022-0728(80)80011-8.
- (12) Nasirizadeh, N.; Shekari, Z.; Nazari, A.; Tabatabaee, M. Fabrication of a Novel Electrochemical Sensor for Determination of Hydrogen Peroxide in Different Fruit Juice Samples. *Journal of Food and Drug Analysis* **2016**, *24* (1), 72–82. https://doi.org/10.1016/j.jfda.2015.06.006.
- (13) Wagner, M.; Lisak, G.; Ivaska, A.; Bobacka, J. Durable PEDOT:PSS Films Obtained from Modified Water-Based Inks for Electrochemical Sensors. *Sensors and Actuators B: Chemical* **2013**, *181*, 694–701. https://doi.org/10.1016/j.snb.2013.02.051.
- (14) Sundfors, F.; Bobacka, J.; Ivaska, A.; Lewenstam, A. Kinetics of Electron Transfer between Fe(CN)63-/4- and Poly(3,4-Ethylenedioxythiophene) Studied by Electrochemical Impedance Spectroscopy. *Electrochimica Acta* **2002**, *47* (13), 2245–2251. https://doi.org/10.1016/S0013-4686(02)00063-4.
- (15) Pigani, L.; Heras, A.; Colina, Á.; Seeber, R.; López-Palacios, J. Electropolymerisation of 3,4-Ethylenedioxythiophene in Aqueous Solutions. *Electrochemistry Communications* **2004**, *6* (11), 1192–1198. https://doi.org/10.1016/j.elecom.2004.09.021.
- (16) Fomo, G.; Waryo, T.; Feleni, U.; Baker, P.; Iwuoha, E. Electrochemical Polymerization. In *Functional Polymers*; Jafar Mazumder, M. A., Sheardown, H., Al-Ahmed, A., Eds.; Polymers and Polymeric Composites: A Reference Series; Springer International Publishing: Cham, 2019; pp 105–131. https://doi.org/10.1007/978-3-319-95987-0_3.
- (17) Le, T.-H.; Kim, Y.; Yoon, H. Electrical and Electrochemical Properties of Conducting Polymers. *Polymers* **2017**, *9* (4), 150. https://doi.org/10.3390/polym9040150.
- (18) Gueye, M.; Carella, A.; Massonnet, N.; Yvenou, E.; Brenet, S.; Faure-Vincent, J.; Pouget, S.; Rieutord, F.; Okuno, H.; Benayad, A.; Demadrille, R.; Simonato, J.-P. Structure and Dopant Engineering in PEDOT Thin Films: Practical Tools for a

- Dramatic Conductivity Enhancement. *Chemistry of Materials* **2016**, *28*. https://doi.org/10.1021/acs.chemmater.6b01035.
- (19) Nie, S.; Li, Z.; Yao, Y.; Jin, Y. Progress in Synthesis of Conductive Polymer Poly(3,4-Ethylenedioxythiophene). *Front Chem* **2021**, *9*, 803509. https://doi.org/10.3389/fchem.2021.803509.
- (20) Asplund, M.; von Holst, H.; Inganäs, O. Composite Biomolecule/PEDOT Materials for Neural Electrodes. *Biointerphases* **2008**, *3* (3), 83–93. https://doi.org/10.1116/1.2998407.
- (21) Wolfart, F.; Dubal, D. P.; Vidotti, M.; Holze, R.; Gómez-Romero, P. Electrochemical Supercapacitive Properties of Polypyrrole Thin Films: Influence of the Electropolymerization Methods. *J Solid State Electrochem* **2016**, *20* (4), 901–910. https://doi.org/10.1007/s10008-015-2960-2.
- (22) Gribkova, O. L.; Nekrasov, A. A. Spectroelectrochemistry of Electroactive Polymer Composite Materials. *Polymers (Basel)* **2022**, *14* (15), 3201. https://doi.org/10.3390/polym14153201.
- (23) Bone, J. M.; Jenkins, J. L. Understanding Polymer Electrodeposition and Conducting Polymer Modified Electrodes Using Electrochemistry, Spectroscopy, and Scanning Probe Microscopy. *J. Chem. Educ.* **2023**, *100* (10), 4062–4071. https://doi.org/10.1021/acs.jchemed.3c00656.
- (24) Massonnet, N.; Carella, A.; Jaudouin, O.; Rannou, P.; Laval, G.; Celle, C.; Simonato, J.-P. Improvement of the Seebeck Coefficient of PEDOT:PSS by Chemical Reduction Combined with a Novel Method for Its Transfer Using Free-Standing Thin Films. *J. Mater. Chem. C* **2014**, *2* (7), 1278–1283. https://doi.org/10.1039/C3TC31674B.
- (25) Edberg, J.; Iandolo, D.; Brooke, R.; Liu, X.; Musumeci, C.; Andreasen, J. W.; Simon, D. T.; Evans, D.; Engquist, I.; Berggren, M. Patterning and Conductivity Modulation of Conductive Polymers by UV Light Exposure. *Adv Funct Materials* **2016**, *26* (38), 6950–6960. https://doi.org/10.1002/adfm.201601794.
- (26) Zozoulenko, I.; Singh, A.; Singh, S. K.; Gueskine, V.; Crispin, X.; Berggren, M. Polarons, Bipolarons, And Absorption Spectroscopy of PEDOT. ACS Appl. Polym. Mater. 2019, 1 (1), 83–94. https://doi.org/10.1021/acsapm.8b00061.
- (27) Tisserant, G.; Fattah, Z.; Ayela, C.; Roche, J.; Plano, B.; Zigah, D.; Goudeau, B.; Kuhn, A.; Bouffier, L. Generation of Metal Composition Gradients by Means of

- Bipolar Electrodeposition. *Electrochimica Acta* **2015**, *179*, 276–281. https://doi.org/10.1016/j.electacta.2015.03.102.
- (28) Lupu, S.; Lakard, B.; Hihn, J.-Y.; Dejeu, J. Novel in Situ Electrochemical Deposition of Platinum Nanoparticles by Sinusoidal Voltages on Conducting Polymer Films. *Synthetic Metals* **2012**, *162* (1), 193–198. https://doi.org/10.1016/j.synthmet.2011.11.031.
- (29) Chen, Z.; Villani, E.; Inagi, S. Recent Progress in Bipolar Electropolymerization Methods toward One-Dimensional Conducting Polymer Structures. *Current Opinion in Electrochemistry* **2021**, *28*, 100702. https://doi.org/10.1016/j.coelec.2021.100702.
- (30) Shida, N.; Inagi, S. Bipolar Electrochemistry in Synergy with Electrophoresis: Electric Field-Driven Electrosynthesis of Anisotropic Polymeric Materials. *Chem. Commun.* **2020**, *56* (92), 14327–14336. https://doi.org/10.1039/D0CC06204A.
- (31) Majhy, B.; Priyadarshini, P.; Sen, A. K. Effect of Surface Energy and Roughness on Cell Adhesion and Growth Facile Surface Modification for Enhanced Cell Culture. *RSC Adv 11* (25), 15467–15476. https://doi.org/10.1039/d1ra02402g.
- (32) Kozbial, A.; Li, Z.; Conaway, C.; McGinley, R.; Dhingra, S.; Vahdat, V.; Zhou, F.; D'Urso, B.; Liu, H.; Li, L. Study on the Surface Energy of Graphene by Contact Angle Measurements. *Langmuir* **2014**, *30* (28), 8598–8606. https://doi.org/10.1021/la5018328.
- (33) Arima, Y.; Iwata, H. Effect of Wettability and Surface Functional Groups on Protein Adsorption and Cell Adhesion Using Well-Defined Mixed Self-Assembled Monolayers. *Biomaterials* **2007**, 28 (20), 3074–3082. https://doi.org/10.1016/j.biomaterials.2007.03.013.
- (34) Gindl, M.; Sinn, G.; Gindl, W.; Reiterer, A.; Tschegg, S. A Comparison of Different Methods to Calculate the Surface Free Energy of Wood Using Contact Angle Measurements. *Colloids and Surfaces A: Physicochemical and Engineering Aspects* **2001**, *181* (1), 279–287. https://doi.org/10.1016/S0927-7757(00)00795-0.

Chapter 5

The Effects of Bipolar Size on Electric Field Distribution

5. The Effects of Bipolar Size on Electric Field Distribution

5.1. Introduction

An interesting observation of Chapter 4 was that the wireless polymerisation of poly(3,4-ethylenedioxythiophene), PEDOT, could occur at regions of the bipolar electrode (BPE) where the induced potential is insufficient to create cation EDOT radicals. Bipolar electrochemistry functions through the generation of an electric field facilitated by the presence of feeder electrodes.^{1,2} Electric fields are formed around charged objects which results in an electric force on charged particles that enter the field.³ This therefore highlights the necessity for investigating the migration of charged radicals in the field during the polymerisation, which could result in deposition at negative voltages. Modelling of the electric field distribution using Elmer indicates that the shape and size of the bipolar electrode should have a direct effect on the distribution of the electric field, potentially causing 'U' shaped, straight, or 'n' shaped polymerisation regions (Section 5.3.3). When the field strength is fixed (fixed voltage difference applied to feeders), altering the size of the bipolar electrode should also have a direct effect on the voltage being induced at both ends of the BPE.

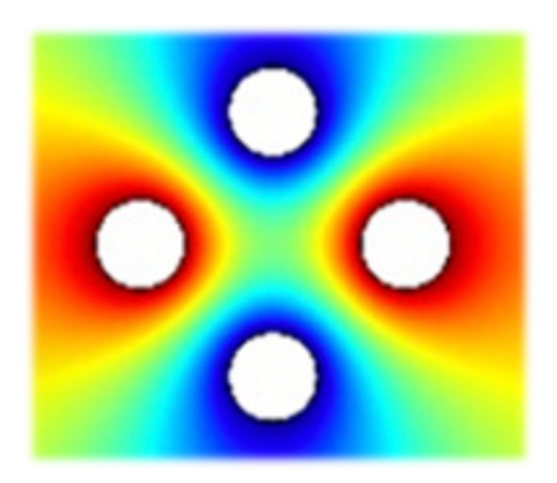


Figure 5. 1. Schematic of the electric field distribution generated by four feeder electrodes using COMSOL software. Extracted from Forster.⁴

Additionally, the electric field distribution can be controlled through the use of multiple feeder electrodes which can be seen in the COMSOL mapping of four feeder electrodes in Figure 5.1.⁴ Having the ability to modify and shape electric fields would enable template free patterning of the regions where a conducting polymer is deposited and allow a doping gradient across the film to be established. This approach would significantly impact the wireless electrostimulation of biological materials and act as a stepping-stone toward 3D electroceuticals, having the ability to predict the electric field distribution.⁴

In this chapter, the wireless deposition of PEDOT using optimised conditions on substrates of different size is reported. Changing the bipolar electrode length can provide information on the distribution of the electric field and potential gradient across the electrode. The electrodes of varying lengths were characterised based on deposition distance by microscope, surface coverage by cyclic voltammetry, impedance, and scanning electron microscopy. Additionally, the use of four feeder electrodes in two different configurations was investigated to understand the field distribution and the ability to shape the electric field. Modelling of the potential gradient within the solution was also performed so that the potential distribution induced in the bipolar electrode could be elucidated.

5.2. Materials and Methods

5.2.1. Materials

All materials used throughout this experimentation were of reagent grade and were obtained from Merck. Fluorine doped tin oxide glass (10 cm x 10 cm x 2.3 mm) was purchased from Merck and cut using a diamond glass cutter purchased from Amazon. Purified water used throughout this experimentation had a resistivity of $18.2 \text{ M}\Omega$ cm.

5.2.2. Bipolar Setup

Two Feeder Setup

The bipolar electrochemical cell was designed using FreeCAD and printed in acrylonitrile butadiene styrene (ABS) filament using the Ultimaker S5 3D printer. The cell was designed with a 3 cm separation between feeder electrodes and a 2 cm x 1 cm internal cavity for the BPE, to ensure central alignment. A well and tweezer slot were placed below and to the side of the FTO slot for easy removal. The objects were unified and cut out using the Boolean operation on FreeCAD, and then exported to an stl file. Cura software was used to adjust specific parameters (resolution, infill density, temperature) for 3D printing. The cell was printed using normal resolution of 0.15 mm with an infill

density of 20%, and was printed at a temperature of 230°C. The voltage drop across the feeder electrodes was achieved using an Elektro-Automatik EA-PS 5200-02A power supply. FTO glass was used as the BPE and titanium as the feeder electrodes. FTO electrodes of 2 cm x 1 cm (± 0.2 cm both sides) for the two feeder set up were cut using a diamond glass cutter, sonicated in an alcohol (ethanol/ isopropanol) and dried using nitrogen gas prior to use. A multimeter was used to determine which side of the glass had the FTO layer by measuring the resistance. Titanium electrodes (2cm x 1 cm x 2 mm) were sanded using 1600 grit sand paper (10-11 µm particle size) between experiments. The bipolar polymerisation was carried out using 3 ml (two feeder) 10 mM EDOT in deionised water. The voltage drop across the length of the bipolar electrode was calculated using the following equation (Eqt.1.1):⁵

$$\Delta E_{elec} = E_{tot} \left(\frac{l_{elec}}{l_{channel}} \right)$$
 Eqt.1.1

where $l_{channel}$ is the distance between driving electrodes, l_{elec} is the length of the BPE, and E_{tot} is the total voltage applied to the system.

Four Feeder Setup

The four feeder bipolar electrochemical cell was designed using FreeCAD and printed in acrylonitrile butadiene styrene (ABS) filament using the Ultimaker S5 3D printer. The cell was designed with a 3 cm separation between opposite feeder electrodes and a 1.5 cm x 1.5 cm internal cavity for the BPE, to ensure central alignment. FTO electrodes of approximately 1.5 cm x 1.5 cm (\pm 0.2 cm both sides) for the four feeder set up were cut using a diamond glass cutter, sonicated in an alcohol (ethanol/ isopropanol) and dried using nitrogen gas prior to use. Bipolar polymerisation was achieved using 6 ml of 10 mM EDOT in deionised water. All other experimental conditions remained the same as described in the two feeder setup.

5.2.3. Electrochemical Setup

Cyclic voltammetry was performed using an AutoLab (Metrohm) systems potentiostat. For CV and EIS experiments, the area of the working FTO electrode was controlled by masking using teflon tape; surface area of 1 cm² (two feeder) and 1.5 cm² (four feeder). An Ag/AgCl (saturated KCl) was used as the reference electrode, and a coiled platinum wire counter electrode (≈3.62 cm²) completed the three electrode setup. All films were cycled in 0.1 M LiClO₄ solutions.

Surface coverage was calculated using the following:⁶

$$\Gamma = Q/nFA$$
 Eqt. 2.1

where Γ is the surface coverage of the deposited film in mol/cm², Q is the charge (capacitance × potential window of 0.6 V), n is the number of transferred electrons (assuming 2.25), F is Faraday's constant, and A is the surface area of the electrode in cm².

5.2.4. Impedance

All impedance measurements were carried out using an Autolab potentiostat (Metrohm) with an applied AC amplitude of 0.01 V in potentiostatic mode. Impedance measurements were performed using a three-electrode system with a working electrode area of 1 cm² for the two-feeder set up and 2.25 cm² for the four-feeder set up, Ag/AgCl reference electrode, and a coiled platinum wire. A frequency of 1x10⁵ Hz to 0.1 Hz with an applied voltage of 0.2 V. All impedance measurements were recorded in 0.1 M LiClO₄. Nova software was used to fit the EIS data to the appropriate circuit as shown in Figure 5.4 (d).

5.2.5. Microscopy

A Nikon eclipse ME600 microscope was used to determine the polymerisation distance on the BPE electrode. This was achieved by measuring the edge at which polymerisation begins to the location where no blue film could be seen. This method could underestimate the region over which PEDOT is deposited since it does not have the sensitivity to detect very thin layers/monolayers. The microscope images were captured using a camera

inserted into the microscope and were displayed using S-EYE software. The percentage surface coverage was calculated by dividing the measured polymerisation distance by the length of the BPE.

5.2.6. Scanning Electron Microscopy

A Jeol JSM-IT 100 InTouchScope electron microscope was used to image the bipolar PEDOT films on FTO using an accelerating voltage of 2.0 kV and a secondary electron detector. The BPE was placed on SEM specimen stub and stuck down using a conductive carbon adhesive sticker.

5.2.7. Electric Field Mapping

Modelling of the electric field distribution was performed using FreeCAD, Salome, and Elmer software. Firstly, the cell design was created in FreeCAD with titanium electrodes of dimensions 1 cm (Length) x 2 cm (Height) x 2 mm (Depth). For the two-feeder model, a cell of 3 cm x 1 cm was created, and for the four-feeder model a 3 cm x 3 cm cell was used. The files were then converted to BREP files and were imported into Salome. In Salome, the objects (feeders and cell) were rescaled to centimetres, as this software converts items to metres. Individual solid objects were created and then partitioned into discrete entities so that their properties, e.g., conductivity or permittivity could be controlled. The objects were then converted into meshes as this allows for every part of the surface to be considered in the electric field distribution. The project was saved as a UNV file and imported into Elmer software. In Elmer, the bodies were divided to create boundaries on each surface. The surfaces on each body were then unified, so each body had their own boundary. The material of each body was based on the relative permittivity of the material. In this case the cell was given a relative permittivity of 80, and the titanium electrodes were assigned a relative permittivity value of 1x10⁶ as the relative permittivity value of a metal is infinite.^{7,8}

5.3. Results and Discussion

5.3.1. The Effects of Electrode Size on Electric Field Distribution

To gain further insight into the potential distribution, electric field shape, and mass transport processes, EDOT was polymerised on BPEs of varying length (1.4 cm, 2.0 cm, and 2.6 cm). The applicability of the linear potential gradient model and voltage drop across the BPE equation (Eqt. 1.1) were investigated by comparing the predicted potentials across the positive BP pole and the potentials at which experimentally observed polymerisation stops. By changing the size of the BPE, it is possible to investigate the influence of potential as the distance between the BPE and feeder electrodes become reduced.

5.3.1.1. CAD and 3D Printing

FreeCAD was used to design the in house bipolar electrochemical cell. The cell was based on a two 2 mm feeder electrode, one bipolar electrode system. After troubleshooting various designs, the following design was used for all experimentation. The titanium feeder electrodes were separated by a distance of 3 cm. A 2 cm x 1 cm BPE slot was incorporated in the design to ensure accurate alignment of the BPE (to ensure 0 V occurs at the centre of the BPE) and consistency in FTO sizes. A 1 cm x 1 cm well was also incorporated in the design to prevent the FTO suctioning to the base of the cell. A tweezer slot was place perpendicular to the FTO slot for ease of FTO removal after polymerisation. Cura software was used to adjust printing parameters for 3D printing.

5.3.1.2. Characterisation of the PEDOT Modified BPEs

BPE Length	PEDOT Coverage	Theoretical Voltage BP Anode	Theoretical Voltage at which Polymerisation Stops (based on microscope exp.)
1.4 cm	25 %	7 V	5.25 V
1.65 cm	27 %	8.25 V	6 V
2.1 cm	30 %	10.5 V	7.4 V
2.3 cm	27 %	11.5 V	8.4 V
2.4 cm	29 %	12 V	8.5 V
2.65 cm	29 %	13.25 V	9.4 V
2.7 cm	22 %	13.5 V	10.5 V

Figure 5. 2. Diagram of BP PEDOT polymerisation on BPEs of varying lengths. Polymerisation was performed on an FTO BPE in 10 mM EDOT Milli-Q water solution at 30 V for 20 minutes. Percentage coverage was determined experimentally as described in Section 5.2.5. Maximum voltages at the tip of the BPE anode were calculated using Eqt. 1.1. Theoretical voltages where polymerisation stops was calculated by measuring the polymerisation distance as described in Section 5.2.5. The voltage where the polymerisation stopped was then calculated using Eqt. 1.1.

PEDOT was polymerised wirelessly on BPEs of varying lengths in the standard two feeder bipolar system and the results are as shown in Figure 5.2. These experiments were performed to gain insights into the potential gradient, electric field distribution, and to investigate the BPE potential distribution equation (Eqt. 1.1). Firstly, the maximum theoretical voltages that could be generated at the edge of the BPE anodes were calculated using Eqt.1.1.9,10,11 This equation was also used to calculate the voltage at which PEDOT

polymerisation stopped which was initially determined as described in Section 5.2.5. The percentage coverage was calculated by measuring polymerisation distance using a microscope (Section 5.2.5). It is important to note that polymerisation distance was determined visually, so areas where the film is very thin, e.g., monolayers, are not considered leading to potential underestimates of the area. The polymerisation distance was divided by the length of the BPE to calculate the percentage coverage. If a linear potential decay was occurring on the BPE, polymerisation would be expected to finish at 0.85 V, which is the onset voltage for electropolymerisation of PEDOT.¹² With this assumption, a linear increase in the percentage coverage of PEDOT would be expected with increasing BPE length. However, this is not the case as the percentage surface coverage ranges from 22 - 30%, with a possible outlier at 22%. As seen in Figure 5.2, percentage coverage is within the same range for all samples considering some slight changes in percentages due to the accuracy of the visual test. This behaviour cannot be explained by the linear potential model suggesting that alternative factors, ^{13,14} other than the magnitude of the potential induced in the BPE play significant roles. Another observation is the consistency in percentage surface coverage (22-30%); however, as the electrode length increases, the quantity of material deposited increases which can be seen visually in Figure 5.3 (but the percentage coverage does not change significantly). It is also possible that migration is playing a role in the deposition surface coverages due to the movement of cationic radicals and oligomers from the positive end of the BP pole, to the negatively charged feeder electrode. 15,16,17 These results also show that Eqt. 1.1 is not an accurate method of representing the potential gradient across the BPE.

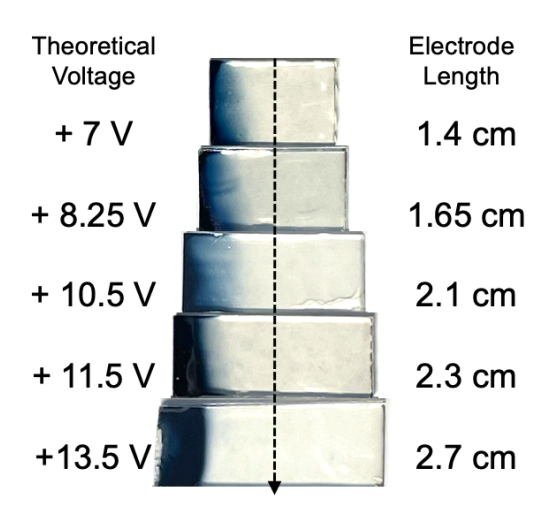


Figure 5. 3. BP PEDOT polymerisation on FTO BPEs of increasing length, ranging from 1.4 cm to 2.7 cm. Polymerisation was performed in an electrolyte free solution. Theoretical voltages were calculated using Eqt. 1.1.

An important visual observation was the changing deposition shape of the BP PEDOT films. As the electrode length increases, the polymerisation end point visually becomes more defined, which could be attributed to a reduction in migration effects as a result of the changing electric field. Another observation is that the optimised 30 V 20 minute BP film produces 'U' shaped films (in the BP width), however, as shown in Figure 5.3, polymerisation ends with a straight line from samples 1.4 cm to 2.3 cm and obtains an 'n' shaped film at 2.7 cm, further confirming that the electric field is changing with the size of the BPE.

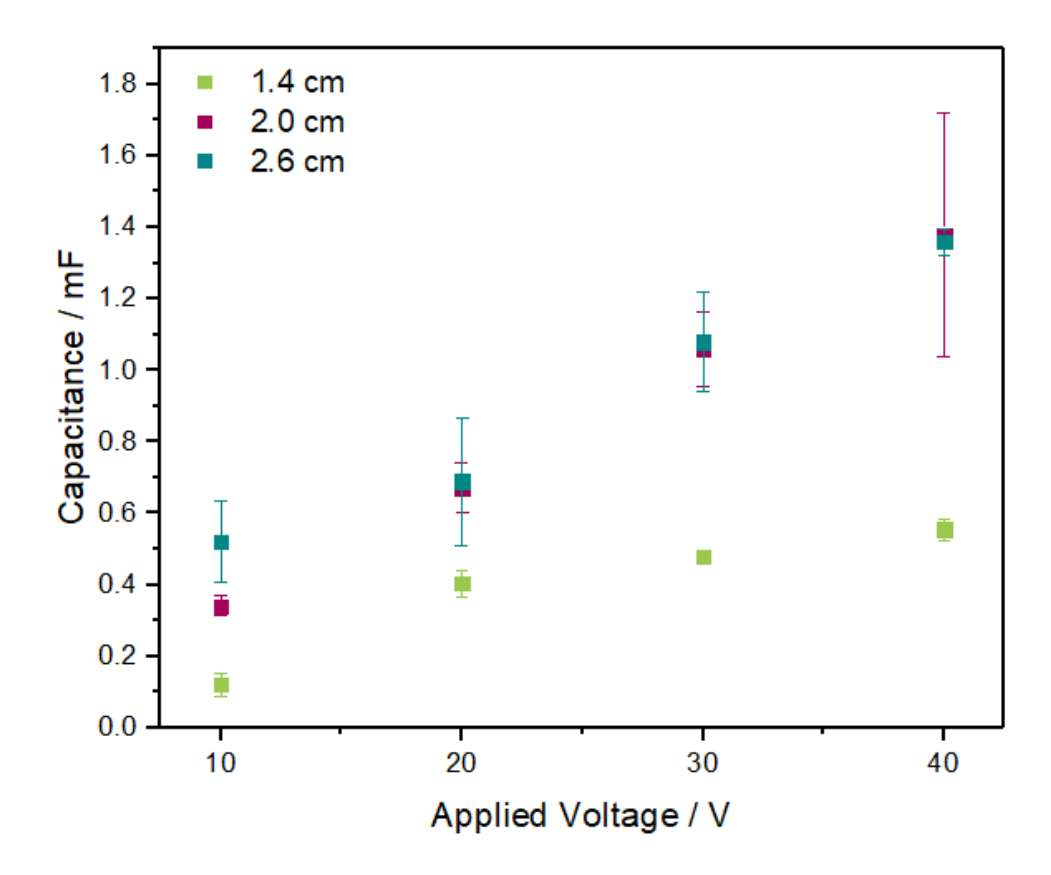


Figure 5. 4. Capacitance of BP polymerised EDOT in 10 mM EDOT Milli-Q water on FTO BPEs of varying lengths (1.4 cm, 2.0 cm, and 2.6 cm) at voltages of 10, 20, 30, and 40 V for 10 minutes. Capacitance was calculated from scan rates studies. Samples were performed in triplicate.

To investigate the quantity of material deposited on the BPEs of varying lengths, a set of scan rate studies (5 mV/s - 100 mV/s) were performed from which the capacitance was calculated. Capacitance was calculated by plotting the current at 0.2 V versus scan rate and obtaining the slope of the line. ¹⁸¹⁸⁷ The capacitance of bare FTO was also calculated (1×10^{-6} F) but was deemed negligible in these calculations. Therefore, the calculated capacitance is a representation of the amount of PEDOT deposited on the electrode surface. Figure 5.4 displays the results of these calculations for electrodes of three different lengths and four different voltages. Firstly, the smallest electrode measured, 1.4 cm, does not show a linear capacitance increase with increasing voltage. The initial jump from 10 V to 20 V results in a substantial increase of capacitance which later tapers off from 20V to 40 V which is not expected. This is not expected as current BP theory suggests a gradient potential across the BPE, leading to the assumption that by doubling the voltage, the quantity of the deposited material would also be doubled. The 2.0 cm

BPE demonstrates a linear increase with increasing potential which is exactly what would be expected based on the potential decay studies as per Figure 4.8 and current bipolar theory. The difference in capacitance measurements between the 1.4 cm and 2.0 cm BPEs are what would be expected for this work. As the BPE increases in size, the voltage experienced across the BPE also increases, therefore more PEDOT material is expected to be deposited which is effectively shown in Figure 5.4 sample 1.4 cm and 2.0 cm. The 2.6 cm BPEs also increase linearly, however, interestingly the quantity of PEDOT present on the surface of the BPE is similar to that of the 2.0 cm electrodes. This is an important observation as it could suggest that there is a limiting process occurring as the BPE approaches the feeder electrodes, however further experimentation at longer feeder electrodes would be required to prove this.

5.3.1.3. Impedance

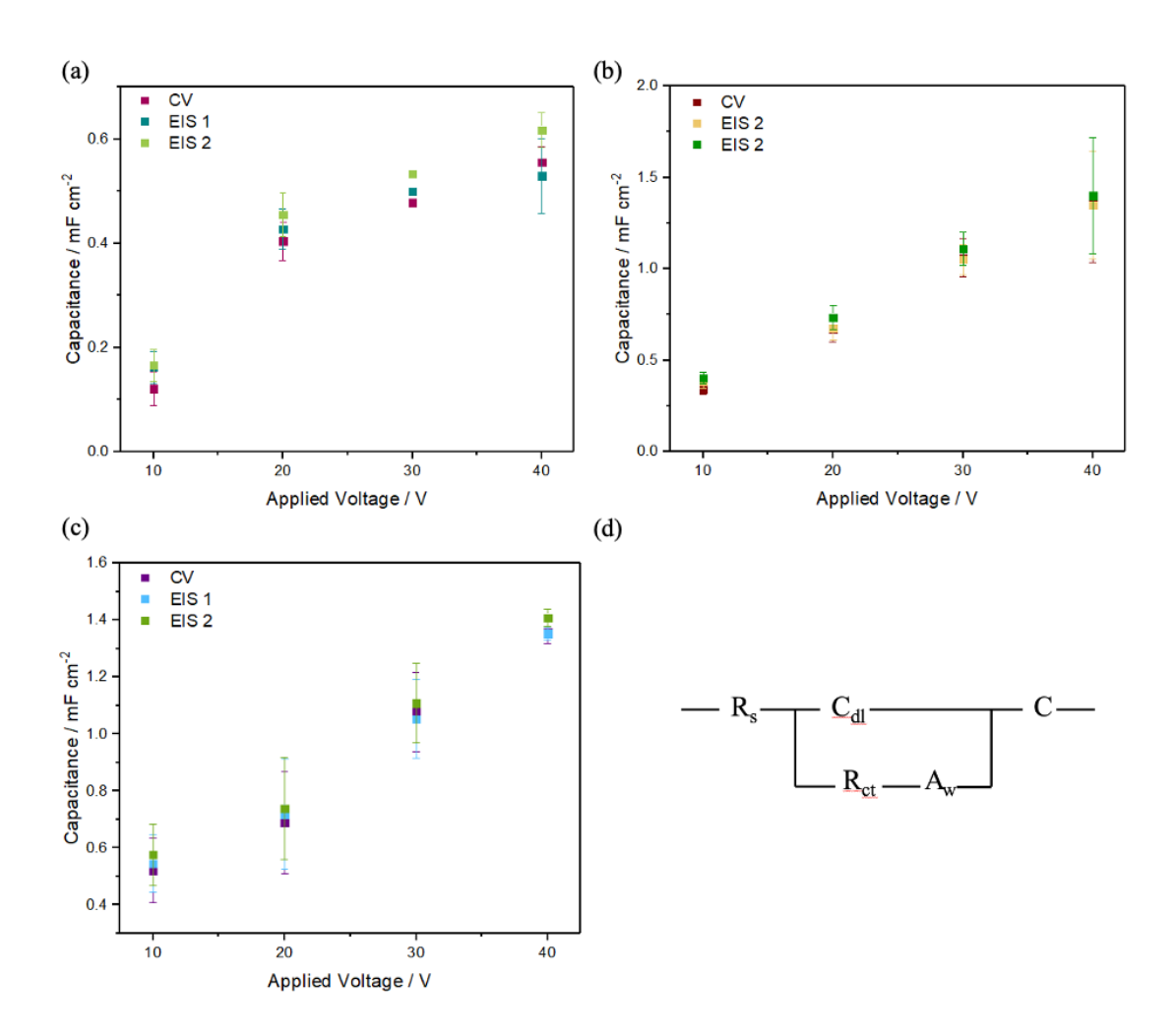


Figure 5. 5. EIS and CV data of the BPEs of varying length in 0.1 M LiClO₄. (a) 1.4 cm BPE capacitance results for initial EIS (EIS 1), scan rate study (CV), and second EIS measurement (EIS 2). (b) 2.0 cm BPE capacitance results for initial EIS (EIS 1), scan rate study (CV), and second EIS measurement (EIS 2). (c) 2.6 cm BPE capacitance results for initial EIS (EIS 1), scan rate study (CV), and second EIS measurement (EIS 2). BP PEDOT films were formed by BP polymerisation at 30 V for 20 minutes in 10 mM EDOT in Milli-Q water. A frequency range of 1x10⁵ Hz to 0.1 Hz at 0.2 V was used for all impedance results. (d) The circuit used for EIS data fitting using Nova software.

To further investigate the quantity of PEDOT deposited on the BPEs of different sizes, electrochemical impedance spectroscopy (EIS) was recorded at 0.2 V. This data was then

used to compare capacitance values with that generated from scan rate studies in Figure 5.4. A series of circuit elements describe the system including solution resistance R_s, capacitance of the double layer at the electrode-electrolyte interface C_{dl}, charge transfer resistance R_{ct}, diffusion as a result of film charging A_w, and finally capacitance of the polymer film C. ^{19,20,21} Nova software was used to fit the impedance data to the appropriate circuit shown in Figure 5.5 (d). The second capacitance was used as this element represents the capacitance as a result of the polymer film on the electrode surface. 22,23,24 EIS was performed prior to scan rate studies and after, to confirm that the capacitance being observed was due to the polymer film on the electrode surface. The EIS performed after the scan rate studies was performed to ensure stability of the polymer film, further confirming the accuracy of the CV measurements. From the EIS results, it is clear that the capacitance values measured using CV accurately represent the quantity of PEDOT on the BPE surface. In Figure 5.5 (a), the 1.4 cm BPE shows a non-linear increase of capacitance with increasing voltage. In Figure 5.5 (b) and (c) which shows both the 2.0 cm and the 2.6 cm BPE, a linear capacitance increase can be seen for both BPEs with increasing voltage, which is what is expected based on the BP linear model.^{25,13}

5.3.1.4. Scanning Electron Microscopy

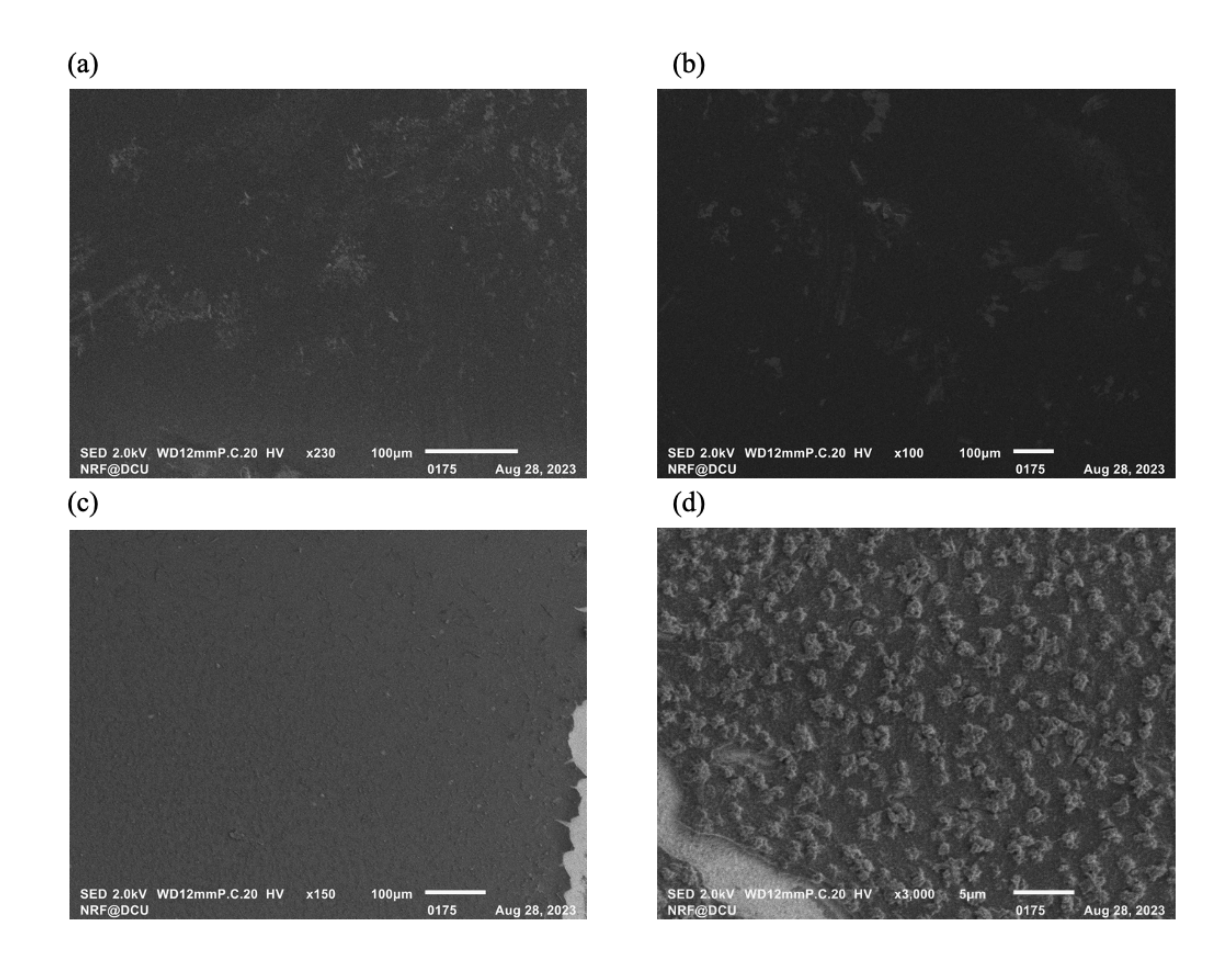


Figure 5. 6. SEM images of BP polymerised PEDOT at 30 V for 20 minutes in 10 mM EDOT Milli-Q water solution. (a) 1.4 cm BPE (b) 2.1 cm BPE (c) 2.7 cm BPE (d) 2.7 cm BPE. BP films were polymerised using a two-feeder electrode system (Figure 5.2).

SEM was used to understand the film morphologies at varying electrode lengths. All figures correspond to the positive end of the BPE. Figure 5.6 (a) displays the PEDOT film formed on the 1.4 cm BPE, the smallest electrode length. The film formed was smooth with no visible aggregates on the surface of the BP anode. At 2.1 cm, the BP PEDOT film also appeared to have a smooth surface, however toward the edge of the FTO with the deposited material (positive BP pole), polymer could be seen flaking off the surface of the electrode. This could be due to shrinkage stress during drying. ²⁶ This was seen for all films past this electrode length. At 2.7 cm, the film is of rougher texture (Figure 5.6 (c)). It is possible that the increased voltage being exerted on the system results in PEDOT clusters on the surface of the BPE. ²⁷ The BPEs from 2.1 cm to 2.7 cm in Figure 5.6 show

a rough surface, however, film flaking is an issue at these electrode lengths, making these substrates unsuitable for cell adhesion. This issue can be combatted by polymerising at a shorter timescale and a lower voltage, therefore reducing the quantity of PEDOT being deposited on the BPE. Overall, the morphologies of the films at different lengths are changing with increasing BPE length, from smooth films to rougher films with small aggregates.

5.3.2. Shaping the Electric Field

5.3.2.1. CAD and 3D Printing

FreeCAD was used to design a four feeder bipolar electrochemical cell. The cell design was based on a novel four feeder setup, in which titanium feeder electrodes were separated by equal distances of 3 cm. This design included a BPE cut out which was of square shape (1.5cm x 1.5cm). A tweezer slot was also included in the design to allow the FTO slide to be removed without damaging the PEDOT film. The CAD file was printed using the Ultimaker 3D printer in acrylonitrile butadiene styrene (ABS) filament. Figure 5.7 (a) includes the CAD design for the four-feeder set up, with the printed cell in ABS filament being shown in Figure 5.7 (b).

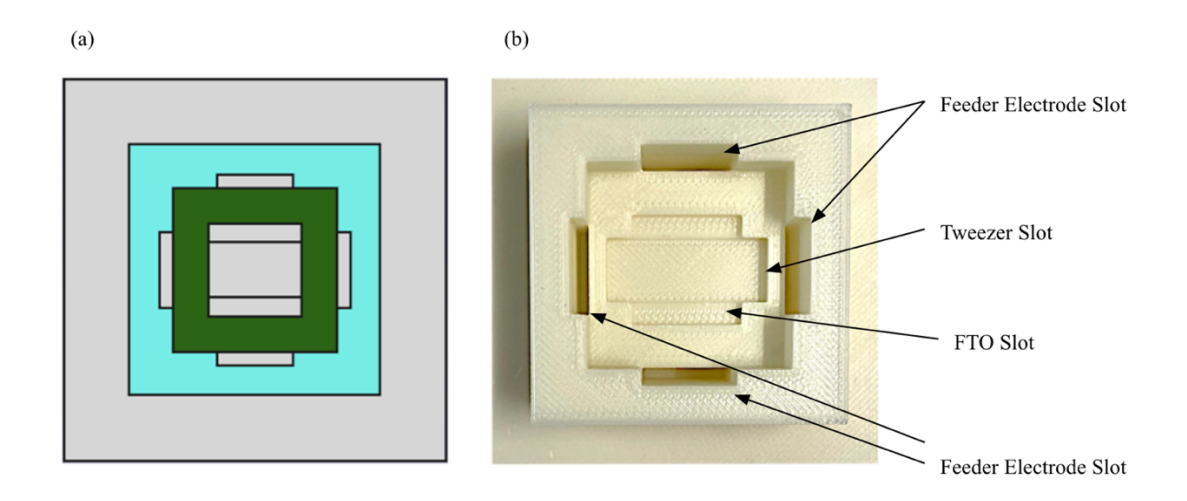


Figure 5. 7. (a) FreeCAD design of the four-feeder set up including four 2 cm x 1 cm x 2 mm feeder electrode slots and one 1.5 cm x 1.5 cm FTO BPE slot (b) four feeder BP cell printed in acrylonitrile butadiene styrene.

5.3.2.2. Bipolar Polymerisation of EDOT using the Four Feeder Setup

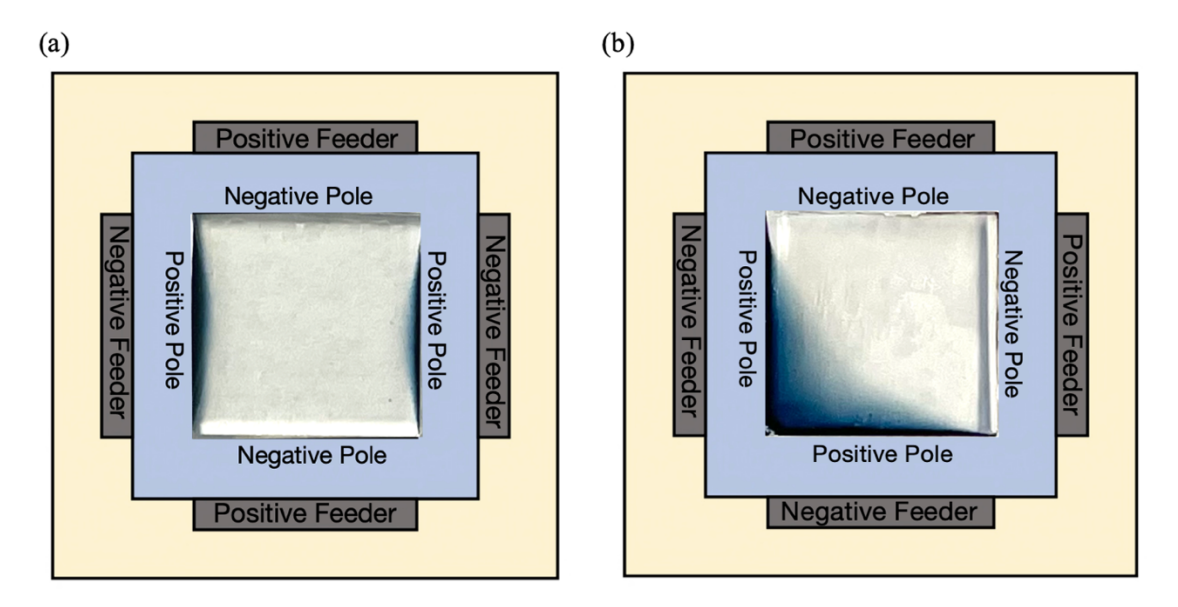


Figure 5. 8. FTO BPE polymerised in 10 mM EDOT Milli-Q water solution at 30 V for 20 minutes (a) Configuration 1: Positive and negative feeders are opposing each other (b) Configuration 2: Positive feeders and negative feeders are located beside each other.

The bipolar electropolymerisation of EDOT using four feeder electrodes is portrayed by two different configurations as shown in Figure 5.8. Configuration 1 involves two pairs of feeder electrodes that oppose one another. PEDOT deposits at the two positive poles of the bipolar electrode, taking the form of two narrow arcs. From this image it appears that the electric field being generated by the feeder electrodes does not drive significant polymerisation across more than 80% of the BPE surface. In Configuration 2, the positive and negative feeders are adjacent to one another, resulting in PEDOT depositing in an approximately triangular region between the two negative feeder electrodes. Interestingly, by changing the feeder configuration, we generate a completely different electric field, thus polymerising in different shapes.

In order to quantify the amount of PEDOT being deposited on the BPE, a scan rate study was performed. The capacitance was calculated by the current at 0.2 V versus scan rate and obtaining the slope of the line. Figure 5.9 shows the flat and featureless cyclic voltammograms of both Configuration 1 and 2, which are expected for PEDOT as no faradaic processes are expected within this potential window. The film capacitance was

converted to charge by multiplying the capacitance by the potential window of 0.6 V.²⁸ From this, the surface coverage (mol/ cm²) was calculated using Eqt. 2.1.²⁹ In conclusion, Configuration 1 deposited 1.06×10⁻⁹ mol/cm² of EDOT, while Configuration 2 deposited 4.31×10⁻⁹ mol/cm² of EDOT. By simply changing the feeder configuration, four times the amount of polymer can be deposited on the BPE. This is likely happening because of the feeder setup in Configuration 1 resulting in interferences between the feeder electrodes. Another reason why this may be occurring is cationic radicals and oligomers are migrating in the complex electric field.

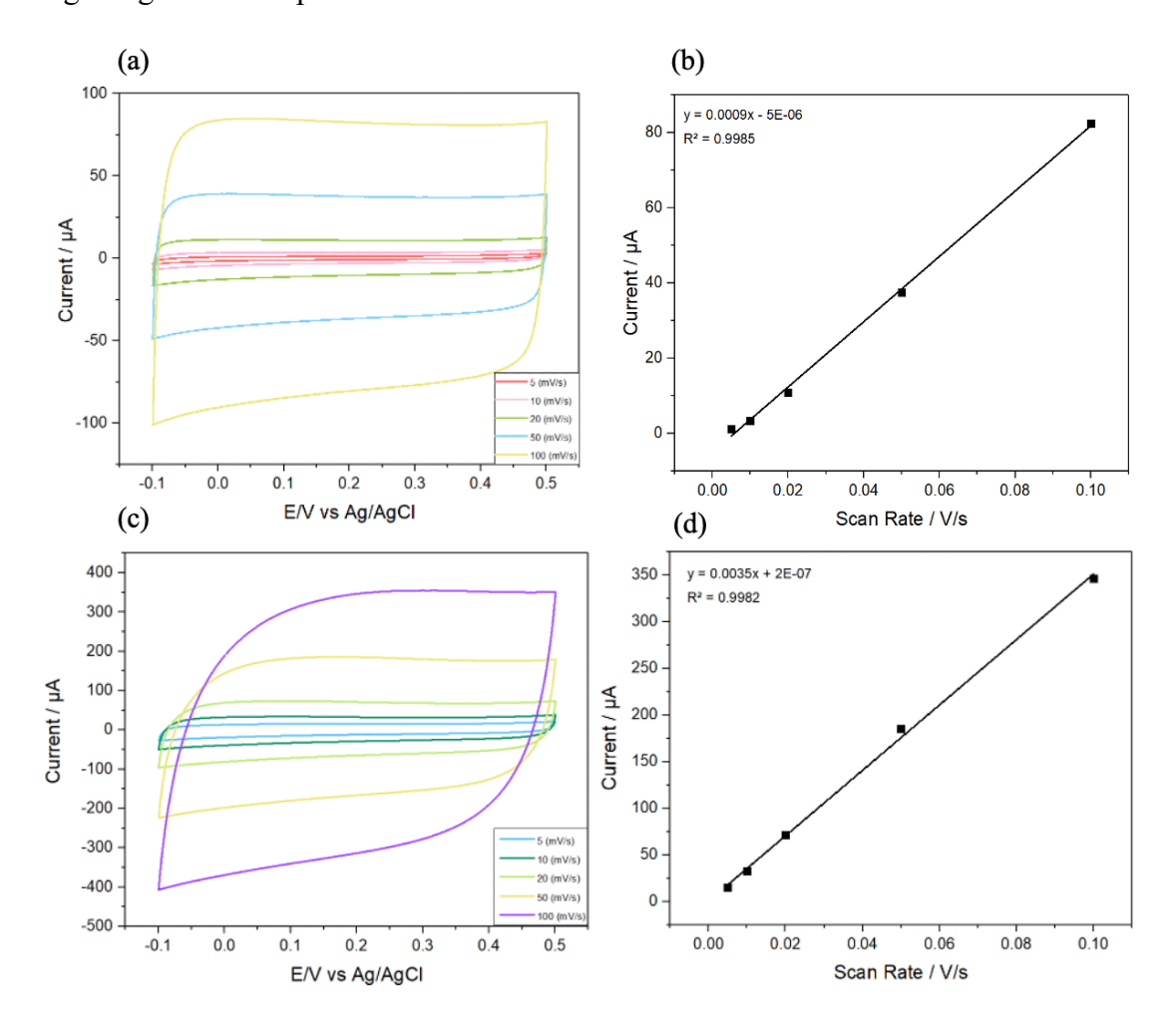


Figure 5. 9. Four feeder BP polymerisation of 10 mM EDOT in Milli-Q water at 30 V for 20 minutes. Each BPE was cycled in 0.1 M LiClO₄. Scan rates of 5, 10, 20, 50 and 100 mV/s were used for the scan rate study. (a) Configuration 1 (b) Current versus scan rate of configuration 1 (c) Configuration 2 (d) Current versus scan rate of configuration 2.

5.3.2.3. Scanning Electron Microscopy

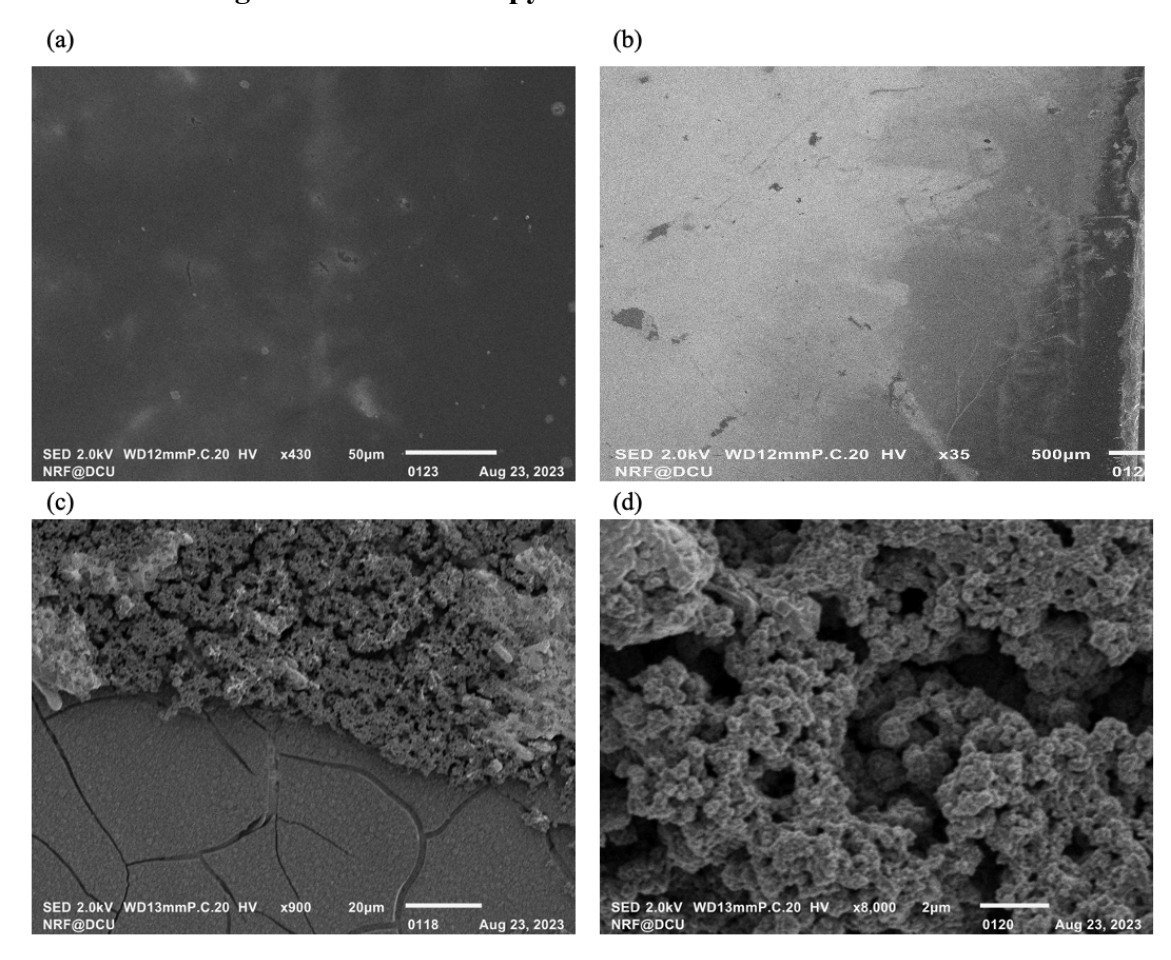


Figure 5. 10. SEM images for PEDOT deposited by bipolar polymerisation using four feeder electrodes at 30 V for 20 minutes in 10 mM EDOT Mill-Q water solution. (a) and (b) represent Configuration 1, (c) and (d) represent Configuration 2.

The morphology of both films was investigated using SEM. Figure 5.10 (a) and (b) correspond to Configuration 1, while Figure 5.10 (c) and (d) correspond to Configuration 2. The PEDOT film shown in Configuration 1 shows a smooth morphology, with a film thickness gradient toward the edge of the FTO slide which is identified by the darker colour. Configuration 2 shows a substantially rougher film, with globular aggregates in areas toward the corner of the FTO substrate due to thicker deposition as a result of higher potentials. The film becomes thinner toward the centre of the FTO, resulting in a smoother, cracked morphology, which could be due to the film drying or film thickness.²⁶

5.3.3. Electric Field Mapping using Simulation Software

FreeCAD, Salome, and Elmer free software packages were used to model the electric field distribution and to determine the potentials induced in the bipolar electrode. The cell design, which included the two feeder electrodes or four feeder electrodes and main cell which contained the solvent were created using FreeCAD. The designs were then converted to the correct format as described in Section 5.2.7, where they were imported into Salome software. The designs were rescaled to their original sizes of centimetres as Salome software converts designs to metres. After this, the three objects were transformed into meshes, which allowed each triangular mesh to possess a vector. In the Elmer software, it was essential to create different boundaries between each feeder electrode and the cell. The experimental potential was also applied to the specific feeder electrodes which was either +10 V or -10 V. Once the parameters were applied, the potential distribution, electric field, and electric flux were calculated.

Potential Distribution

The potential distribution refers to the gradient in voltage that is produced within the solution of the bipolar cell due to the potential applied to the feeder electrodes. The bipolar electrode is easily polarised and so its potential shifts to match the solution phase value. Thus, it is important to understand the solution phase potential so that the potentials at which polymerisation is occurring are known.

Electric Field

An electric field is a field that is generated by the repulsion and attraction of electrical charge.^{30,31} The electric field is a vector field, having both magnitude and direction.

Electric Flux

The electric flux is the measure of the electric field flow through a surface.³²

5.3.3.1. Two Feeder Electrode Setup

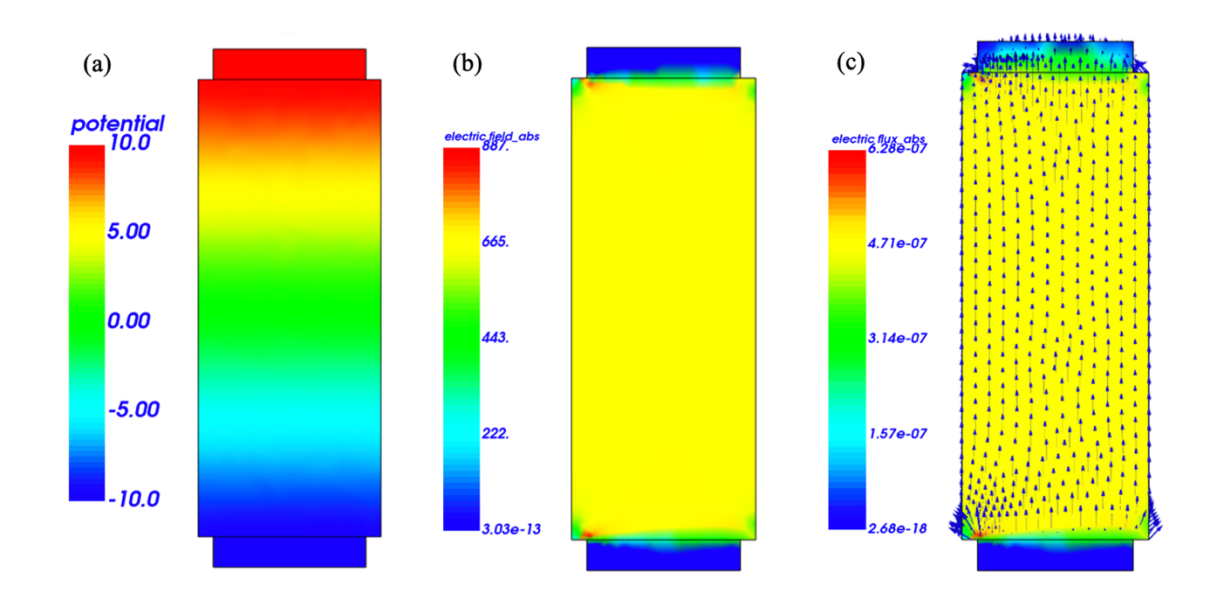


Figure 5. 11. Electric field modelling of the two-feeder electrode set up, investigating (a) potential gradient (b) electric field and (c) electric flux.

Figure 5.11 displays the Elmer modelling of the two feeder set up without the BPE present in the cell. Figure 5.11 (a) represents the potential distribution across the 20 V bipolar cell. From this mapping, we can see a gradient potential decay across the solution in the BP electrochemical cell which has been described in the literature. The gradient potential decay is shown in Figure 5.11 (a) with the red banded area representing +10 V which gradually decreases to the blue -10 V, with the centre of the cell (green) representing 0 V. From the electrode length experimentation (Section 5.4) and the polymerisation time experimentation (Section 4.3.5) this is not an accurate representation of the system as (a) at longer electrode lengths of 2.7 cm, polymerisation does not continue close to the centre of the BPE (Figure 5.3) (b) the percentage coverage of all BPE regardless of length is approximately the same (Figure 5.2) and (c) polymerisation is occurring beyond the zero volts point at the centre of the BPE (Figure 4.10). This therefore shows that by inserting the BPE into the cell, the field shape is changing and deviating from the expected linear potential decay. In the electric field mapping, the strength of the electric field appears consistent throughout the BP cell, with some areas toward the corner of the feeder electrode experiencing stronger fields which is portrayed by the colour red. A thin bright

blue band can also be seen at both feeder electrodes, which is likely to be a loss of electric field strength due to the formation of the double layer on feeder electrodes. Figure 5.11 (c) shows the electric flux distribution throughout the bipolar setup with the use of vectors. At the left side of the anode feeder, there appears to be a stronger flux represented by vectors with a slightly greater magnitude than the rest of the cell. Toward the cathode feeder electrode, the electric flux decreases, which is depicted by a reduction in the magnitude of the vectors. Mapping in the presence of an FTO glass BPE would allow a more in-depth analysis of the effects of the BPE size and shape on the electric field distribution.

5.3.3.2. Four Feeder Bipolar Setup – Configuration 1

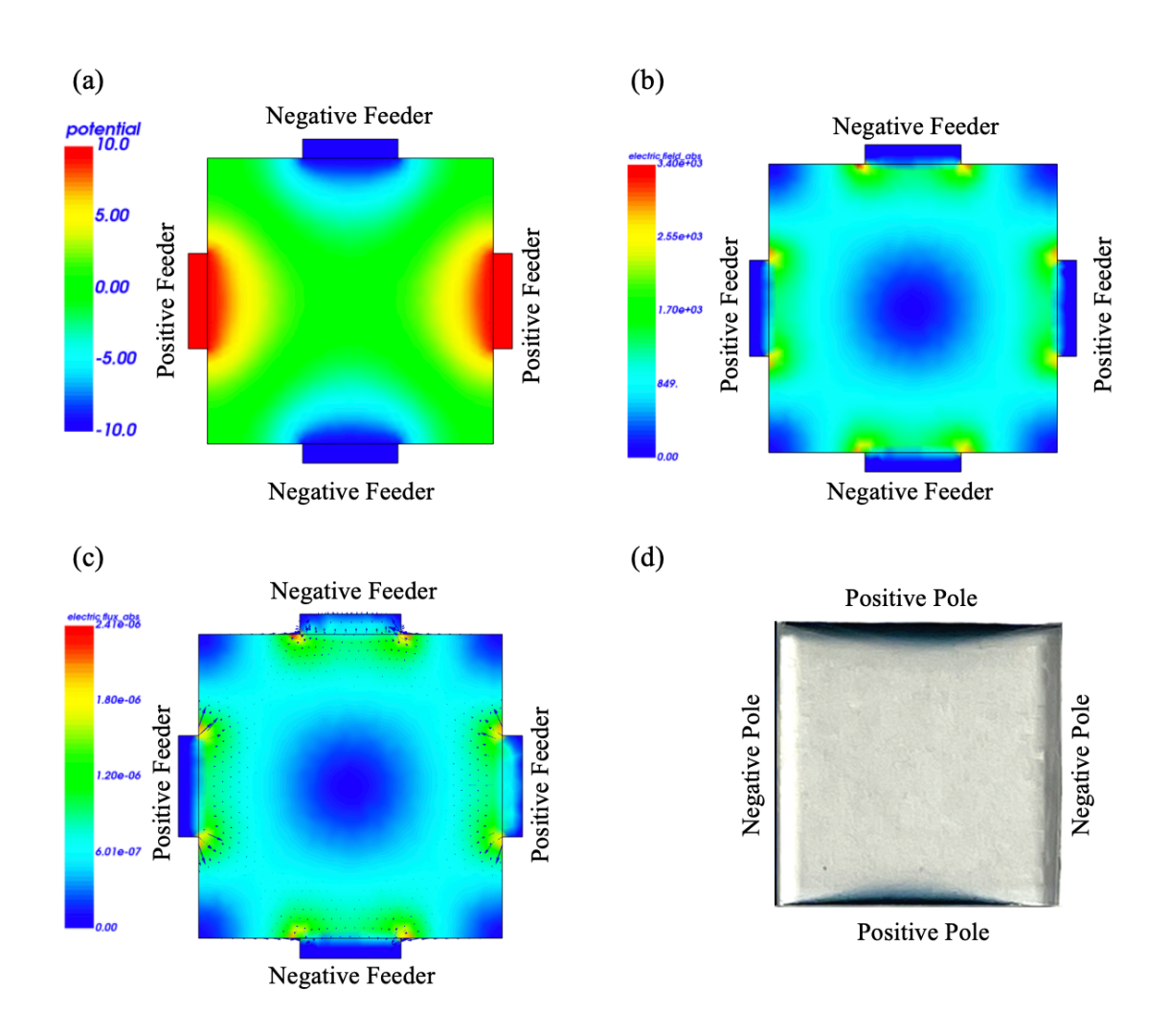


Figure 5. 12. Electric field mapping of the four-feeder setup without the BPE (Configuration 1), investigating (a) potential gradient (b) electric field (c) electric flux

and (d) image of PEDOT deposited by Configuration 1 on FTO (1.5 x 1.5 cm). Applied potential of -10 V on the negative feeders and +10 V on the positive feeders.

Figure 5.12 displays the Elmer generated simulations of the four-feeder electrode Configuration 1 without the BPE. The initial observation is the similarity between the experimental BP PEDOT deposition shown in Figure 5.12 (d) and the correlating potential distribution shown in Figure 5.12 (a). The blue 'n' shaped distribution represents the negative feeders which are at -10 V, which are opposite to the positive feeders at +10V. The simulated solution potential shown in Figure 5.12 (a) shows the 'n' shaped saturated potential at all four feeder electrodes. Interestingly, the negative feeder electrode solution potential is the exact shape of the deposited PEDOT film on the positive pole of the BPE. Figure 5.12 (b) displays the electric field for the four feeder Configuration 1 setup which once again shows a strong electric field at the corners of the feeder electrodes as indicated by the red and yellow area. The centre of the cell shows a low or no electric field which is likely due to the interactions between the feeder electrodes. Figure 5.12 (c) demonstrates the electric flux generated in the system. Interestingly, the negative feeder at the top of the bipolar cell possesses increased electric flux than that of the opposing negative feeder which is indicated by a more pronounced red and yellow area at the corners of the feeder electrode. Interestingly, this is also seen in the deposition on the FTO substrate in Figure 5.12 (d) as the deposition at the top of the FTO visually has more deposited PEDOT than that of the bottom deposition. This correlates with the electric flux distribution, having a greater electric flux at the top negative feeder electrode and thus the top positive BP pole.

5.3.3.3. Four Feeder Bipolar Setup – Configuration 2

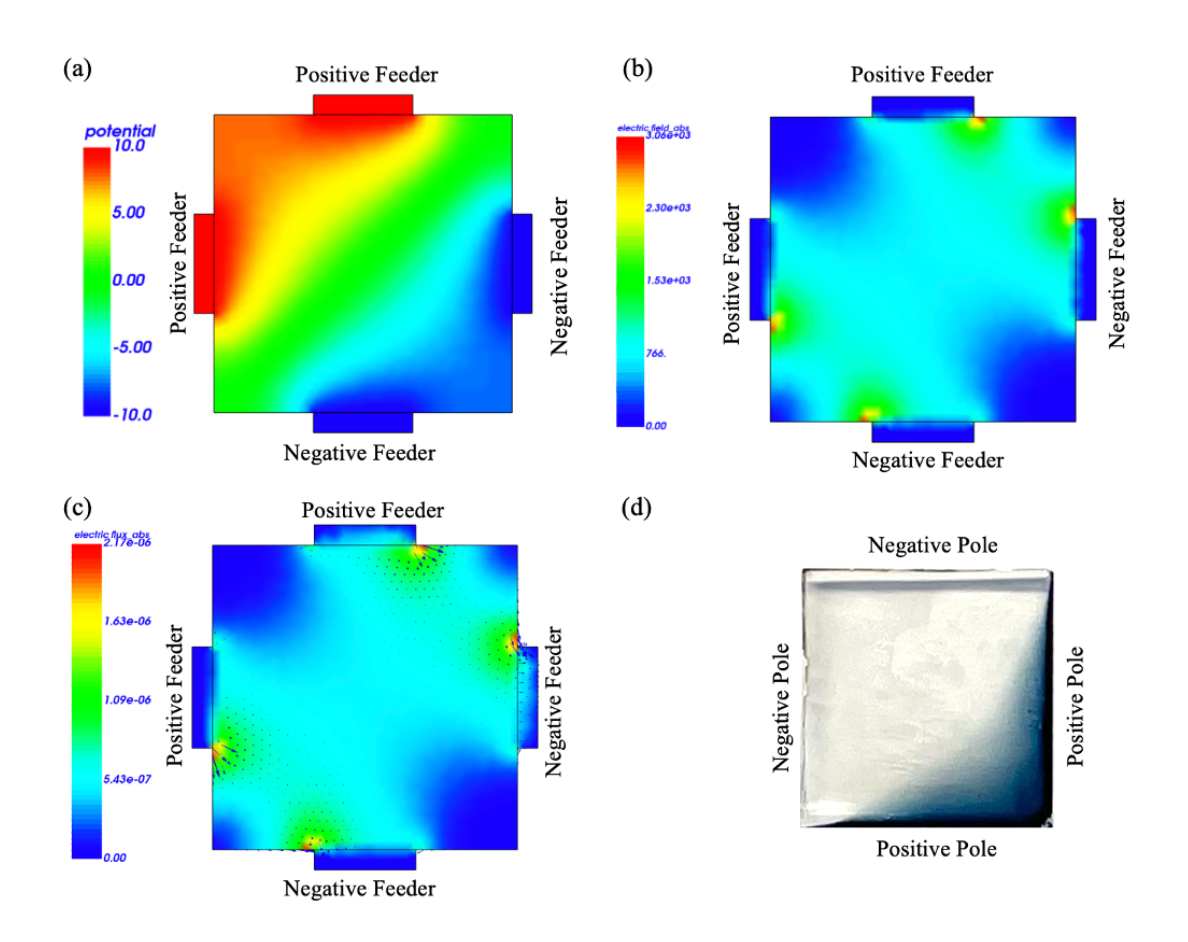


Figure 5. 13. Electric field mapping of the four-feeder electrode set up (Configuration 2), investigating (a) potential gradient (b) electric field (c) electric flux and (d) image of PEDOT deposited by Configuration 2 on FTO (1.5 x 1.5 cm). Applied potential of -10 V on feeder cathodes and +10 V on feeder anodes.

Figure 5.13 shows the potential, electric field, and electric flux simulations generated using Elmer software for the four feeder electrode Configuration 2 without the BPE. Figure 5.13 (a) shows the solution potential for the four feeder Configuration 2 which shows +10 V at both positive feeders which is indicated by the colour red, and -10 V at the negative feeders, indicated by blue. The solution potential in Figure 5.13 (a) shows a strong correlation between the experimental polymerisation of PEDOT in Figure 5.13 (d), as the blue bands of the negative feeder electrodes demonstrate the same shape as the polymerised PEDOT on the positive BP poles. The result is triangular shaped deposition that stops just before the diagonal halfway point which is also indicated in the solution

potential simulation (Figure 5.13 (a)). However in Figure 5.13 (d), the actual BP polymerisation shows a thick PEDOT film at the edges of the BPE, indicated by the dark navy colour, which is not demonstrated in the solution phase potential in Figure 5.13 (a). Figure 5.13 (b) shows the electric field distribution of the four feeder Configuration 2 setup, showing a low or no field between two feeder electrodes of the same charge that is indicated by a blue area. The strongest field is shown to occur at the feeder corner that is nearest to the opposing charge feeder electrode. This simulation also shows that the is a low electric field between feeder electrodes that are opposite one another regardless of the fact that they are different charges. Figure 5.13 (c) displays the electric flux of the system with vectors, showing the interactions between the feeder electrodes. Interestingly, the vectors that are coming from the positively charged feeder electrodes have a greater magnitude than other vectors in the system, showing that there is a strong electric flux from the corners of the positive feeder electrodes.

5.4. Conclusion

This work demonstrates the wirefree polymerisation of PEDOT to develop a further understanding of the electric field distribution generated during bipolar electrochemical processes. Bipolar electrodes (BPE) of different lengths |(1.4 cm, 2.0 cm, 2.6 cm) were used to gain further insight into the effects of the BPE on the distribution of the electric field, and therefore the potential experienced at that electrode. From this work, it was determined that the quantity of PEDOT material being deposited on the electrode surface was increasing with increasing electrode length, however the percentage surface coverage remained the same. This work therefore contradicts Eqt. 1.1 and the linear potential decay model, as these would imply a linear potential decay across the BPE with the centre of the BPE equating to zero volts. Eqt. 1.1 is not suitable to describe the potential distribution across the BPE, as the potential at which polymerisation is stopping is increasing in voltage with increasing electrode length as shown in Figure 5.2, which is not expected. It would be expected that the potential at which polymerisation stops would remain the same based on these models. The latter work describes the use of multi-feeder electrodes and their ability to shape and change the electric field. This work is promising to understand the potential distribution in the presence of two electric fields. This work has potential for use in cell stimulation or multi-analyte sensing, having the flexibility to alter the field lines based on the feeder configurations.

Finally, simulation software was used to map the electric field in solution. In the two-feeder set up, a linear potential decay could be seen in solution which is not what is seen in experimentation, leading to the conclusion that the introduction of the BPE has a significant impact on the shaping of the electric field (the BPE was not mapped in the software as the computer did not have the ability to run the simulation). Secondly, the four-feeder BP system was investigated using simulation software. Interestingly, the solution potential gradient generated by the software does in fact replicate what is being polymerised on the BPE for both configurations. Overall this work provides an in-depth mapping and modelling of the electric field being generated using two and four feeder electrodes which poses questions for the current bipolar linear potential decay model.

5.5. References

- (1) Abad, L.; Rajnicek, A. M.; Casañ-Pastor, N. Electric Field Gradients and Bipolar Electrochemistry Effects on Neural Growth: A Finite Element Study on Immersed Electroactive Conducting Electrode Materials. *Electrochimica Acta* **2019**, *317*, 102–111. https://doi.org/10.1016/j.electacta.2019.05.149.
- (2) Kuhn, A.; Crooks, R. M.; Inagi, S. A Compelling Case for Bipolar Electrochemistry. *ChemElectroChem* **2016**, *3* (3), 351–352. https://doi.org/10.1002/celc.201500569.
- (3) 2 Fundamentals of Electric Fields. In *Electromagnetics Explained*; Schmitt, R., Ed.; EDN Series for Design Engineers; Newnes: Burlington, 2002; pp 25–49. https://doi.org/10.1016/B978-075067403-4/50003-3.
- (4) Forster, R. J. Wirefree Electroceuticals: 3D Electrical and Electrochemical Stimulation of Biological Systems. *Current Opinion in Electrochemistry* **2023**, *39*, 101297. https://doi.org/10.1016/j.coelec.2023.101297.
- (5) Crooks, R. M. Principles of Bipolar Electrochemistry. *ChemElectroChem* **2016**, *3* (3), 357–359. https://doi.org/10.1002/celc.201500549.
- (6) Nasirizadeh, N.; Shekari, Z.; Nazari, A.; Tabatabaee, M. Fabrication of a Novel Electrochemical Sensor for Determination of Hydrogen Peroxide in Different Fruit Juice Samples. *Journal of Food and Drug Analysis* **2016**, *24* (1), 72–82. https://doi.org/10.1016/j.jfda.2015.06.006.
- (7) Fitterman, D. V. 11.10 Tools and Techniques: Active-Source Electromagnetic Methods. In *Treatise on Geophysics (Second Edition)*; Schubert, G., Ed.; Elsevier: Oxford, 2015; pp 295–333. https://doi.org/10.1016/B978-0-444-53802-4.00193-7.
- (8) Professor Robert B. Laughlin, Department of Physics, Stanford University. http://large.stanford.edu/courses/2007/ap272/peng1/ (accessed 2023-12-18).
- (9) Mavré, F.; Anand, R. K.; Laws, D. R.; Chow, K.-F.; Chang, B.-Y.; Crooks, J. A.; Crooks, R. M. Bipolar Electrodes: A Useful Tool for Concentration, Separation, and Detection of Analytes in Microelectrochemical Systems. *Anal. Chem.* 2010, 82 (21), 8766–8774. https://doi.org/10.1021/ac101262v.
- (10) Duval, J.; Kleijn, J. M.; van Leeuwen, H. P. Bipolar Electrode Behaviour of the Aluminium Surface in a Lateral Electric Field. *Journal of Electroanalytical Chemistry* **2001**, *505* (1), 1–11. https://doi.org/10.1016/S0022-0728(01)00461-2.

- (11) Zhan, W.; Alvarez, J.; Crooks, R. M. Electrochemical Sensing in Microfluidic Systems Using Electrogenerated Chemiluminescence as a Photonic Reporter of Redox Reactions. J. Am. Chem. Soc. 2002, 124 (44), 13265–13270. https://doi.org/10.1021/ja020907s.
- (12) Pigani, L.; Heras, A.; Colina, Á.; Seeber, R.; López-Palacios, J. Electropolymerisation of 3,4-Ethylenedioxythiophene in Aqueous Solutions. *Electrochemistry Communications* **2004**, *6* (11), 1192–1198. https://doi.org/10.1016/j.elecom.2004.09.021.
- (13) Koizumi, Y.; Shida, N.; Ohira, M.; Nishiyama, H.; Tomita, I.; Inagi, S. Electropolymerization on Wireless Electrodes towards Conducting Polymer Microfibre Networks. *Nat Commun* 2016, 7 (1), 10404. https://doi.org/10.1038/ncomms10404.
- (14) Mwanza, C.; Ding, S.-N. Newly Developed Electrochemiluminescence Based on Bipolar Electrochemistry for Multiplex Biosensing Applications: A Consolidated Review. *Biosensors* **2023**, *13* (6), 666. https://doi.org/10.3390/bios13060666.
- (15) Shida, N.; Inagi, S. Bipolar Electrochemistry in Synergy with Electrophoresis: Electric Field-Driven Electrosynthesis of Anisotropic Polymeric Materials. *Chem. Commun.* **2020**, *56* (92), 14327–14336. https://doi.org/10.1039/D0CC06204A.
- (16) Shida, N.; Zhou, Y.; Inagi, S. Bipolar Electrochemistry: A Powerful Tool for Electrifying Functional Material Synthesis. *Acc. Chem. Res.* **2019**, *52* (9), 2598–2608. https://doi.org/10.1021/acs.accounts.9b00337.
- (17) Karimian, N.; Hashemi, P.; Afkhami, A.; Bagheri, H. The Principles of Bipolar Electrochemistry and Its Electroanalysis Applications. *Current Opinion in Electrochemistry* **2019**, *17*, 30–37. https://doi.org/10.1016/j.coelec.2019.04.015.
- (18) Jiang, H.; Yang, L.; Li, C.; Yan, C.; Lee, P. S.; Ma, J. High–Rate Electrochemical Capacitors from Highly Graphitic Carbon–Tipped Manganese Oxide/Mesoporous Carbon/Manganese Oxide Hybrid Nanowires. *Energy Environ. Sci.* **2011**, *4* (5), 1813–1819. https://doi.org/10.1039/C1EE01032H.
- (19) Mei, B.-A.; Munteshari, O.; Lau, J.; Dunn, B.; Pilon, L. Physical Interpretations of Nyquist Plots for EDLC Electrodes and Devices. J. Phys. Chem. C 2018, 122 (1), 194–206. https://doi.org/10.1021/acs.jpcc.7b10582.
- (20) Lazanas, A. Ch.; Prodromidis, M. I. Electrochemical Impedance Spectroscopy—A Tutorial. *ACS Meas. Sci. Au* **2023**, *3* (3), 162–193. https://doi.org/10.1021/acsmeasuresciau.2c00070.

- (21) Hass, R.; García-Cañadas, J.; Garcia-Belmonte, G. Electrochemical Impedance Analysis of the Redox Switching Hysteresis of Poly(3,4-Ethylenedioxythiophene) Films. *Journal of Electroanalytical Chemistry* **2005**, *577* (1), 99–105. https://doi.org/10.1016/j.jelechem.2004.11.020.
- (22) Vacca, A.; Mascia, M.; Rizzardini, S.; Corgiolu, S.; Palmas, S.; Demelas, M.; Bonfiglio, A.; Carlo Ricci, P. Preparation and Characterisation of Transparent and Flexible PEDOT:PSS/PANI Electrodes by Ink-Jet Printing (97), Electropolymerisation. *RSC* Advances 2015, 5 79600–79606. https://doi.org/10.1039/C5RA15295J.
- (23) Bobacka, J.; Lewenstam, A.; Ivaska, A. Electrochemical Impedance Spectroscopy of Oxidized Poly(3,4-Ethylenedioxythiophene) Film Electrodes in Aqueous Solutions. *Journal of Electroanalytical Chemistry* **2000**, *489* (1), 17–27. https://doi.org/10.1016/S0022-0728(00)00206-0.
- (24) Macdonald, J. R. Impedance Spectroscopy. *Ann Biomed Eng* **1992**, *20* (3), 289–305. https://doi.org/10.1007/BF02368532.
- (25) Tisserant, G.; Fattah, Z.; Ayela, C.; Roche, J.; Plano, B.; Zigah, D.; Goudeau, B.; Kuhn, A.; Bouffier, L. Generation of Metal Composition Gradients by Means of Bipolar Electrodeposition. *Electrochimica Acta* **2015**, *179*, 276–281. https://doi.org/10.1016/j.electacta.2015.03.102.
- (26) Tomar, B. S.; Shahin, A.; Tirumkudulu, M. S. Cracking in Drying Films of Polymer Solutions. *Soft Matter* **2020**, *16* (14), 3476–3484. https://doi.org/10.1039/C9SM02294E.
- (27) Romyen, N.; Thongyai, S.; Praserthdam, P.; Sotzing, G. Enhancement of Poly(3,4-Ethylenedioxy Thiophene)/Poly(Styrene Sulfonate) Properties by Poly(Vinyl Alcohol) and Doping Agent as Conductive Nano-Thin Film for Electronic Application. *Journal of Materials Science: Materials in Electronics* **2013**, *24*. https://doi.org/10.1007/s10854-013-1188-0.
- (28) Jadli, U.; Mohd-Yasin, F.; Amini Moghadam, H.; Nicholls, J.; Pande, P.; Dimitrijev, S. The Correct Equation for the Current Through Voltage-Dependent Capacitors. *IEEE Access* 2020, 8, 98038–98043. https://doi.org/10.1109/ACCESS.2020.2997906.
- (29) Tsai, T.-H.; Chen, T.-W.; Chen, S.-M.; Ramiah, S. Nickel, Copper and Manganese Hexacyanoferrate with Poly(3,4-Ethylenedioxythiophene) Hybrid Film Modified

- Electrode for Selectively Determination of Ascorbic Acid. *Russian Journal of Electrochemistry* **2012**, *48*. https://doi.org/10.1134/S1023193512030147.
- (30) Kusakari, S.; Okada, K.; Shibao, M.; Toyoda, H. High Voltage Electric Fields Have Potential to Create New Physical Pest Control Systems. *Insects* **2020**, *11* (7), 447. https://doi.org/10.3390/insects11070447.
- (31) Theoretical Solid State Physics; Courier Corporation, 1985.
- (32) O'Sullivan, C. A Reflection on the Use of 'Electric Flux' in Introductory Physics Instruction. *Eur. J. Phys.* **2018**, *39* (4), 045708. https://doi.org/10.1088/1361-6404/aaba3d.

Chapter 6Conclusion

6. Thesis Conclusion

The overarching aim of this project was the creation of an 'on demand' drug delivery system, tackling one of the most formidable issues in modern society, which is cancer. The drug delivery system was based on the use of biocompatible, multifunctional, electronically conducting polymers so as to enable more effective therapy for cancer patients, whilst reducing common side effects. Based on the redox switching of conducting polymers, a drug delivery system was created using PEDOT as the drug release vehicle, having the ability to load and release materials upon oxidation and reduction. The second part of the project focused on the fundamentals of 'wirefree' or bipolar electrochemistry. The main focus of this work was to challenge current theories in the field, to provide a thorough, in-depth understanding of the technique. By combining both works, a future project of a wirelessly stimulation release of therapeutics from biocompatible conducting polymers can be achieved, providing a new, innovative method for the delivery of therapeutics.

The initial work shown in Chapter 2 provides a comprehensive study of the doping and de-doping procedures of the conducting polymer PEDOT. In this work, the bulky anion dodecylbenzenesulfonate is entrapped in the PEDOT film upon electropolymerisation. The immobilisation of the anion in the film leads to an exchange of cations, rather than the expected anion exchange for *p*-type doping polymers. This chapter provides an important foundation of the polymerisation and doping processes of PEDOT that is vital for the interpretation of the following chapters.

Chapter 3 further investigates the work performed in Chapter 2, delving deeper into the redox behaviour of PEDOT. This work demonstrates the polymer's ability to load (dope) and release (de-dope) therapeutics upon the application of specific potentials. The influence of the initial primary dopant is thoroughly investigated in this chapter, showing that the size of the initial dopant greatly influences the polymer's ability to load and release the anti-inflammatory drug naproxen. Diffusion coefficients for both films were calculated to determine the time taken for the therapeutic to diffuse to and from the film. The kinetics of the spontaneous and controlled release of the therapeutic were also calculated to understand which material exhibited a slow release. The second part of this work explores the effect of film thickness on the loading and release of anti-cancer

therapeutic mitoxantrone. This work indicates that upon increasing the film thickness, the quantity of therapeutic incorporated into the film increases linearly.

The second aspect of the project explores wireless electrochemistry and the inaccuracy and restrictions with current theories. Chapter 4 investigates the electropolymerisation of EDOT using the bipolar method, analysing the effects of time and voltage on the quantity of PEDOT deposited and the length of deposition. This work entirely contradicts the current theory of the linear decay model that has been used to describe bipolar electrochemistry. The electropolymerisation of EDOT using both bipolar and conventional methods is also described in this work, ultimately confirming that both methods produce a similar PEDOT material.

Chapter 5 provides a further investigation into the electric field distribution on the BPE. In this work, BPE of varying sizes are used to review the accuracy of the potential distribution equation and to further emphasis the flawed linear decay model. This work illustrates that the centre of the electrode does not always equate to 0 V, and that the potential distribution equation does not accurately represent all systems. The use of multiple feeder electrodes is also studied in this chapter, showing that the electric field can be shaped by changing the multi feeder electrode configuration. Simulation software was also used to analyse the electric field distribution in both two feeder and four feeder settings.

In combining the work presented in this thesis, a thorough understanding of conducting polymer drug delivery and wireless electrochemistry has been established. Further building on this work could see the development of a wirelessly triggered conducting polymer-based drug delivery system that could be used as a minimally or non-invasive method for delivering therapeutics to patients.

Chapter 7Future Work

7. Future Work: Wireless Release of Naproxen from Poly(3,4-ethylenedioxythiophene) Films

7.1. Aim

The aim of this work is to develop a wirelessly stimulated drug delivery system through the use of the well-known redox characteristics of conducting polymers and 'wirefree' electrochemistry. The purpose of this work would be the delivery of chemotherapeutic drugs in a safe, controlled, and targeted manner, minimising the cytotoxic effects of chemo drugs.¹ In Ireland, the annual cost of treatment is approximately €13,500 per cancer patient. This work would also focus on targeted, precision dosing, resulting in a reduction in the quantity of drug required for the treatment of patients and thus, a reduction in cost to the state.

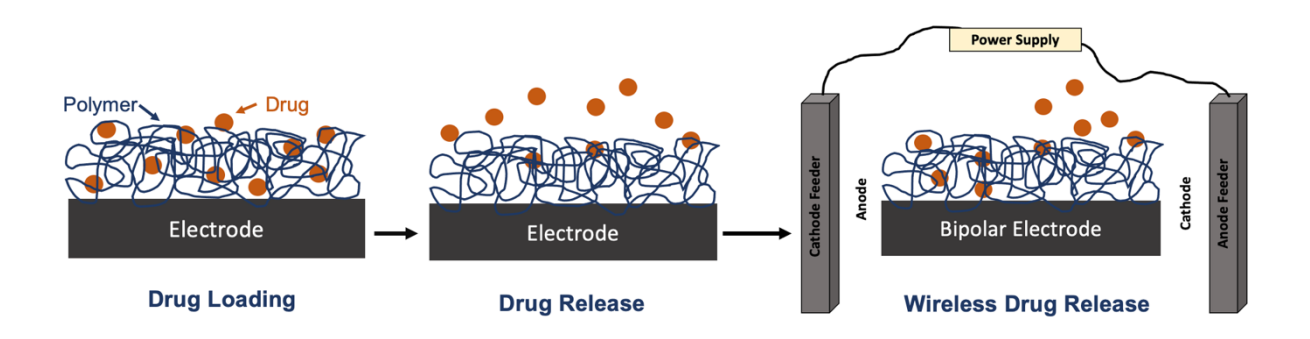


Figure 7.1. Schematic representation of the wirelessly stimulated drug release from conducting polymers.

Based on the work outlined in Chapter 2 to Chapter 5, a wireless drug delivery system would be the next gradual step for the development of the project. Building on the drug loading and release mechanisms described using EQCM in Chapter 3, upon the application of positive and negative potentials, therapeutics can be loaded and released from polymer films. From the thorough investigation of the bipolar system, specific potentials can be applied to achieve the necessary voltage to de-dope the therapeutics from the polymers, resulting in a controlled release of the drug wirelessly.

Work Package 1: Conventional Loading and Wireless Release of Anti-Inflammatory Drug Naproxen

Naproxen sodium salt would firstly be used to demonstrate the doping and wireless release of therapeutics as the compound in significantly cheaper to purchase than an anticancer therapeutic. PEDOT/ClO₄ films would be formed using cyclic voltammetry for 25 cycles in 10 mM EDOT 0.1 M LiClO₄ solution on FTO glass (2 cm x 1 cm). Using the standard three electrode setup, the perchlorate ion would be de-doped from the PEDOT film upon application of -0.5 V for 300 seconds. The PEDOT film would then be loaded with the anti-inflammatory drug naproxen upon the application of +0.5 V for 300 seconds. The drug loaded PEDOT film on the FTO substrate would then be transferred to the two feeder BP setup, and a voltage would be applied to release the drug. The quantity of drug released wirelessly would be monitored at two-minute intervals. Naproxen is a UV active molecule, thus, UV-Vis spectrometry would be used to determine the quantity of drug released wirelessly from the PEDOT films at various intervals.

Work Package 2: Conventional Loading and Wireless Release of Anti-Cancer Drug Cisplatin

Cisplatin is an anti-cancer drug used in the treatment of ovarian, testicular, bladder and lung cancers.² It is a negatively charged molecule and would therefore be an ideal drug for a PEDOT based drug delivery system. Similar to Work Package 1, PEDOT/ClO₄ films would be formed using cyclic voltammetry for 25 cycles in 10 mM EDOT 0.1 M LiClO₄ solution on FTO glass (2 cm x 1 cm). Using the standard three electrode setup, the perchlorate ion would be de-doped from the PEDOT film upon application of -0.5 V for 300 seconds. The PEDOT film would then be loaded with the anti-cancer drug cisplatin upon the application of +0.5 V for 300 seconds. The drug loaded PEDOT film on the FTO substrate would then be transferred to the two feeder BP setup, and a voltage would be applied to release the drug. Cisplatin is not a UV active molecule, therefore HPLC analysis would be used to quantify the amount of drug wirelessly released from the PEDOT film.³

7.2. Conclusion

The development of a wirefree drug delivery system is a novel concept, providing a major advancement in the way patients are treated. Using the inexpensive wireless approach to deliver therapeutics provides a targeted, minimally invasive, and more effective treatment for patients, as well as reducing the side effects of high drug concentrations. Based on the findings from Chapter 2 to Chapter 5, Work Package 1 would continue the work performed on the anti-inflammatory drug naproxen by wirelessly releasing the drug as well as quantifying the material released. Incorporating the anti-cancer drug cisplatin to the drug delivery system would result in the first wirelessly released anti-cancer drug to the best of our knowledge.

7.3. References

- (1) Rébé, C.; Ghiringhelli, F. Cytotoxic Effects of Chemotherapy on Cancer and Immune Cells: How Can It Be Modulated to Generate Novel Therapeutic Strategies? *Future Oncol* 2015, *11* (19), 2645–2654. https://doi.org/10.2217/fon.15.198.
- (2) Dasari, S.; Tchounwou, P. B. Cisplatin in Cancer Therapy: Molecular Mechanisms of Action. *Eur J Pharmacol* 2014, 740, 364–378. https://doi.org/10.1016/j.ejphar.2014.07.025.
- (3) Qin, C.; Yue, Z.; Forster, R. J.; Chen, J.; Wallace, G. G. On Demand, Wireless Electrochemical Release of Brain Derived Neurotrophic Factor. *Electrochemistry Communications* 2023, *157*, 107626. https://doi.org/10.1016/j.elecom.2023.107626.